FREQUENCY CONTROL VIA DISTRIBUTED DEMAND RESPONSE IN SMART GRID

MOHAMMAD REZA VEDADY MOGHADAM N.

NATIONAL UNIVERSITY OF SINGAPORE

2015

FREQUENCY CONTROL VIA DISTRIBUTED DEMAND RESPONSE IN SMART GRID

MOHAMMAD REZA VEDADY MOGHADAM N.

(*B. Eng. Shahid Beheshti University*)

A THESIS SUBMITTED
FOR THE DEGREE OF DOCTOR OF PHILOSOPHY
DEPARTMENT OF ELECTRICAL AND COMPUTER ENGINEERING
NATIONAL UNIVERSITY OF SINGAPORE

2015

To my dear parents

Nasrin & Mahrooz

and

my lovely wife

Katayoun

Declaration

I hereby declare that this thesis is my original work and it has been written by me in its entirety.

I have duly acknowledged all the sources of information which have been used in the thesis.

This thesis has also not been submitted for any degree in any university previously.

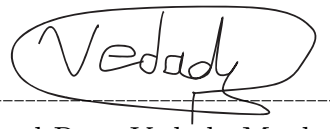

Mohammad Reza Vedady Moghadam N.

5 Agust 2015

Acknowledgments

Accomplishing the Ph.D. as well as this thesis was an amazing journey that would not have been possible without the support and encouragement of my advisors, family, group members, and friends.

My deepest gratitude goes to my advisor, Dr. Rui Zhang, for giving me a wonderful opportunity to complete my Ph.D. under his supervision, which is truly an honor. I have been amazingly fortunate to have an advisor who gave me the freedom to explore on my own, and at the same time provided the guidance to help me recover when my steps faltered. His patience and support helped me overcome many obstacles in my research to complete this thesis.

I would like to deeply thank my co-supervisor, Dr. Richard T. B. Ma. He has always been a great reference and support for my research. His insightful comments and constructive criticisms at various stages in my research were always thought-provoking and very helpful.

I am also very grateful to Prof. Asghar Mirarefi for his advice and encouragement over the course of theses few years. I truly admire his support and guidance to students.

To my current and former group members, Jie Xu, Liang Liu, Xun Zhou, Shixin Luo, Yinghao Guo, Seunghyun Lee, Shuowen Zhang, Reuben Stephen, Suzhi Bi, Yong Zeng, Gang Yang, Lu Yang, Hyungsik Ju, and Nguyen Duy Hieu, thank you for listening, offering me advice, and supporting me through this entire process. Many appreciation also goes to my dear friends Maryam, Omid, Dorsa, Amey,

Saima, Ahmed, Aisan, Farshad, Amna, Anshoo, Shima, Vahid, Sufi, Yasam, Hamed, Neda, Ehsan, Atieh, Pouya, Mohammad, Mohsen, and many more, for all of the enlightening and joyful moments we have had.

I would like to express my deepest gratitude to my family. Words cannot express how grateful I am to my parents, Nasrin and Mahrooz, for their unconditional love. I thank my sisters, Sanaz and Parisa, who always encourage me and express confidence in my abilities. I am very much thankful to my loving wife for her unlimited love, understanding, prayers and continuous support to complete my study. My gratitude also goes to my in-laws, Akram, Mehdi, Armita, and Atousa. I wish them nothing but the best.

Lastly, I gratefully acknowledge the funding sources that helped me pursue my Ph.D. education in Singapore. My work was fully supported by Singapore International Graduate Award (SINGA), funded by Singapore Agency of Science, Technology and Research (A*STAR).

Table of Contents

Summary

Frequency control is essential to maintain the stability and reliability of a power system. Traditionally, primary/secondary/tertiary reserve services with fossil-fuel based generation units are used to stabilize the power system frequency upon a contingency of supply-demand power imbalance, which, however, incur high operational costs. In future smart grid, demand response (DR) is an effective method to control the power consumption of distributed users in real time, which can be utilized to stabilize the power system frequency at low cost. This thesis is devoted to investigating efficient algorithms for DR-enabled distributed frequency control in smart gird.

This thesis starts with proposing a new frequency control algorithm based on randomized on-off operation of distributed smart appliances (SAPPs), to stabilize the power system frequency without the need of conventional primary reserve service. We characterize various the impacts of SAPPs' randomized responses on the system frequency in terms of its mean and variance over time. Based on the proposed frequency analysis, we then determine the average frequency recovery time, the average number of responded SAPPs over time, and the probability of frequency overshoot/undershoot, which provide important guidelines for designing SAPPs' response rates in practical system.

Next, we extend the proposed algorithm (for SAPPs) to frequency control via distributed charging/discharging operation of electric vehicles (EVs) that are connected to the grid. Accordingly, we formulate an optimization problem to design

the response rates of EVs to minimize the cost of implementing frequency control subject to given performance requirements. Although the formulated problem is non-convex, we solve it approximately and efficiently under certain practical assumptions.

Lastly, we study a real-time pricing scheme to incentivize distributed self-interested aggregators to reschedule their demand upon a contingency of supply deficit to achieve cost-effective secondary/tertiary reserve services. By assuming that the system operator has full knowledge of the behavior of aggregators, we formulate a bilevel optimization problem to design real-time electricity prices for the system operator to shape the sum demand of all aggregators in a way that minimizes the total operational cost of the grid, including the frequency control cost. Although the formulated problem is non-convex in general, we develop an efficient algorithm to solve it locally optimally by exploring its equivalent one-level problem. Moreover, we propose an iterative algorithm to solve the bilevel pricing problem sub-optimally, which enables the system operator to design real-time electricity prices even without any presumed knowledge of the aggregators.

List of Tables

List of Figures

List of Abbreviations

AGC	Automatic Generation Controller
BDPP	Bilevel Discount Pricing Problem
CICE	Conventional Internal Combustion Engine
CSMA	Carrier Sense Multiple Access
DLC	Direct Load Control
DR	Demand Response
ESS	Energy Storage System
EV	Electric Vehicle
FERC	Federal Energy Regulatory Commission
HEV	Hybrid Electric Vehicle
ILC	Indirect Load Control
KKT	Karush-Kuhn-Tucker
LP	Linear Programming
NEMS	National Electricity Market of Singapore
NPCC	Northeast Power Coordination Council
ODPP	One-Level Discount Pricing Problem
PDR	Price Based Demand Response
PHEV	Plug-in Hybrid Electric Vehicle
PV	Photovoltaic
RES	Renewable Energy Source
RHS	Right Hand Side

RS	Randomized Search
SAPP	Smart Appliance
SCP	Sequential Convex Programming
UFLS	Under Frequency Load Shedding
WSCC	Western System Coordinating Council

List of Symbols

Throughout this thesis, scalars are denoted by regular-face letters, vectors denoted by bold-face lower-case letters, and matrices denoted by bold-face upper-case letters. In addition, we define the following symbols:

$\mathbf{1}_{\{\cdot\}}$	Indicator Function
$\boldsymbol{x}^T$	Transpose of Vector $\boldsymbol{x}$
$\approx$	Approximately Equal to
$\gg$	Much Greater Than
$\ll$	Much Lesser Than
$\|\boldsymbol{x}\|_p$	L_p Norm of Vector $\boldsymbol{x}$
$\|\boldsymbol{x}\|_\infty$	Infinity Norm of Vector $\boldsymbol{x}$
$\|x\|$	Absolute Value of Variable x
$\|A\|$	Cardinality of Set A
$\mathbb{P}r\{x\}$	Probability Operator
$\mathbb{P}r\{x\|y\}$	Conditional Probability Operator
$\mathbb{E}[x]$	Exception Operator
$\mathbb{E}[x\|y]$	Conditional Exception Operator
$\mathbb{V}\text{ar}[x]$	Variance Operator
$\mathbb{V}\text{ar}[x\|y]$	Conditional Variance Operator

Chapter 1

Introduction

1.1 Smart Grid

Smart grid refers to an electric power system that deploys bidirectional communications and advanced signal processing techniques to gather and process information from the suppliers (generation companies), distributors (transmission system operators), and demand-side users (residential, commercial, and industrial) to operate the system in a reliable, cost-efficient, and environmentally friendly manner. For instance, the real-time information gathered from the installed sensors such as current and voltage meters in remote transmission lines and substations can help estimate the power system state more accurately. This enables the system operator to achieve autonomous fault detection and self-healing functions [1], which are able to withstand severe disturbances without interrupting power delivery to the users. Furthermore, the information exchanged among the suppliers (offered electricity prices) and users (willingness to pay for each unit of energy) help them adopt more rational and flexible operational strategies. Particularly, the users can schedule their demand over time in response to the electricity prices offered by the suppliers to save their electricity bills, e.g., defer portions of their deferrable loads such as dishwashers and/or cloth dryers to the off-peak-demand period with a lower electricity price. As a result, the need for high-cost generation units such as diesel generators during the peak-demand period decreases, which reduces the generation cost of suppliers and also makes a greener power system.

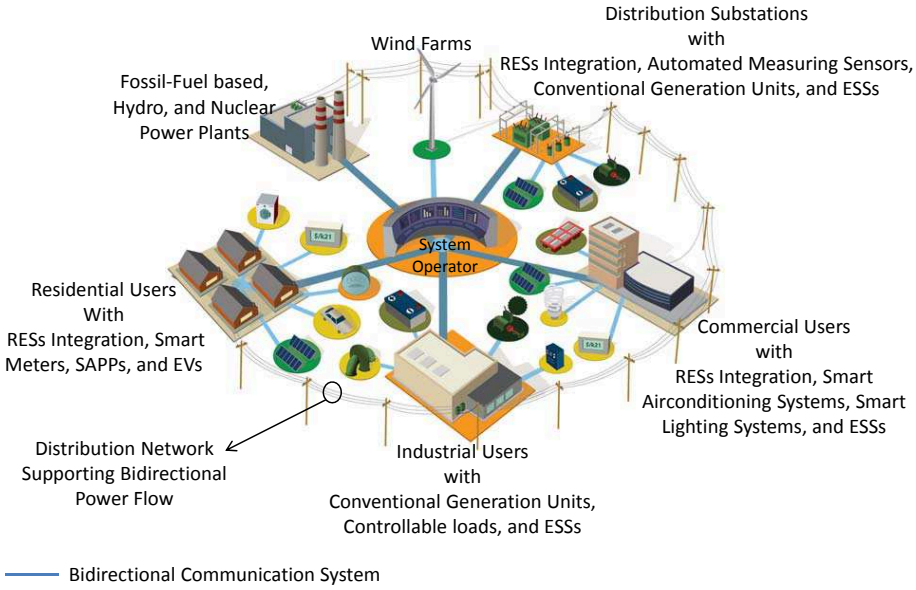

Figure 1.1: Smart grid schematic.

As shown in Fig. 1.1, smart grid supports bidirectional power flow, i.e., each user can either draw power from the grid or inject power to it, which helps increase the penetration rate of renewable energy sources (RESs) such as solar and wind in the power system. Moreover, there is a globally increasing trend for generating green energy with RESs in large scale. For example, the installed capacity of solar photovoltaic (PV) panels in the Singapore power grid has exponentially increased from 1MW in 2009 to 14.6MW in 2014 [2]. In the future, it is expected that users can widely deploy distributed renewable energy generators to meet their individual demand locally, store the surplus energy (if any) in their energy storage systems (ESSs) for future use, and/or trade it with the system operator or other users to gain monetary reward.

The massive deployment of RESs can significantly reduce both the carbon dioxide emissions of traditional fossil-fuel based power plants and the energy transmission losses from power plants to far apart users [3]. However, the intermittent and stochastic characteristics of RESs can cause imbalanced supply with demand and yield fluctuations in the power system frequency and/or voltage. Although ESSs can

be utilized to smooth out the power fluctuations in the renewable energy generation, they are costly and not environmentally friendly since toxic chemicals such as nickel and cadmium are commonly used to make rechargeable batteries. An alternative greener solution is to adjust users' power consumption over time to match the power generation of their renewable energy generators as closely as possible. This solution can also help each user to minimize the power drawn from the grid, especially during the peak-demand period to avoid causing significant disturbance to the grid. The active engagement of users in rectifying their power consumption is known as demand response (DR) in smart grid.

1.2 Demand Response (DR) in Smart Grid

According to the Federal Energy Regulatory Commission (FERC), DR is defined as [4]:

> "Changes in electric usage by end-use customers from their normal consumption patterns in response to changes in the price of electricity over time, or to incentive payments designed to induce lower electricity use at times of high wholesale market prices or when system reliability is jeopardized."

In smart grid, the bidirectional communications are required to enable DR for real-time information sharing among different entities in the system. Hence, users can adjust their instantaneous demand in response to the power system condition or a change in the electricity price. In practice, DR can be realized using either direct load control (DLC) or indirect load control (ILC) schemes [5, 6], which are explained in the following.

The DLC scheme is usually implemented in a centralized manner, under which the system operator jointly designs the power consumption of individual users over

time to achieve a certain goal. For instance, the system operator can switch off some users' loads during the peak-demand period or upon a contingency of supply shortfall to improve the power grid stability. However, the privacy issue and the communication delay in gathering information from distributed users, as well as the complexity of solving the required optimization problem involving many decision variables and constraints, e.g., each user has various loads that need to be scheduled over a given time interval, are the three main barriers to implement the DLC in practice. To facilitate the implementation of DLC, aggregators are introduced as coordinating agents between the system operator and preassigned groups of residential, commercial, and/or industrial users, under which the system optimization can be solved in hierarchical manner with lower complexity in general.

In contrast, the ILC scheme is generally implemented in a distributed manner, under which each user controls its demand independently according to the signal received from the system operator. The signal can represent either the real-time electricity price or a request for load shedding when an emergency event occurs in the power grid. If users ignore the received signal by keeping their demand unchanged, a cost is generally incurred, e.g., the users need to pay higher electricity bills or get their electricity supply completely cut off. One potential challenge for implementing the ILC is to avoid simultaneous responses of users. For example, when the electricity price is cheap, the users are likely to reschedule their future demand to the current time to reduce their electricity bills. This can result in a sudden spike in the aggregate demand which causes frequency/voltage instability in the power grid. Note that this problem occurs due to the fact that the ILC scheme is implemented in a distributed manner and thus there is no centralized control over the responses of users.

It is worth noting that both DLC and ILC schemes have been previously studied in the literature to reshape users' demand to achieve various goals [7–23]. Specifically, the optimal demand scheduling for a group of residential users to minimize

the total power generation cost of the system over a finite time horizon was studied in [7–12]. The portfolio maximization of a generation utility via designing the electricity prices offered to price-responsive users, in both day-ahead and real-time pricing scenarios, was investigated in [13–15]. The peak-to-valley minimization of the aggregate demand of users by scheduling their deferrable and reducible loads was also considered in [16–18]. Another prominent application of DR is to provide reserve (ancillary) services such as the voltage control [19, 20] and the frequency control [21–23] in order to support continuous and reliable operation of the power system.

In the following, we discuss the importance of frequency control in the power system and introduce the conventional frequency controllers. Then, we explain how DR can be used for frequency control in smart grid.

1.3 Frequency Control in Power System

The main goal of a power system is to deliver power to its users reliably and stably. To achieve this goal, the power system should be able to withstand severe disturbances without interrupting power delivery to the users. In practice, according to the criterion proposed by Northeast Power Coordination Council (NPCC) [24], the power system should be able to return to an equilibrium operating state subject to any loss in each of its components by deploying various reserve services, e.g., the system frequency and voltage controllers. Specifically, the reserve services facilitate the power system to realize continuous flow of electricity from suppliers to the users such that the supply meets the demand all the time.

Upon a contingency of supply-demand power imbalance due to e.g. the insufficient RES supplies, failures of power plants, breakdown of transmission lines, and/or unexpected spikes in the total demand, the system frequency can deviate from its nominal value, e.g., 50Hz in Singapore or 60Hz in North America. The magnitude

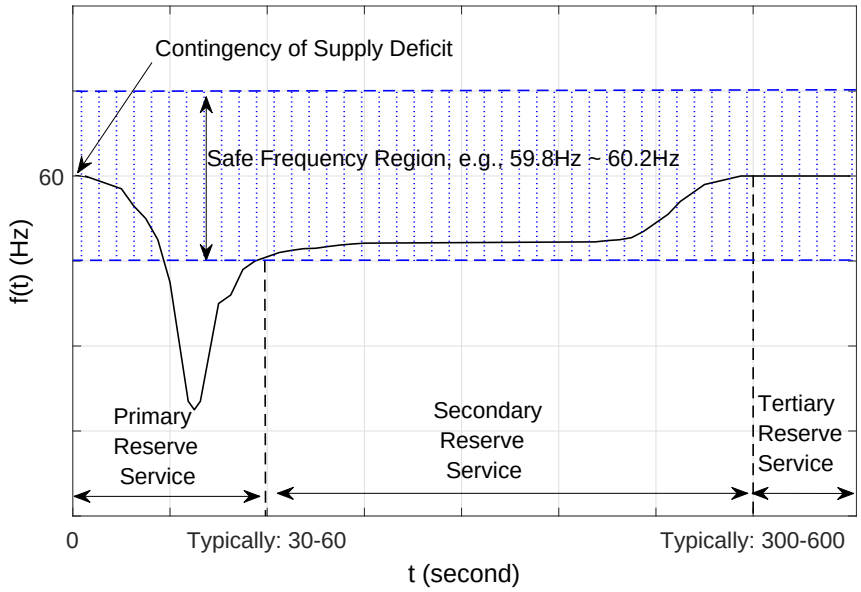

Figure 1.2: Impact of reserve services on the system frequency after a contingency of supply deficit, where $f(t)$ denotes the system frequency over time $t \geq 0$ with the nominal value of 60Hz.

and speed of the frequency deviation depends on various parameters such as the amount of the power imbalance, the power system's size and topology, etc. Generally, given a fixed power imbalance level, the system frequency in a large power system with higher mechanical inertia deviates less significantly than that in a small power system with lower mechanical inertia. A sufficiently large frequency deviation can jeopardize the power system reliability and cause serious damages to the system components and industrial machinery. For instance, under a low-frequency event due to the supply shortfall, generators, transformers, and heavy motors become overheated, since the volts/hertz ratio increases in the power system [25]. Therefore, the system frequency deviation needs to be restored quickly to prevent damages.

Conventionally, power plants providing reserve services are responsible for returning the system frequency back to its nominal value after each contingency. As shown in Fig. 1.2, the reserve services can be categorized into three main classes

as primary (regulatory), secondary, and tertiary (replacement), based on their different activation times [27]. The primary reserve service refers to the immediate responses of turbine governors and/or automatic generation controllers (AGCs) of fast-ramping synchronized generation units that do not inject power to the grid or inject power less than their maximum capacities when the system is under its normal condition. The primary reserve service arrests the system frequency decline, which is very sharp initially, and restores it to a new steady state level in the vicinity of the system frequency nominal value ($\pm 1\%$ deviation in general) in typically 20–30 seconds. After this quick service, moderate-ramping synchronized generation units deliver the secondary reserve service. This service returns the system frequency back to its nominal value by adjusting the supply to perfectly match the demand in a couple of minutes, say, 5–10 minutes. Last, since the number of power plants providing primary and secondary reserve services is limited in practice, the system operator activates the tertiary reserve service that is slow-ramping through the real-time electricity market, which is used to free the primary and secondary reserve services for future use. The tertiary reserve service is usually provided by desynchronized (standby) generation units.

Deploying the conventional primary and secondary reserve services for frequency control incurs high operational costs, since they are provided by fast/moderate ramping generation units, e.g., diesel and gas-turbine generators, which have high generation costs due to their low fuel-to-energy efficiency in general. For instance, according to the report of PJM energy market in 2013 and 2014 [28], on average, 16.6% and 15.4% of the electricity cost were due to the reliability and reserve services, respectively. Besides the cost consideration, the overall efficiency of the power system reduces when power plants are partially loaded to be enabled to provide reserve services. Last but not least, the conventional reserve services are mostly provided by power plants consuming fossil fuels that are not environmentally green.

In smart grid, an alternative and more cost-effective solution for controlling the system frequency is via DR, which is discussed next.

1.4 DR for Frequency Control

In a conventional power system, demand can provide reserve services in the form of interruptible users and/or under-frequency load shedding (UFLS) [29–31]. Under these two programs, the system operator interrupts power delivery to the users in specific geographical areas for a short time period after the contingency so as to reduce the demand to match the decreased supply. Note that this is in contrast to the generation side controllers that increase the supply to match the demand. As a result, users in the affected areas will experience electricity cut-off temporarily, without prior notice. This degrades the users' comfort levels.

In smart grid, bidirectional communications together with the advanced control tools used in smart appliances (SAPPs), e.g., *LG Smart THINQ^{TM} Appliances* or *Whirlpool® Smart Duet Pair with 6th Sense Live^{TM} Technology*, as well as electric vehicles (EVs) enable the control of the power consumption of distributed loads independently to regulate the system frequency smoothly and swiftly, which is discussed next.

Under the DLC scheme, the system operator can remotely switch on/off certain SAPPs, e.g., low priority loads such as dishwashers and cloth dryers, or change the operational modes (charging, idle, and discharging) of grid-connected EVs in response to the system frequency deviation [21, 32–40]. There are two main disadvantages of using the DLC scheme to control the system frequency. First, the communication delay for collecting information from all SAPPs/EVs and the computation time required to jointly design their responses can increase the overall delay for activating DR. As a result, the DLC cannot be used in replacement of the conventional primary reserve service in practice. Second, the DLC scheme creates

serious privacy concern, since the system operator can infer personal information of users based on the collected information [55].

Under the ILC scheme, SAPPs/EVs are designed to measure the system frequency locally and adjust their power consumption independently in response to the system frequency deviation using their respective control algorithms [41–53]. As an example, when an EV detects that the system frequency is below a given threshold, it can stop its ongoing charging process and/or inject power to the grid to help boost the system frequency. However, when the system frequency recovers to its safe range for a sufficient amount of time and the supply deficiency is compensated using the secondary and tertiary reserve services, SAPPs/EVs can deactivate their frequency control and resume their normal operation.

Besides improving the system flexibility to manage the variability and uncertainty of the aggregate power supply resulting from the massive deployment of RESs, using DR for frequency control has other benefits over the conventional frequency controllers, as listed below [54]:

- Fast response time: the response time of the frequency controllers installed in power plants is usually longer than that of the demand-side controllers due to the high inertia of large mechanical components in power plants, e.g., turbines' shafts and blades.

- Low operational cost: the need for generating extra power using fossil-fuel based generation units decreases; as a result, the total fuel cost decreases.

- Environmentally green: the decrease in consuming fossil fuels can reduce greenhouse gas emissions.

- Higher power quantity: except for must-run demand such as loads of hospitals and military sites, the rest of demand can potentially take part in the frequency control program.

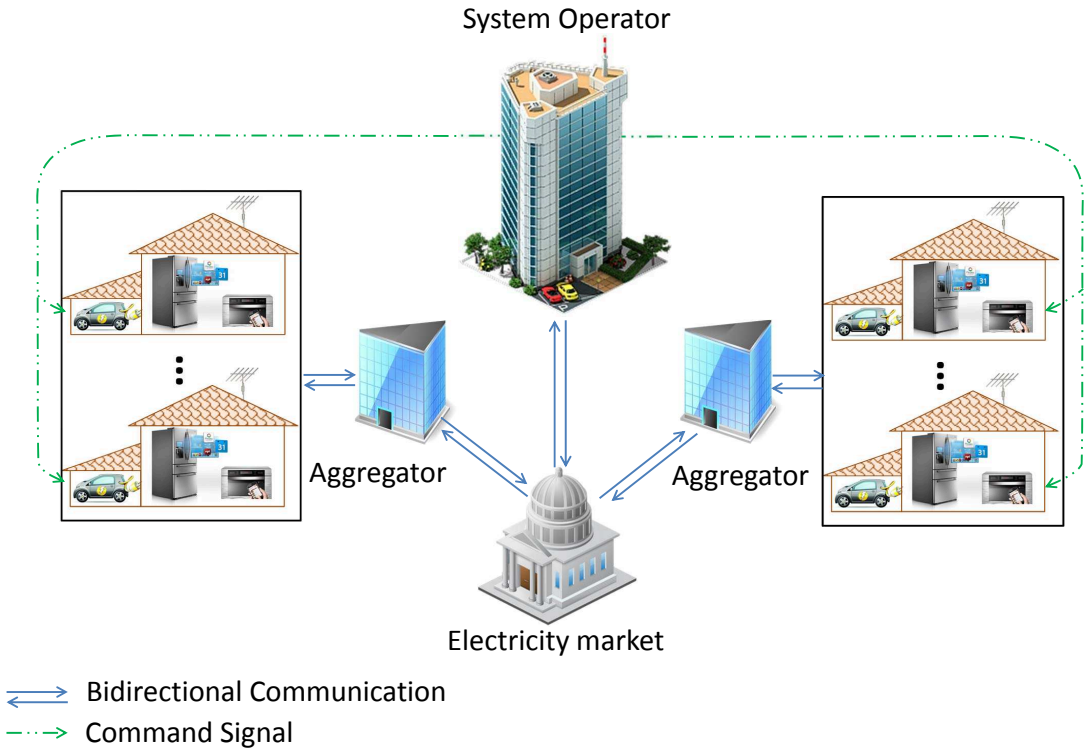

Figure 1.3: The proposed two-stage operation architecture for DR-enabled frequency control in smart grid.

As shown in Fig. 1.3, in this thesis we consider a two-stage operation architecture to utilize DR for frequency control using the ILC scheme. In the first stage, the system operator notifies all users (SAPPs/EVs) to activate their individual frequency control algorithms by sending a command signal (e.g., bit '1') upon a contingency of supply-demand power imbalance. Accordingly, SAPPs/EVs respond to their locally measured system frequency independently to help restore the system frequency to its safe region swiftly, where their responses function similarly as the conventional primary reserve service provided by fast-ramping generation units. In the second stage, the system operator holds the real-time electricity market and negotiates with the aggregators, each of which purchases electric power from the system operator to satisfy the demand of its users, to provide cost-efficient secondary and tertiary reserve services. After the energy transaction is completed, i.e.,

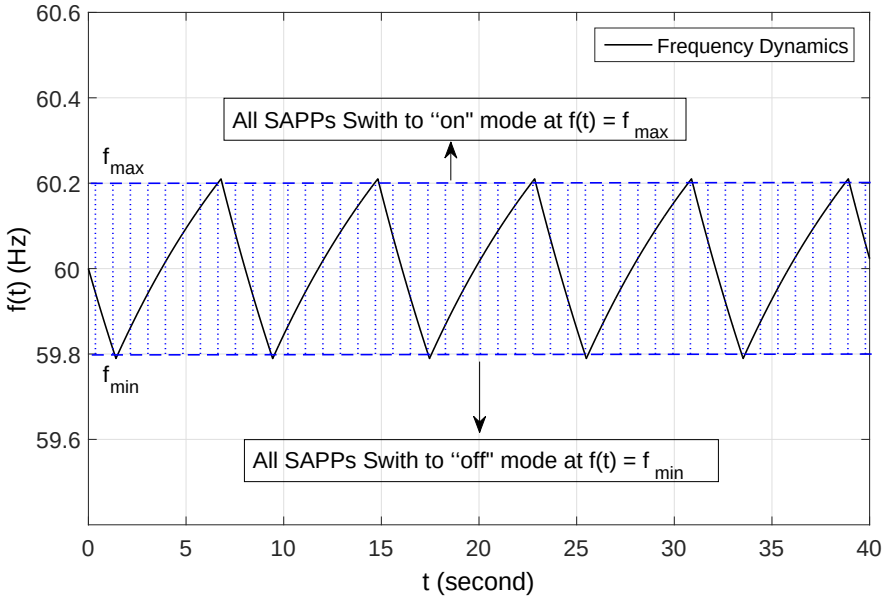

Figure 1.4: Frequency oscillation problem due to synchronized responses of SAPPs.

the demand of aggregators is rescheduled similar to the conventional secondary and tertiary reserve services, the system operator sends a clear command (e.g., bit ‘0’) to all SAPPs/EVs in order to deactivate their frequency controllers and resume their normal operation.

1.5 Motivation

There are three main challenges in designing the proposed two-stage architecture for DR-based frequency control, which are discussed in the following.

1.5.1 Frequency Oscillation Problem

The simultaneous responses of users’ frequency-responsive loads, i.e., SAPPs and EVs, can potentially result in a frequency oscillation problem. To further demonstrate this problem, we consider a simple frequency threshold based on-off load control policy as follows. We assume that all SAPPs continuously monitor

the system frequency and switch their loads off when the frequency drops below a predetermined lower threshold, $f_{\min} = 59.8$Hz, and switch them on again when the frequency goes up to a predetermined upper threshold, $f_{\max} = 60.2$Hz. We assume that all SAPPs use the same frequency thresholds. We implement this load control policy for the IEEE 9-Bus test system that represents a portion of the Western System Coordinating Council (WSCC) power system [56]. By applying this load control policy, a snapshot of the frequency dynamic in the IEEE 9-Bus test system after a contingency of supply shortfall is shown in Fig. 1.4, from which a frequency oscillation is observed. This phenomenon is due to the fact that all SAPPs observe and respond by switching from on(off) to off(on) states at the same time when the system frequency reaches one of the two frequency thresholds. If SAPPs gradually adjust their power consumption in response to the system frequency deviation [36, 38], then the system frequency can recover smoothly and the frequency oscillation problem can be avoided. However, this assumption is not practically valid for many household appliances such as television sets, refrigerators, and washing machines that operate with constant power load. A similar solution is to continuously adjust the power charging/discharging rates of EVs in response to the system frequency deviation [50–53, 57], which, however, is costly to implement in practice.

It is worth noting that randomized algorithms have been widely applied in practice to solve problems in other applications with similar issues as the frequency oscillation problem in the power system. For example, randomized algorithms have been successfully implemented to solve a collision problem in multi-user communication networks (using, e.g., CSMA or ALOHA based protocols [58–60]), by applying random waiting times for each individual transmitter in order to minimize the probability of overlapping transmissions.

In the literature (see e.g. [41–47]), randomized methods to desynchronize responses of SAPPs/EVs, by using either random frequency thresholds for activa-

tion/deactivation of their loads or random waiting times for activating their control, have been proposed to solve the frequency oscillation problem. However, the frequency control algorithms proposed therein require to be implemented continuously in time, i.e., SAPPs/EVs need to monitor the system frequency all the time to respond timely. However, the continuous monitoring of SAPPs/EVs are difficult to be realized in practice due to practically large response times (say, tens of milliseconds) of commercially available frequency measurement sensors. Furthermore, the continuous monitoring of a battery-powered sensor can reduce its operation time significantly. Therefore, how to design efficient and low-cost methods to desynchronize the responses of distributed SAPPs/EVs is still a challenging problem.

1.5.2 Frequency Characterization

The power system frequency upon a contingency can be easily expressed for the case where the amount of power imbalance and the time that it occurs as well as the time instants that SAPPs/EVs respond are known. However, there is no analysis available in the literature for the case where all these variables are random, as in the case of randomized frequency control. In the related prior studies [41–47, 49–53], simulations have been extensively used to validate the performance of proposed frequency control algorithms under different system setups. However, in order to implement frequency control via randomized DR in practice, we need to choose appropriate design parameters such as the average response rate and the inter-response time distributions for frequency-responsive loads given the power system characteristics to optimize the control performance. This is not feasible without a rigorous analysis on the system frequency dynamics under randomized DR. Such analytical results are crucial for the system operator to estimate how the randomized responses of SAPPs/EVs affect the system frequency upon a contingency of supply-demand imbalance. To our best knowledge, there has been no prior work that

rigorously characterized the system frequency dynamics subject to randomized DR.

1.5.3 Optimal DR for Frequency Control

If we use DR to replace the conventional primary reserve service for frequency control in smart grid, DR should be activated quickly, say, within 30 seconds. Thus, it is not practically feasible to jointly design control parameters for a large number of SAPPs/EVs (e.g., for millions of users) in real time. Alternatively, their control parameters can be designed off-line and then applied in real time. However, a mathematical framework to design the control parameters of SAPPs/EVs with randomized responses for frequency control in smart grid is still missing in the literature.

After instantaneous responses of SAPPs/EVs which arrest the system frequency deviation and restore it to a new steady state within its safe range, the system operator is given adequate time to provide DR-enabled secondary and tertiary reserve services through the real-time electricity market. Particularly, the system operator can negotiate with the aggregators by offering discounted electricity prices over off-peak-demand period or other monetary rewards to reschedule their users' demand over time to reduce the overall demand to match the decreased supply. However, designing the real-time electricity prices is a challenging task in general, since aggregators are practically self-interested and aim to maximize their individual utilities even when there is a contingency of supply deficit. As a result , if the real-time electricity prices are not designed appropriately, aggregators may not be motivated to reschedule their loads or they all shift loads into the same time in future, which causes a spike in the aggregate demand. In the literature [61–70], various real-time pricing algorithms have been devolved to design electricity prices for the system operator by assuming that the power grid is operated under the normal condition. However, there has been less effort to investigate real-time pricing for contingency

management, which can improve the power system reliability with minimum cost.

1.6 Thesis Objective and Organization

Motivated by the above discussions, in this thesis we focus our study on addressing the three major challenges in implementing the two-stage architecture in Fig. 1.3 for controlling the power system frequency via distributed DR, which are, respectively, overcoming the frequency oscillation problem due to simultaneous responses of distributed SAPPs/EVs, characterizing the system frequency dynamics subject to the randomized responses of SAPPs/EVs, and optimal DR management to minimize the operational cost of the power system. The thesis is organized as follows.

Chapter 1 presents the motivation, objective, and the major contributions of this thesis.

Chapter 2 proposes a new frequency control algorithm for distributed SAPPs, under which SAPPs locally monitor and respond to the system frequency over randomized discrete times. The impacts of SAPPs' randomized responses on the system frequency dynamics are mathematically characterized, and extensive simulations based on the IEEE 9-Bus test system and the aggregate model of the Ireland power system are provided in order to verify the performance of our proposed frequency control scheme. Specifically, we show that with the proposed control algorithm, using SAPPs' responses can replace the conventional primary reserve service provided by fast-response power plants to restore the system frequency reliably, even under a severe contingency of supply-demand power imbalance up to 10% of the total generation capacity.

Chapter 3 extends the proposed algorithm for SAPPs to control the system frequency by exploiting randomized responses of distributed grid-connected EVs. Accordingly, we characterize the impacts of EVs' randomized responses on the sys-

tem frequency. Furthermore, an optimization problem is formulated and efficiently solved to design EVs' response rates to minimize the expected cost of deploying our proposed frequency control. Last, simulation results are provided to verify the effectiveness of our proposed algorithm to control the system frequency via DR of distributed EVs.

Chapter 4 presents a new real-time pricing scheme to manage the demand rescheduling in a group of self-interested aggregators to provide cost-efficient secondary and tertiary reserve services. A bilevel optimization problem is formulated to optimize real-time discounted electricity prices (cheaper than the day-ahead electricity prices) for the system operator to minimize the frequency recovery cost of the power system after a contingency of supply-demand imbalance. Numerical examples are provided to show that our proposed real-time pricing scheme can effectively reduce the frequency control cost of the power grid, while the aggregators also pay less electricity bills with the designed discounted electricity prices.

Finally, Chapter 5 concludes this thesis and discusses about the future work.

1.7 Major Contributions of the Thesis

The major contributions of this thesis are summarized as follows.

1.7.1 New Randomized Algorithms to Desynchronize Responses of SAPPs/EVs

The first contribution of this thesis is to propose new practical control algorithms to desynchronize the responses of SAPPS/EVs to help recover the system frequency smoothly.

In Chapter 2, we design SAPPs to monitor the system frequency over discrete times (e.g., with the interval of 20–30 seconds) and respond based on a simple frequency threshold based on-off policy. To desynchronize responses of SAPPs, we

impose a constraint that each SAPP must wait a random time between any two consecutive monitoring events, where the waiting times are assumed to be independent and identically distributed (i.i.d.) exponential random variables with a given mean value. The inverse of mean value is named *response rate*. We show via both analytical and simulation results that by designing response rates of SAPPs appropriately, our proposed control algorithm can restore the system frequency smoothly, without frequency oscillation.

In Chapter 3, we present a randomized frequency control algorithm for distributed EVs. The algorithm is in similar spirit of that presented in Chapter 2 for desynchronizing responses of SAPPs, while the discharging control of EVs (i.e., by injecting power to the grid) is considered in addition to the charging control for frequency recovery. Specifically, EVs are designed to monitor the system frequency locally over discrete randomized times and respond independently according to a simple frequency threshold based mode switching policy. As compared to SAPPS, deploying EVs for frequency control has more flexibility due to both charging and discharging control, which can help restore the system frequency more smoothly.

1.7.2 Characterizing Impacts of Randomized Responses of SAPPs/EVs on System Frequency

Under the randomized control of SAPPs/EVs, the system frequency is generally modeled as a stochastic process over time. In Chapters 2 and 3, we investigate the impacts of randomized responses of SAPPs and EVs on the system frequency, respectively. We first derive closed-form expressions for the mean and variance of the system frequency over time upon a contingency of supply-load imbalance. Then, we derive the average frequency recovery time, i.e., the average time needed to recover the system frequency within its safe region after the contingency, the expected number of responded SAPPs/EVs over time, and the probability of frequency over-

shoot over the preassigned threshold in steady state. This analysis provides useful guidelines for the system operator to implement our algorithms in real time.

1.7.3 Optimal DR Management for Frequency Control

In Chapter 3, we formulate an optimization problem for the grid operator to minimize the expected cost of implementing our proposed EV-enabled frequency control by designing EVs' response rates subject to the incentive prices requested by their owners and the given power grid performance requirements. Although the formulated problem is non-convex in general, we approximate it as a linear programming (LP) problem under certain practical assumptions, and then solve it efficiently. In practice, the grid operator can solve the problem in a hourly/daily basis and then send the optimal response rates to the users to set up their individual EVs for implementing frequency control in the future.

In Chapter 4, we formulate a *bilevel optimization problem* [98] to design real-time discounted electricity prices for the system operator to minimize the cost of motivating self-interested aggregators to reschedule their demand upon a contingency. The problem is formulated by first assuming that the system operator has the full knowledge of the behavior of all aggregators. Since the formulated problem is non-convex in general, we develop a sequential convex programming (SCP) based algorithm to solve it locally optimally. Moreover, we propose a randomized search (RS) based algorithm to solve the problem heuristically, which is shown to be able to design electricity prices even when the system operator does not have any presumed knowledge about the aggregators. The performance of two proposed algorithms are compared using a numerical example based on the Singapore power grid data, from which it is observed that our pricing scheme can effectively manage DR of aggregators in real-time electricity market to provide cost-efficient secondary/tertiary reserve services. As shown in our numerical example, the demand rescheduling of aggregators is activated through the real-time electricity market as fast as the con-

ventional secondary reserve service, e.g., in nearly 80 seconds, while it can alleviate the power imbalance for a sufficiently long time interval, e.g., up to 12 hours, which is comparable to the conventional tertiary reserve service.

Chapter 2

Frequency Control via Randomized Responses of Distributed SAPPs

2.1 Introduction

In this chapter, we propose a new frequency control algorithm based on the randomized on-off operation of distributed SAPPs to alleviate the frequency oscillation problem, and stabilize the power system frequency swiftly without the need of conventional primary reserve service. Next, we analyze the performance of our frequency control algorithm upon a contingency of supply shortfall, where the obtained results can help the system operator choose appropriate design parameters such as the average response rates and the inter-response time distributions for SAPPs given the power system parameters to optimize the control performance.

2.2 Literature Review

In one preliminary work on the distributed DR-enabled frequency control in smart grid, the Pacific Northwest National Laboratory (PNNL) [41] used a simple threshold based on-off load switching policy with randomized activation/deactivation frequency thresholds and randomized response delay times for domestic SAPPs to rectify the system frequency fluctuations. The proposed frequency control algorithm by PNNL was implemented on a small-scale demonstration project, including 150 cloth dryers and 50 water heaters, which yielded promising positive results.

However, the theoretical analysis to characterize the system frequency dynamics following the randomized responses of SAPPs has been not provided in [41]; therefore, there is no straightforward approach to verify whether their obtained results are valid for power systems with larger number of SAPPs or not. It is worth noting that the analytical approach proposed in this chapter can be applied to derive the performance analysis for the PNNL algorithm. A novel thermostat control policy for smart refrigerators was investigated in [42]. This control policy was designed to autonomously increase the thermostat's temperature set-point (subject to a given cap, e.g., $-1\,^{\circ}\mathrm{C}$) upon an under-frequency event to switch off the refrigerator's compressor temporarily. It was shown in [42] that the diversity of refrigerators' physical specifications and differences in their initial inner temperatures can desynchronize their responses, and thereby a smooth frequency recovery can be achieved even without the need for the conventional primary reserve service in the generation side. Molina-Garcia *et. al* [43] proposed a multi-regional frequency control algorithm for household SAPPs to achieve faster responses to larger frequency deviations (similar to an over-current protection relay in a transmission line which disconnects the line from the grid faster when the current overshoot in the line increases). To avoid frequency oscillation, [43] applied uniformly distributed turn-on delay times and normally distributed minimum/maximum response time limits for SAPPs. Alternatively, randomized frequency thresholds were deployed in [44] to avoid simultaneous responses of SAPPs. The priority dependent frequency thresholds were proposed in [45] to prevent high priority loads, e.g., lighting systems, from responding to small frequency deviations. It was shown in [45] that utilizing the randomized responses of approximately 200MW of SAPPs for frequency control in the Great Britain's (GB) power system can keep the system frequency over the desired level 49.5Hz upon a contingency of 1320MW supply deficit which is the worst case scenario in the GB's power system. Recently, an experimental implementation of a cost-efficient decentralized load control scheme on the Bornholm Island, Denmark (a

small power grid with 33% penetration of wind energy) was reported in [46]. Specifically, 70 thermostatically controlled loads were equipped with frequency control devices to help regulate the system frequency. It was shown in [46] that deploying frequency-responsive loads for frequency control can decrease both the cost and the time required to stabilize the system frequency as compared to the conventional primary reserve service. Last, Molina-Garcia *et al.* [47] utilized the same frequency control algorithm as that reported in [42] to show that DR-enabled frequency control can enhance the quality of frequency control by reducing the maximum frequency deviation and also increasing the speed of restoring the frequency to its safe region in a power system with high penetration of intermittent wind generation, even up to 20% of the total generation capacity.

The frequency control algorithms proposed in [41–47] require to be implemented continuously in time, while the continuous monitoring of SAPPs are difficult to be achieved as discussed in Section 1.5.1. Hence, we develop a simple frequency control algorithm to distributively switch on/off each SAPP in response to its locally measured system frequency over discrete randomized time instants. Furthermore, [41–47] used simulations and small-scale experiments to validate the performance of their proposed algorithms. However, to implement DR-enabled frequency control in practice, we need to choose appropriate design parameters such as the average response rates and the inter-response time distributions for SAPPs given the power system characteristics, which is not feasible without a rigorous analysis of the system frequency dynamics. This motivates our work to analyze the impacts of randomized responses of distributed SAPPs on the system frequency, which enables the system operator to design their parameters to achieve desired power system stability with the minimum cost. In contrast to [49] that has investigated the behavior of an individual smart refrigerator with random frequency control in response to the system frequency, we focus on characterizing the system frequency by taking the randomized responses of a large group of distributed SAPPs into account.

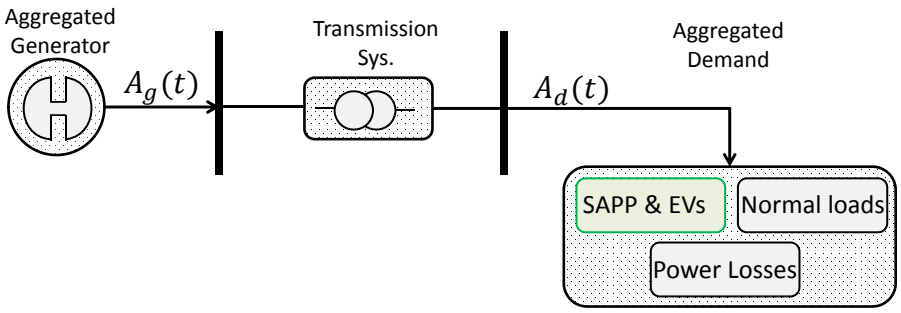

Figure 2.1: Schematic of an aggregate power system model.

2.3 System Model

In this section, we first introduce an aggregate power system model. We next study the frequency dynamics of this system upon a contingency of supply deficit. Herein, we assume that there are no conventional frequency controllers such as turbine governors and/or AGCs in the power system. Furthermore, we assume that DR-enabled frequency controllers are all deactivated for the time being. In Sections 2.4.2 and 3.4.2, we will extend our analysis to capture responses of SAPPs and EVs, respectively, on the system frequency dynamics.

2.3.1 Aggregate Power System Model

We consider a power system under the so-called *synchronous* operating regime, where the whole system operates with a single system-wide frequency even upon emergency events [72]. This assumption is reasonable due to the fact that most power systems are designed to deal with any loss of a single component without losing the system frequency synchronism according to the criterion proposed by the Northeast Power Coordination Council (NPCC) [24]. As a result, we can model the power system in an aggregate form, as shown in Fig. 2.1, where $A_g(t)$ and $A_d(t)$ denote the aggregate output power of generation units and the aggregate demand of energy consumers, respectively. The aggregate demand includes the

power consumption of all residential, commercial, and industrial loads regardless of whether they participate in frequency control or not, together with transmission power losses.

Let $f(t)$ denote the system frequency over time $t \geq 0$, with the nominal value of f_0 at $t = 0$. Since the system voltage can be regulated separately by voltage controllers that inject/absorb reactive power into/from the grid [79,80], the demand power consumption (without responses of demand-side frequency controllers) can be modeled as a function of the system frequency only. Based on the fact that the system frequency deviation from its nominal value is practically small, the aggregate demand power consumption can be expressed as a linear function of the system frequency [72]. Specifically, we have

$$A_d(t) = A_0 + \left(\frac{f(t) - f_0}{f_0}\right) K_f A_0, \ t \geq 0, \tag{2.1}$$

where A_0 denotes the aggregated demand power consumption under the nominal values of frequency and voltage at time $t = 0$. The second term on the right hand side (RHS) of (2.1) indicates the demand power change due to the system frequency deviation, where $K_f > 0$ is the frequency damping coefficient [72]. In fact, K_f models the natural (passive) behaviors of loads such as motors and fans, where the power consumption of each of them depends on the frequency of its supply source. Although the aggregated power consumption of demand may not be a linear function of the system frequency in general, we can still linearize it in the vicinity of the nominal frequency (e.g., $\pm 2\% f_0$) using its first-order Taylor series approximation.

2.3.2 Frequency Dynamics in Power System

The frequency dynamics in a power system are governed by the physics of motion (Newton's laws of motion) and expressed by a so-called *swing equation* [72]

as follows

$$\frac{2E}{f_0}\frac{df(t)}{dt} = A_g(t) - A_d(t),\ t \geq 0, \tag{2.2}$$

where $E > 0$ denotes the stored energy in the rotational parts of the aggregate generator. By substituting (2.1) into (2.2), we obtain

$$\frac{2E}{f_0}\frac{df(t)}{dt} = A_g(t) - A_0 - \left(\frac{f(t) - f_0}{f_0}\right) K_f A_0,\ t \geq 0. \tag{2.3}$$

We now investigate the system frequency upon a contingency of supply-demand power imbalance. Without loss of generality, we assume that the aggregate generation power deviates A_e from its scheduled value at time $t = 0$, where $A_e < 0$ indicates the case of supply deficit and $A_e > 0$ indicates the case of supply surplus. Given the assumption that there are no conventional frequency controllers in the power system, we can set $A_g(t) = A_0 + A_e \mathbf{1}_{\{t \geq 0\}}$, where $\mathbf{1}_{\{.\}}$ is an indicator function. Accordingly, we re-write (2.3) as follows

$$\frac{2E}{f_0}\frac{df(t)}{dt} = A_e - \left(\frac{f(t) - f_0}{f_0}\right) K_f A_0,\quad t \geq 0. \tag{2.4}$$

By solving the above differential equation, we thus obtain

$$f(t) = f_0 + \frac{f_0}{K_f A_0} A_e \left(1 - e^{-\alpha t}\right),\ t \geq 0, \tag{2.5}$$

where $\alpha = (K_f A_0)/(2E)$. In general, a large α corresponds to a power system with small mechanical inertia; thus, the system frequency reaches to its new steady state more quickly after each disturbance [72]. From (2.5), it follows that A_e amount of supply deviation yields $(f_0 A_e)/(K_f A_0)$ amount of frequency deviation in steady state, and this change on the system frequency occurs exponentially fast. In practice, we have $|A_e|/(K_f A_0) < 1$, since $|A_e| \ll A_0$.

In the rest of this thesis, we focus on the case of supply shortfall, i.e. $A_e < 0$,

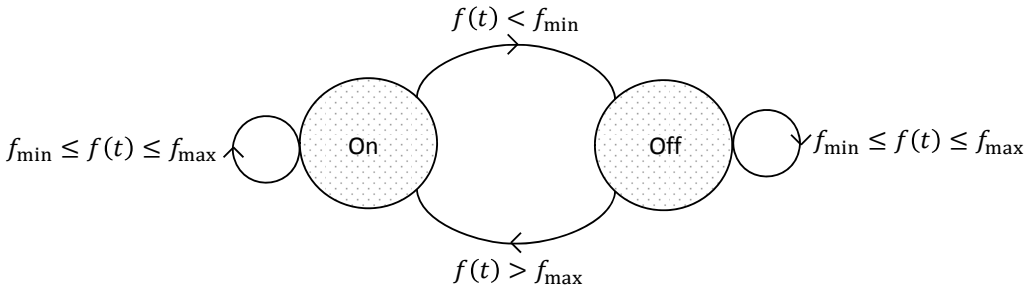

Figure 2.2: Threshold based one-off load control policy for each SAPP.

while all the obtained theoretical results can be readily extended to the case of supply surplus, i.e. $A_e > 0$.

2.4 Frequency Control via Distributed SAPPs

In this section, we introduce our frequency control algorithm with randomized responses of distributed SAPPs. For convenience, in this chapter we assume that there is no EV available in the system, while the power system with EV integration will be investigated later in Chapter 3. Specifically, we assume that the power system consists of $M \geq 1$ SAPPs, indexed by i, $i \in \mathcal{M} = \{1, \cdots, M\}$. We denote the power consumption of SAPP i by $A_i > 0$, which is assumed to be constant regardless of the system frequency and/or voltage deviation.

We assume that each SAPP can monitor the system frequency locally, e.g., by measuring the voltage signal at its connecting point to the grid and then extracting the dominant frequency of the measured signal via the Fast Fourier Transform (FFT) analysis or other signal processing techniques [73]. As discussed in Section 1.4, the system operator will notify all SAPPs via sending a command signal (e.g., bit '1') to activate their frequency controllers, as shown in Fig. 2.2, when the contingency occurs. However, the system operator will send a clear signal (e.g., bit '0') to SAPPs to deactivate their algorithms and resume their normal operation when the system

frequency gets back to its safe range for a sufficient amount of time by deploying cost-efficient secondary/tertiary reserve services, which will be discussed later in Chapter 4.

2.4.1 Frequency Threshold Based On-off Load Control Policy

Let $S_i(t) \in \{0, 1\}$ denote the state of SAPP i at time t, where 0 and 1 indicate the off and on states, respectively. Our proposed load control policy with a given pair of lower and upper frequency thresholds, denoted by $f_{\min} < f_0$ and $f_{\max} > f_0$, respectively, is then given by

$$S_i(t^+) = \begin{cases} 0, & \text{if } S_i(t) = 1 \text{ and } f(t) < f_{\min} \\ 1, & \text{if } S_i(t) = 0 \text{ and } f(t) > f_{\max} \\ S_i(t), & \text{otherwise.} \end{cases} \tag{2.6}$$

where $t^+ = t + \Delta t$, with $\Delta t \to 0^+$, denotes the time immediately after monitoring the system frequency at time t. In the above algorithm, changes in the power consumption of SAPP i can be tracked conveniently by a random process, defined as $X_i(t) = A_i(S_i(t) - S_i(t^+))$, which has three possible values in $\{\pm A_i, 0\}$.

For convenience, we assume that all SAPPs are initially in the on state at time $t = 0$, i.e., we set $S_i(0) = 1$, $\forall i \in \mathcal{M}$. In Section 2.5.2, we then investigate a more general case that the initial states of SAPPs and their power consumption are modeled as stochastic variables.

2.4.2 Randomized Inter-Response Time

As shown in Fig. 1.4, if all SAPPs continuously monitor the system frequency and respond according to the proposed on-off load control policy in (2.6), a frequency oscillation will occur. 1.4. To tackle this issue, we propose that each SAPP

i monitors and responds to the system frequency deviation only over a discrete set of time instances given by the sequence in $\{t_{1,i}, t_{2,i}, \cdots\}$, where $t_{l,i}$ denotes the lth monitoring/response time of SAPP i. Thus, the number of responses of SAPP i can be tracked by a continuous-time counting process $C_i(t)$, defined as $C_i(t) = \sum_{l=1}^{\infty} \mathbf{1}_{\{t \geq t_{l,i}\}}$, where $\mathbf{1}_{\{t \geq t_{l,i}\}}$ indicates whether the lth response of SAPP i has occurred before time t or not. To further desynchronize responses of SAPPs, we impose a constraint that each SAPP has to wait a random time between any two consecutive responses. Specifically, we define the lth inter-response time of SAPP i as $T_{l,i} = t_{l,i} - t_{l-1,i}$, where $t_{0,i} = 0$ by default. Accordingly, we design $T_{l,i},\ l = 1, 2, \cdots$, to be independent and identically distributed (i.i.d.) exponential random variables with the same mean $1/\lambda_i \geq 0$, where λ_i is called the response rate of SAPP i. Under the above setting, it follows that $C_i(t)$ is a Poisson process with the rate λ_i.

Let $A_a = \sum_{i=1}^{M} A_i$ denote the aggregate load that can be shed by all SAPPs when they switch their loads off upon the contingency (note that it is assumed that SAPPs are on initially). Due to the fact that $A_a \ll A_0$ holds in practice, we can safely assume that A_0 remains constant after responses of SAPPs. Accordingly, by taking responses of all SAPPs into account, we can modify the aggregate demand model given in (2.1) as $A_d(t) = A_0 + ((f(t) - f_0)/f_0)\, K_f A_0 - \sum_{i=1}^{M} \sum_{l=1}^{C_i(t)} X_i(t_{l,i}) \mathbf{1}_{\{t \geq t_{l,i}\}}$. By substituting this result in (2.2) and solving the obtained differential equation for $A_g(t) = A_0 + A_e \mathbf{1}_{\{t \geq 0\}}$, we can modify (2.5) to capture the impacts of SAPPs on the system frequency as follows

$$f(t) = f_0 + \frac{f_0}{K_f A_0} \left(A_e \left(1 - e^{-\alpha t}\right) + \sum_{i=1}^{M} \sum_{l=1}^{C_i(t)} X_i(t_{l,i}) \left(1 - e^{-\alpha (t - t_{l,i})^+}\right) \right),\ t \geq 0, \quad (2.7)$$

where $(z)^+ = \max\{z, 0\}$. From (2.7), it follows that when a particular SAPP i switches its load off at its lth monitoring event in $t = t_{l,i}$, the system frequency increases over $t \geq t_{l,i}$, since $X_i(t_{l,i}) = A_i$. The opposite is also true when SAPP

i switches its load on. Furthermore, since $t_{l,i}$'s are random variables, the grid frequency given in (2.7) is a random process in general, where its statistical characterizations such as the mean and variance over time will be investigated in the next section.

2.5 Analysis of System Frequency

In this section, we first present a numerical example to take some useful insight into the different impacts of the supply shortfall and SAPPs' responses on the system frequency. We next provide our theoretical results on deriving the statistical characteristics of the system frequency.

2.5.1 Impacts of Supply Deficit and Responses of SAPPs on System Frequency

First, we study the effect of supply deficit A_e on the system frequency $f(t)$ given in (2.7). For convenience, we define a power threshold

$$A_{e,\min} = \frac{K_f A_0}{f_0}(f_{\min} - f_0), \tag{2.8}$$

which denotes the minimum value of supply deficit under which the grid frequency will reach the given lower frequency threshold $f_{\min}$ at some time $t > 0$. Specifically, from (2.5), it follows that if $A_{e,\min} \leq A_e < 0$, then the system frequency will not drop below the lower frequency threshold $f_{\min}$. Thus, SAPPs do not change their states, i.e., we have $X_i(t) = 0$, $\forall i \in \mathcal{M}$, over time $t \geq 0$. Accordingly, $f(t)$ given in (2.7) can be simplified to (2.5). However, if $A_e < A_{e,\min}$, then the system frequency drops below $f_{\min}$ at a certain time $t = t_0$ (see Fig. 2.3), after which SAPPs respond by changing their states according to the on-off control policy given in(2.6). From

(2.5), we can derive

$$t_0 = -\frac{1}{\alpha} \ln \left(1 - \frac{A_{e,\min}}{A_e} \right). \tag{2.9}$$

Next, by assuming $A_e < A_{e,\min}$, we study the effect of the aggregate power response of SAPPs A_a on $f(t)$. For convenience, we define the following two power thresholds

$$A_{a,\min} = \frac{K_f A_0}{f_0}(f_{\min} - f_0) - A_e, \tag{2.10}$$

$$A_{a,\max} = \frac{K_f A_0}{f_0}(f_{\max} - f_0) - A_e, \tag{2.11}$$

where $A_{a,\min}$ denotes the minimum value of A_a that is required to recover the grid frequency to $f_{\min}$ in steady state after A_e amount of supply deficit, while $A_{a,\max}$ denotes the minimum amount of A_a required to recover the grid frequency to $f_{\max}$ in steady state. Given $A_e < A_{e,\min}$, we thus discuss the following three cases.

- Case 1: $A_a < A_{a,\min}$. In this case, from (2.7) it follows that $f(t)$ will not recover back to $f_{\min}$ even though all SAPPs respond after t_0.

- Case 2: $A_{a,\min} \leq A_a \leq A_{a,\max}$. In this case, it can be shown from (2.7) that $f(t)$ recovers back to $f_{\min}$ at a certain time $T_r > t_0$, termed *frequency recovery time*, which can be more explicitly defined as the smallest time $t > t_0$ solving the following equation:

  $$f(t) = f_{\min}, \tag{2.12}$$

  with $f(t)$ given in (2.7). However, $f(t)$ will not overshoot the upper frequency threshold $f_{\max}$, regardless of the SAPPs' response rate λ_i's.

- Case 3: $A_a > A_{a,\max}$. In this case, $f(t)$ may or may not overshoot $f_{\max}$ depending on λ_i's.

Note that Case 3 is most challenging to investigate since in this case the response rates of SAPPs will play a key role in adjusting the resulting trade-off between

minimizing the probability of frequency overshoot versus minimizing the frequency recovery time.

As an illustrative example, we consider the IEEE 9-Bus test system [56] with the given parameters in Table 2.1 (see Section 2.6) under a contingency when the system experiences a generation power loss that results in $A_0 = -20$MW. We assume that all SAPPs in the system have the identical power consumption $A_i = 3$kW and response rate $\lambda_i = \lambda$, for $i = 1, \ldots, M$. Furthermore, we set the lower and upper frequency thresholds of the control algorithm as $f_{\min} = 59.8$Hz and $f_{\max} = 60.2$Hz, respectively, which result in $A_{a,\min} = 17.5$MW and $A_{a,\max} = 22.5$MW.

Fig. 2.3 shows the above three cases in the IEEE 9-Bus test system, when the number of appliances is set as $M = 5000$, $M = 7000$, and $M = 10000$ in Cases 1, 2, and 3, respectively. Therefore, the aggregated power response of all appliances, i.e., A_a, is obtained as 15MW, 21MW, and 30MW in Cases 1, 2, and 3, respectively. The trade-off between the frequency recovery time minimization and the frequency overshoot avoidance is clearly depicted in Fig. 2.3 (c) for different values of λ. As observed, a higher value of response rate $\lambda = 0.2$Hz results in a shorter frequency recovery time as compared to $\lambda = 0.05$Hz, but at the cost of a system frequency overshoot upon $f_{\max}$. A more detailed analysis on the average frequency recovery time and the probability of frequency overshoot will be given later in Sections 2.5.3 and 2.5.5, respectively. At last, since Case 1 is not of our interest, in the rest of this paper, we will focus only on Cases 2 and 3, i.e., $A_a \geq A_{a,\min}$.

2.5.2 Mean and Variance of System Frequency

With the randomized frequency control algorithm proposed in the previous section, the system frequency $f(t)$ given in (2.7) is a random process in general. Specifically, we are interested to study the behavior of this random process over time $t_0 \leq t \leq T_r$, under which the system frequency is below the threshold $f_{\min}$ and

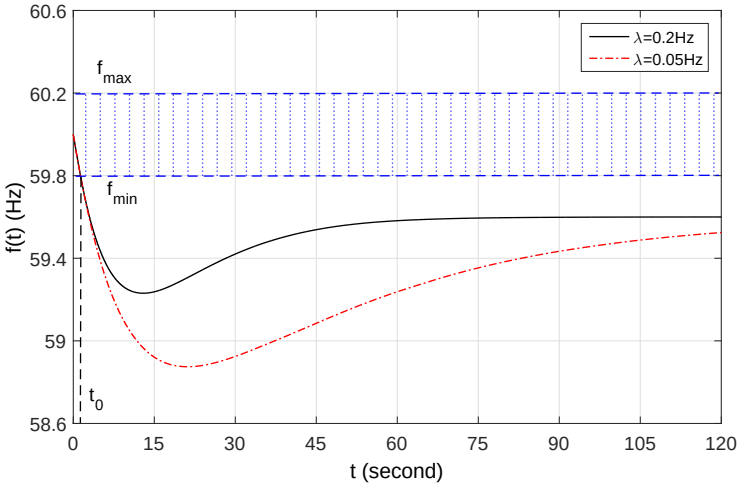

(a) Case 1

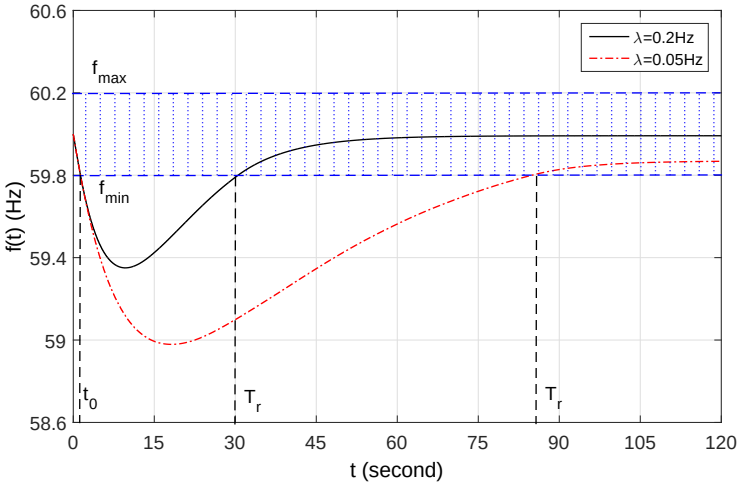

(b) Case 2

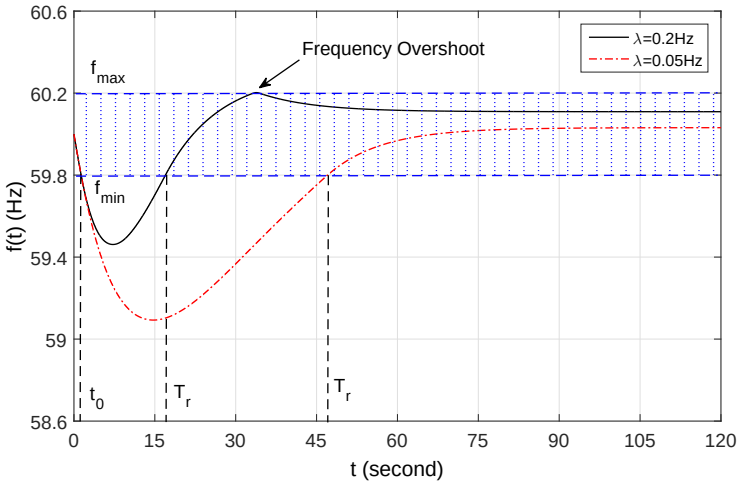

(c) Case 3

Figure 2.3: Simulated system frequency of IEEE 9-Bus test system for the case $A_e < A_{e,\min}$.

thus SAPPs respond by switching their loads off to recover the system frequency. To investigate the statistical characteristics of $f(t)$, we first derive closed-form expressions for its mean and variance over time in the following two propositions, respectively, given the assumption $S_i(0) = 1,\ i = 1, \ldots, M$. Next, we extend the obtained results to a more general case that the initial states of SAPPs and their power consumption are modeled as stochastic variables, but with known distributions.

Proposition 2.5.1. Given $A_e < A_{e,\min}$ and $A_a \geq A_{a,\min}$, the mean value of the system frequency over time $t_0 \leq t \leq T_r$ is given by

$$\mathbb{E}[f(t)] = f_0 + \frac{f_0}{K_f A_0} \left(A_e \left(1 - e^{-\alpha t}\right) + \sum_{i=1}^{M} h_\alpha(A_i, \lambda_i, t - t_0) \right), \tag{2.13}$$

where $h_\alpha(A, \lambda, s) = A(1 - u_\alpha(\lambda, s))$ and $u_\alpha(\lambda, s)$ is defined as

$$u_\alpha(\lambda, s) = \begin{cases} \dfrac{\lambda e^{-\alpha s} - \alpha e^{-\lambda s}}{\lambda - \alpha}, & \text{if } \lambda \neq \alpha \text{ and } s > 0 \\ (\lambda s + 1) e^{-\lambda s}, & \text{if } \lambda = \alpha \text{ and } s > 0 \\ 1, & \text{if } s = 0. \end{cases} \tag{2.14}$$

Proof. Please see Appendix A. □

The mean frequency given in (2.13) is due to both the deterministic frequency dynamics without DR and that contributed by randomized responses of SAPPs, where $h_\alpha(A_i, \lambda_i, t - t_0) f_0/(K_f A_0)$ represents the contribution of SAPP i on the mean system frequency over time. The contribution of SAPP i to the mean of the system frequency takes effect only for $t > t_0$, with t_0 given in (2.9). This is due to the fact that over $t \leq t_0$, although SAPP i monitors the system frequency, it does not respond by switching its load off since $f(t) \geq f_{\min}$. From $h_\alpha(A_i, \lambda_i, t - t_0)$, it also follows that the mean contribution of SAPP i to restore the system frequency is linearly proportional to its power consumption A_i, but takes effect over time

according to $1 - u_\alpha(\lambda_i, s)$, which is exponentially fast.

Fig. 2.4 plots $h_\alpha(A_i, \lambda_i, s)$ for both the Ireland power system ($\alpha = 0.15$Hz) and the IEEE 9-Bus test system ($\alpha = 0.1$Hz), by setting $A_i = 1$W. It is observed that given the same λ_i, the impact of SAPP i on the system frequency recovery is faster in the Ireland power system as compared to the IEEE 9-Bus test system. This phenomenon is due to the fact that the mechanical inertia of the Ireland power system is smaller than IEEE 9-Bus test system; thus, its frequency response is faster (cf. (2.5)). Furthermore, it is observed that under a fixed α, the impact of SAPP i on the system mean frequency is more pronounced with higher values of response rate λ_i. Last, it is observed that $h_\alpha(A_i, \lambda_i, s)$ is upper-bounded by $A_i(1 - e^{-\alpha s})$ when $\lambda_i \to \infty$, which corresponds to the case that SAPP i continuously monitors the system frequency and thus its resulting frequency contribution is deterministic over time. This can be easily verified from (2.14).

Proposition 2.5.2. Given $A_e < A_{e,\min}$ and $A_a \geq A_{a,\min}$, the variance of the system frequency over time $t_0 \leq t \leq T_r$ is given by

$$\mathbb{V}\mathrm{ar}[f(t)] = \sum_{i=1}^{M} \left(\frac{f_0}{K_f A_0}\right)^2 q_\alpha(A_i, \lambda_i, t - t_0), \tag{2.15}$$

where $q_\alpha(A, \lambda, s) = A^2(u_{2\alpha}(\lambda, s) - (u_\alpha(\lambda, s))^2)$.

Proof. Please see Appendix B. □

Proposition 2.5.2 shows that the variance of the system frequency is the sum of SAPPs' individual variance contributions over time.

Fig. 2.5 plots $q_\alpha(A_i, \lambda_i, s)$ for both the Ireland power system ($\alpha = 0.15$Hz) and the IEEE 9-Bus test system ($\alpha = 0.1$Hz), by setting $A_i = 1$W. It is observed that for a fixed value of λ_i, the impact of SAPP i on the system frequency variance is more pronounced in the Ireland power system as compared to the IEEE 9-Bus test system. This is mainly because given fixed λ_i, $u_\alpha(\lambda_i, s)$ changes faster with a

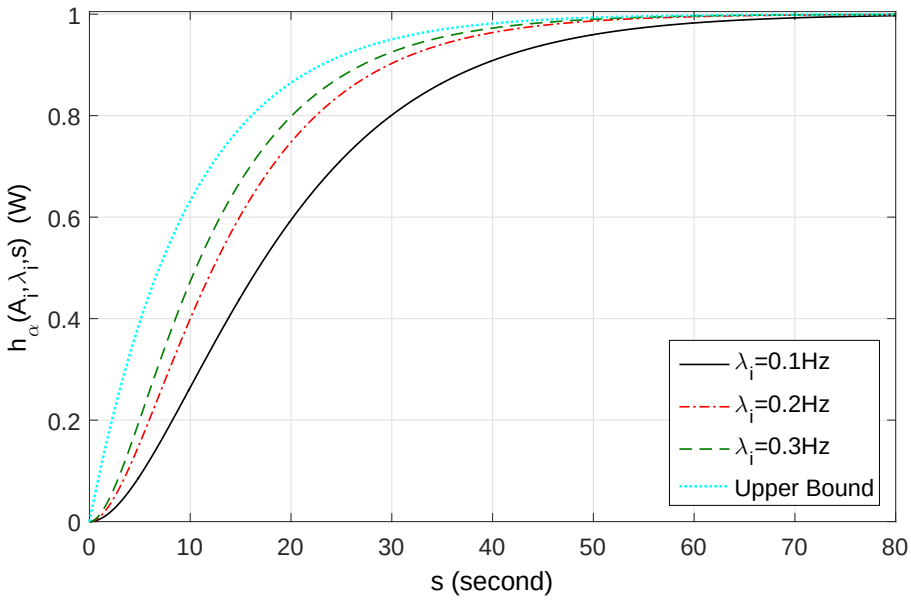

(a) IEEE 9-Bus test system with $\alpha = 0.1$Hz.

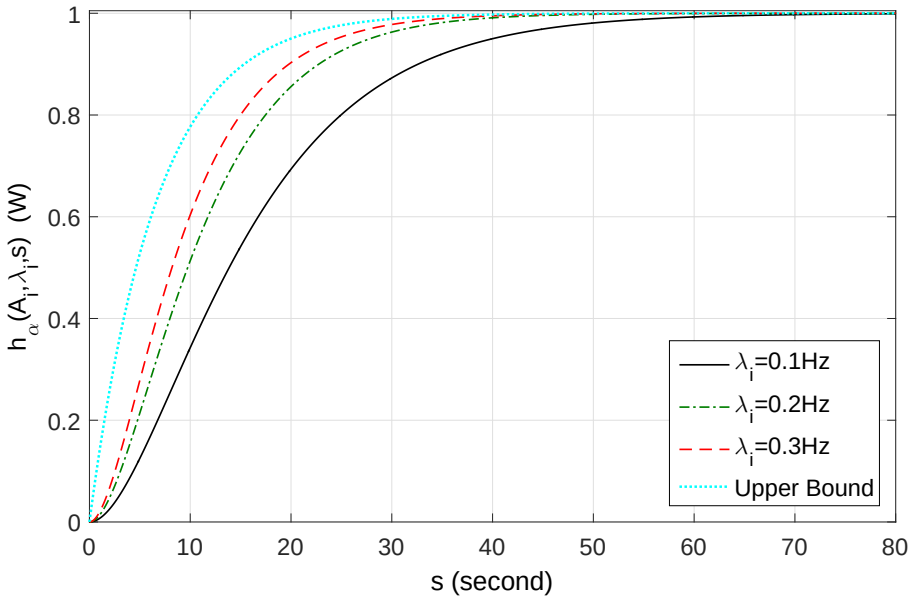

(b) Ireland power system with $\alpha = 0.15$Hz.

Figure 2.4: Frequency mean characterization function of SAPP i, $h_\alpha(A_i, \lambda_i, s)$.

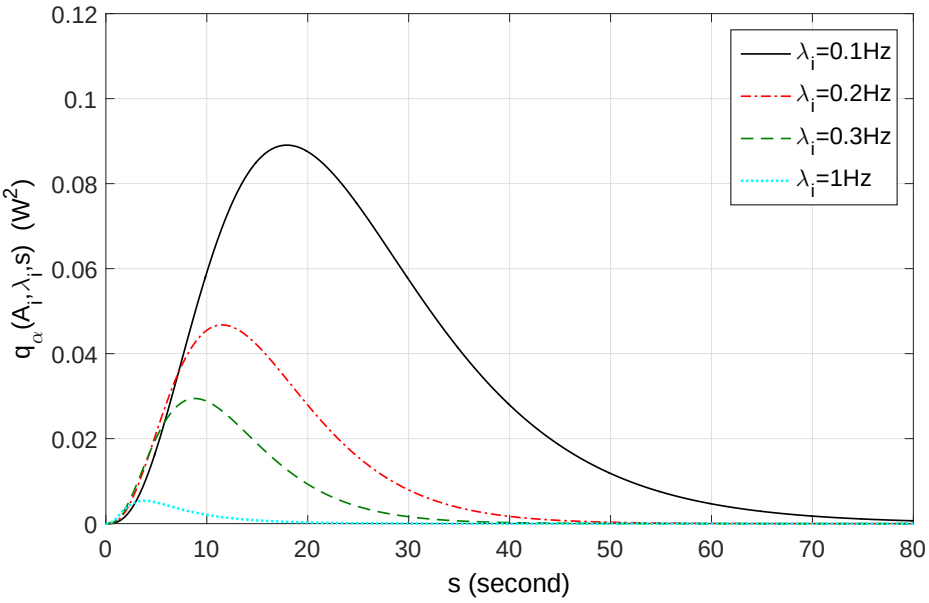

(a) IEEE 9-Bus test system with $\alpha = 0.1$Hz.

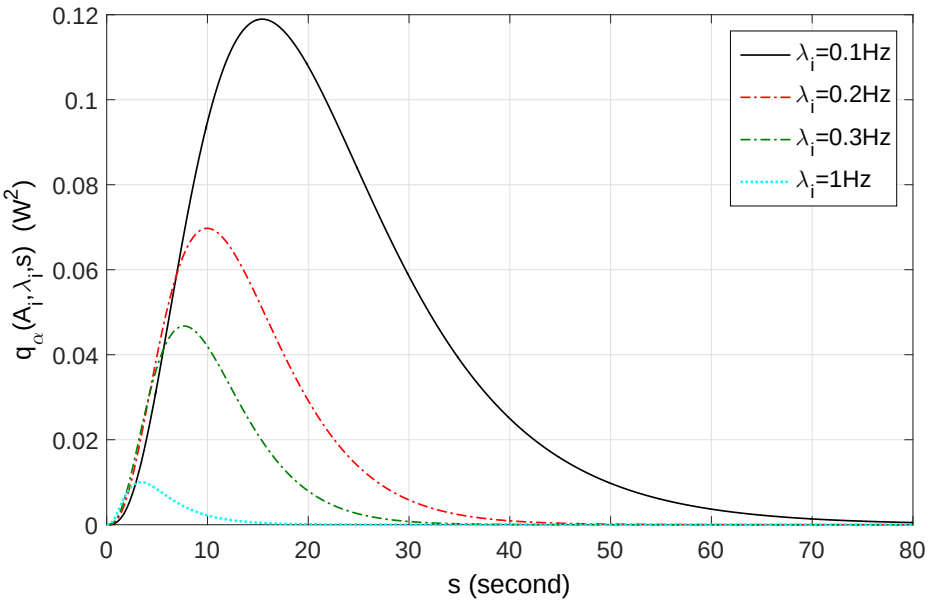

(b) Ireland power system with $\alpha = 0.15$Hz.

Figure 2.5: Frequency variance characterization function of SAPP i, $q_\alpha(A_i, \lambda_i, s)$.

lager value of α. We also observe that the variance contribution of SAPP i follows a single-peak pattern. To explain this observation, we consider a special case that $\alpha \gg \lambda_i$. Under this assumption, we can simplify the normalized frequency variance characterization function to be $q_\alpha(A_i, \lambda_i, s) = A_i^2(e^{-\lambda_i s} - e^{-2\lambda_i s})$, which has the global maximum at $s^* = (\ln 2)/\lambda_i$. Therefore, when the system time $s < s^*$, the resulting variance contribution of SAPP i to the system frequency grows with time since the probability of monitoring the system frequency by this particular SAPP increases with s. However, when the system time $s \geq s^*$, the variance contribution decreases since it becomes more likely that SAPP i has already responded by time s. In addition, it is observed that a larger response rate will result in an earlier peak in the variance contribution, which is in accordance to s^* in this case. It is also worth noting that the variance contribution of SAPP i will asymptotically vanish to zero as $\lambda_i \to \infty$. This is due to the fact that SAPP i monitors the system frequency continuously over time when $\lambda_i \to \infty$; as a result, its resulting response becomes deterministic.

Finally, we extend our results given in Propositions 2.5.1 and 2.5.2 to the case that $S_i(0)$ and A_i of each SAPP $i \in \mathcal{M}$ are modeled as stochastic variables with known distributions, as discussed in the following. In particular, we model $S_i(0)$ as a binary random variable with $\Pr\{S_i(0) = 1\} = \zeta_i$, $0 \leq \zeta_i \leq 1$, and $\Pr\{S_i(0) = 0\} = 1 - \zeta_i$. Given $S_i(0) = 1$, we model A_i as a random variable of arbitrary given distribution (either continuous or discrete) with the mean $\overline{A}_i > 0$, i.e., $\mathbb{E}[A_i \mid S_i(0) = 1] = \overline{A}_i$, and the variance $\sigma_i \geq 0$, i.e., $\mathbb{V}\text{ar}[A_i \mid S_i(0) = 1] = \sigma_i$. Otherwise, given $S_i(0) = 0$, we thus have $A_i = 0$. We assume that $S_i(0)$ and $\boldsymbol{t}_i$ as well as A_i and $\boldsymbol{t}_i$ are independent random variables. This assumption is valid, since the monitoring events of SAPP i are independent of its operational state and power consumption rate in practice. Accordingly, we extend the mean and variance functions of the system frequency given in Propositions 2.5.1 and 2.5.2 in the two following corollaries, respectively.

Corollary 2.5.1. Under the proposed stochastic models of $S_i(0)$'s and A_i's, the mean value of the system frequency over time $t_0 \leq t \leq T_r$ is given by

$$\mathbb{E}[f(t)] = f_0 + \frac{f_0}{K_f A_0}\left(A_e\left(1 - e^{-\alpha t}\right) + \sum_{i=1}^{M} \zeta_i h_\alpha(\overline{A}_i, \lambda_i, t - t_0)\right). \tag{2.16}$$

Corollary 2.5.2. Under the proposed stochastic models of $S_i(0)$'s and A_i's, the variance of the system frequency over time $t_0 \leq t \leq T_r$ is given by

$$\mathbb{V}\text{ar}[f(t)] = \sum_{i=1}^{M}\left(\frac{f_0}{K_f P_0}\right)^2 \dot{q}_\alpha(\zeta_i, \overline{A}_i, \sigma_i, \lambda_i, t - t_0), \tag{2.17}$$

where $\dot{q}_\alpha(\zeta, \overline{A}, \sigma, \lambda, s)$ is defined as

$$\begin{aligned}\dot{q}_\alpha(\zeta, \overline{A}, \sigma, \lambda, s) = \zeta(\sigma + \overline{A}^2)\left(1 + u_{2\alpha}(\lambda, s) - 2u_\alpha(\lambda, s)\right) \\ - \zeta^2\overline{A}^2\left(1 + \left(u_\alpha(\lambda, s)\right)^2 - 2u_\alpha(\lambda, s)\right).\end{aligned} \tag{2.18}$$

The results given in corollaries 2.5.1 and 2.5.2 can be simplified to the results given in Propositions 2.5.1 and 2.5.2, respectively, by simply setting $\zeta_i = 1$, $\overline{A}_i = A_i$, and $\sigma_i = 0$, $\forall i \in \mathcal{M}$.

Based on the above analysis, in the following sections we investigate how different values of SAPPs' response rates λ_i's can affect the frequency recovery time as well as the expected number of SAPPs switching their loads off to regulate the system frequency. These results will help design optimal λ_i's to meet a given requirement on the frequency recovery time, and yet minimize the number of responded SAPPs for load shedding or equivalently the amount of service interruptions.

2.5.3 Average Frequency Recovery Time

Denote the average frequency recovery time by $\overline{T}_r = \mathbb{E}[T_r]$. Since in general it is difficult to obtain the distribution of T_r from (2.12), we approximate $\overline{T}_r$ by using the

mean of the system frequency $\mathbb{E}[f(t)]$ obtained in Proposition 2.5.1. This is justified due to the fact that in a practical power system, although there are many SAPPs, their individual power consumption are much smaller than the system aggregate demand ($A_i/A_0 \to 0$, $i = 1, \ldots, M$); therefore, the variance of the system frequency given in (2.17) is usually very small and thus can be safely ignored in our analysis. This assumption will be validated later via simulations in Section 2.6.1 (see Fig. 2.7). Given $S_i(0) = 1,\ \forall i \in \mathcal{M}$, we have the following proposition.

Proposition 2.5.3. Given $A_e < A_{e,\min}$ and $A_a \geq A_{a,\min}$, the average frequency recovery time $\overline{T}_r$ is approximated by the smallest $t > t_0$ which is the solution of the frequency equation $\mathbb{E}[f(t)] = f_{\min}$, where $\mathbb{E}[f(t)]$ is given in (2.13).

Note that the result given in Proposition 2.5.3 can be easily extended to the case that $S_i(0)$'s and A_i's are modeled as random variables by using $\mathbb{E}[f(t)]$ given in (2.16) in replacement of that given in (2.13).

2.5.4 Expected Number of Responded SAPPs

Without loss of generality, we assume that the power system consists of $J \geq 1$ different classes of SAPPs, indexed by j, $j \in \mathcal{J} = \{1, \ldots, J\}$. We denote $M_j \geq 1$, $\tilde{A}_j > 0$, and $\tilde{\lambda}_j \geq 0$ as the number of SAPPs, power consumption, and response rate of each individual SAPP from Class j, respectively. To be consistent with our previous notations, we also set $\sum_{j=1}^{J} M_j = M$. For convenience, we again assume that all SAPPs are initially in the on state at time $t = 0$, i.e., we have $S_i(0) = 1$, $i = 1, \ldots, M_j$, $\forall j \in \mathcal{J}$.

Let $N_j(t)$ be a random process that counts the number of responded SAPPs from Class j which have responded by switching their loads off by time t, $t_0 \leq t \leq T_r$. Accordingly, we state our result in the following proposition.

Proposition 2.5.4. Given $A_e < A_{e,\min}$ and $A_a \geq A_{a,\min}$, the average number of responded SAPPs from Class $j \in \mathcal{J}$ which have switched their loads off by time t,

$t_0 \leq t \leq T_r$, is given by

$$\mathbb{E}[N_j(t)] = M_j \left(1 - e^{-\tilde{\lambda}_j(t-t_0)}\right). \tag{2.19}$$

Proof. Please see Appendix C. □

From Proposition 2.5.4, it immediately follows that the average demand that has been shed by all SAPPs from Class j by time t, $t_0 \leq t \leq T_r$, is given by $M_j\tilde{A}_j(1 - e^{-\tilde{\lambda}_j(t-t_0)})$.

2.5.5 Probability of Frequency Overshoot

Now, we derive the probability that the system frequency overshoots the upper threshold $f_{\max}$ due to over-response of SAPPs. Particularly, we assume $A_a > A_{a,\max}$ holds in this section; otherwise, a frequency overshoot will not occur (see Cases 2 and 3 in Section 2.5.1).

Since it is assumed $S_i(0) = 1$, $i = 1, \ldots, M_j$, $\forall j \in \mathcal{J}$, the total demand that has been shed by SAPPs from all classes by time t, $t_0 \leq t \leq T_r$, is obtained as $\sum_{j=1}^{J} \tilde{A}_j N_j(t)$. Let $n_j = N_j(T_r)$, $j = 1, \ldots, J$, i.e., n_j is one realization for the random variable $N_j(T_r)$. The set of all possible values of $\boldsymbol{n} = [n_1, \ldots, n_J]^T$ that will cause the system frequency overshoots $f_{\max}$ is then given in the set $\mathcal{O}$, which is defined as

$$\mathcal{O} = \{\boldsymbol{n} \mid 0 \leq n_j \leq M_j,\ j = 1, \ldots, J,\ \sum_{j=1}^{J} \tilde{A}_j n_j > A_{a,\max}\}. \tag{2.20}$$

The probability that each SAPP from Class j has responded by switching its load off by time t, $t_0 \leq t \leq T_r$, can be expressed as $1 - e^{-\tilde{\lambda}_j(t-t_0)}$. Since SAPPs respond independently, the conditional probability that $0 \leq n_j \leq M_j$ out of M_j SAPPs from Class j have responded by switching their loads off by a given frequency

recovery time $T_r = s$, with $s > t_0$, is derived as

$$\mathbb{P}\mathrm{r}\{N_j(T_r) = n_j \mid T_r = s\} = \binom{M_j}{n_j} \left(1 - e^{-\tilde{\lambda}_j(s-t_0)}\right)^{n_j} \left(e^{-\tilde{\lambda}_j(s-t_0)}\right)^{M_j - n_j}. \quad (2.21)$$

The following proposition thus follows.

Proposition 2.5.5. Given $A_e < A_{e,\min}$ and $A_a > A_{a,\max}$, the probability that the system frequency overshoots $f_{\max}$ is approximated as

$$P_{os} \approx \sum_{\boldsymbol{n} \in \mathcal{O}} \prod_{j=1}^{J} \binom{M_j}{n_j} \left(1 - e^{-\tilde{\lambda}_j(\overline{T}_r - t_0)}\right)^{n_j} \left(e^{-\tilde{\lambda}_j(\overline{T}_r - t_0)}\right)^{M_k - n_j}, \quad (2.22)$$

where $\overline{T}_r$ is given in Proposition 2.5.3.

Proof. Please see Appendix D. □

2.6 Simulation Results

In this section, we provide simulation results to validate our proposed analysis in this chapter. For the purpose of exposition, we consider two power systems: one is the IEEE 9-Bus test system [56], and the other is the aggregate model of Ireland power system [25,26], for which simulation results are presented in the following two sections, respectively.

2.6.1 IEEE 9-Bus Test System

We consider the IEEE 9-Bus test system consisting of 3 generators and 9 buses with the initial steady state as shown in Fig. 2.6, which has been used widely in the literature for the power system stability study. The aggregate model of this power system can be characterized by the corresponding parameters given in Table 2.1. It is assumed that SAPPs are equally distributed among load Buses 5, 6, and

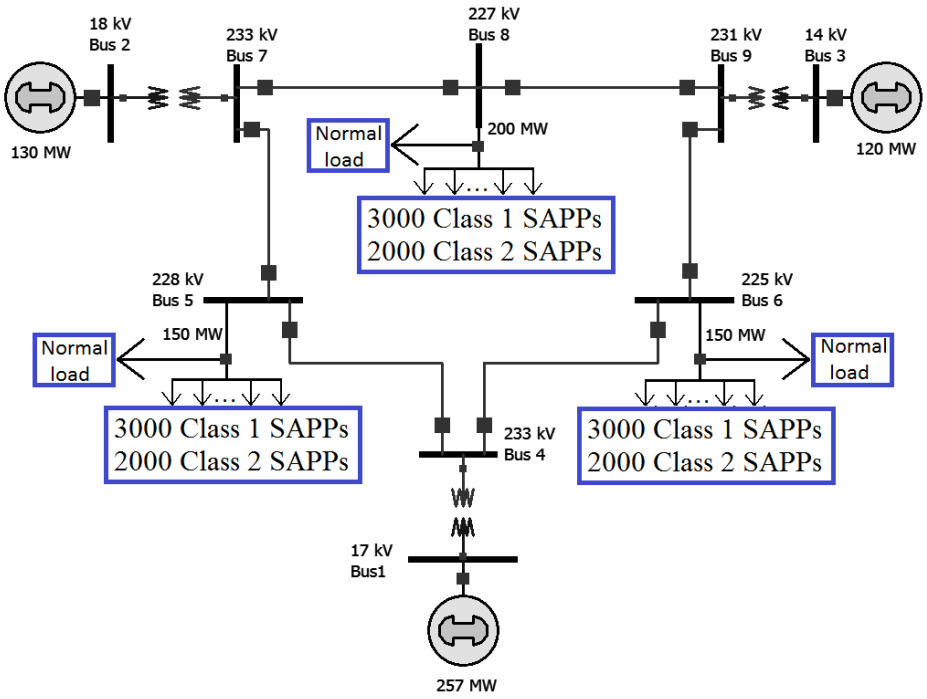

Figure 2.6: Schematic of IEEE 9-Bus test system.

Table 2.1: Parameters of IEEE 9-Bus test system and Ireland power system.

System	Parameters			
	A_0(MW)	f_0(Hz)	K_f	α(Hz)
IEEE 9-Bus	500	60	1.5	0.1
Ireland	6065	50	2.5	0.15

8 (see Fig. 2.6). We further assume that there are two classes of SAPPs, which in total correspond to 5% of the aggregate demand. The Class 1 SAPPs consist of a set of $M_1 = 9000$ electrical water heaters, while Class 2 SAPPs consist of a set of $M_2 = 6000$ electric ovens. It is assumed that SAPPs operate separately and thus they respond to the system frequency deviation independently. The more detailed parameters of SAPPs from each class are provided in Table 2.2. We consider that a contingency occurs at $t = 0$ when the system experiences a generation power loss due to the partial failure of the connected generator to Bus 3 (see Fig. 2.6), which results in $A_e = -20$MW. From (2.5) it thus follows that this amount of generation loss will

Table 2.2: Parameters of SAPPs.

System	Parameters			
	$\tilde{A}_1$(kW)	$\tilde{A}_2$(kW)	$f_{\min}$(Hz)	$f_{\max}$(Hz)
IEEE 9-Bus	3.0	0.5	59.80	60.20
Ireland	3.0	0.5	49.95	50.05

reduce the steady state frequency by 1.6Hz if DR and generation side frequency controllers are all deactivated.

First, we plot the frequency dynamics of the IEEE 9-Bus test system in Fig. 2.7, where simulated results obtained using the PowerWorld simulator [74] are compared with our analytical results assuming the aggregate power system model. We set the response rates of SAPPs for the two classes as $(\tilde{\lambda}_1, \tilde{\lambda}_2) = (0.06, 0.06)$Hz or $(\tilde{\lambda}_1, \tilde{\lambda}_2) = (0.12, 1.2)$Hz, which means that under the first (second) setting, each SAPP in classes 1 and 2 on average monitors the system frequency every 16.66 and 8.33 seconds, respectively. With 100 randomly generated simulations under the above setting, we plot the simulated mean frequency function over time as well as the upper and lower extreme values of the frequency for each set of response rates in Fig. 2.7. It is observed that for the small response rates, $(\tilde{\lambda}_1, \tilde{\lambda}_2) = (0.06, 0.06)$Hz, the system frequency is recovered within 24.5 seconds without any overshoot while the maximum system frequency undershoot on average is 0.64Hz, which is practically acceptable. On the other hand, for the large response rates, $(\tilde{\lambda}_1, \tilde{\lambda}_2) = (0.12, 1.2)$Hz, the system frequency is recovered within 14 seconds with a single overshoot around 29.5 seconds, while the maximum system frequency undershoot on average is 0.38Hz. Although increasing the response rates of SAPPs can simultaneously reduce both the maximum system frequency undershoot and the frequency recovery time, it may result in a frequency overshoot as shown in Fig. 2.7. Consequently, there is a natural trade-off between minimizing the maximum value of the system frequency undershoot/recovery time versus minimizing the probability of frequency overshoot.

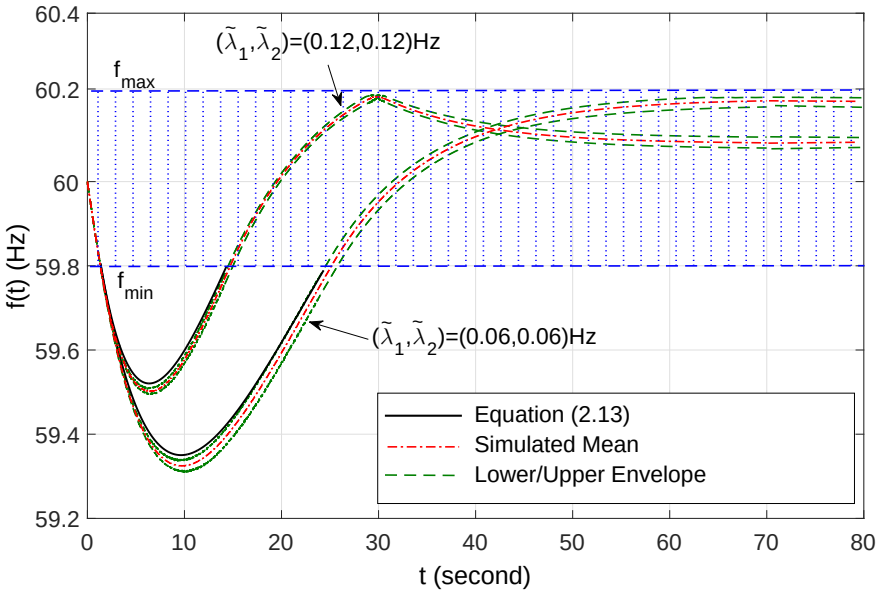

Figure 2.7: Frequency dynamics of IEEE 9-Bus test system.

Furthermore, it is observed that the frequency variance is very small, which is in accordance with the result in Proposition 2.5.1. Lastly, it is observed that the analytical mean frequency given by (2.13) in Proposition 2.5.1 tightly fits the simulated mean frequency over time, while a small discrepancy is due to our assumed aggregate power system model, which has ignored the topology and nonlinear frequency response characteristics of the actual power system.

Next, we investigate the average system frequency recovery time T_r and the expected number of responded SAPPs which have switched their loads off (turn to the off state) by the frequency recovery time T_r, under different values of $\tilde{\lambda}_1$ with fixed $\tilde{\lambda}_2 = 0.1$Hz. Figs. 2.8 and 2.9 compare the average frequency recovery time and the expected number of responded SAPPs based on simulations versus Propositions 2.5.3 and 2.5.4, respectively. As observed, the simulation results closely match our analytical results. In particular, the variance of the frequency recovery time is observed to be sufficiently small for it to be properly approximated by its mean value as assumed in Proposition 2.5.5. Furthermore, we observe that when the response

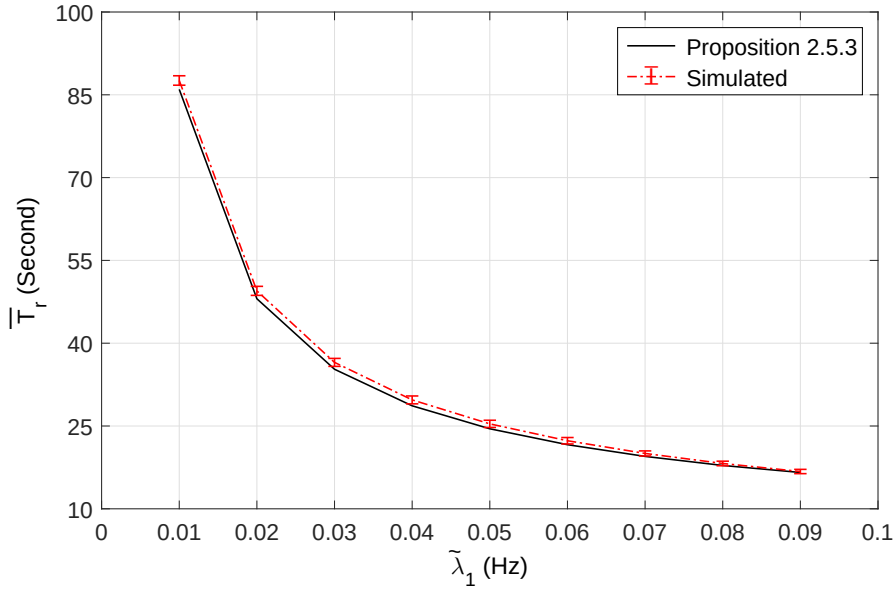

Figure 2.8: Average frequency recovery time of the IEEE 9-Bus test system.

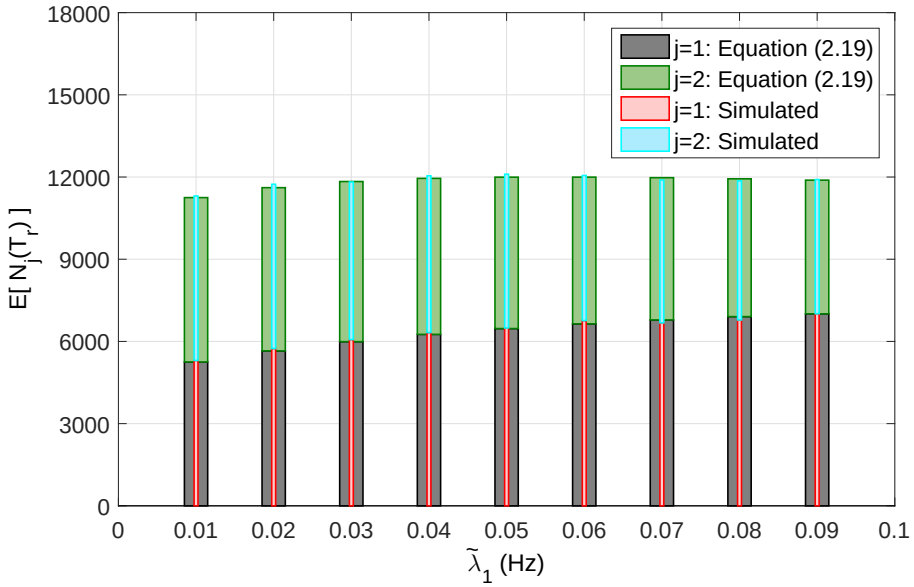

Figure 2.9: Expected number of responded SAPPs in IEEE 9-Bus test system by the frequency recovery time.

rate $\tilde{\lambda}_1$ increases, the system recovery time decreases, since SAPPs from class 1 tend to respond faster on average.

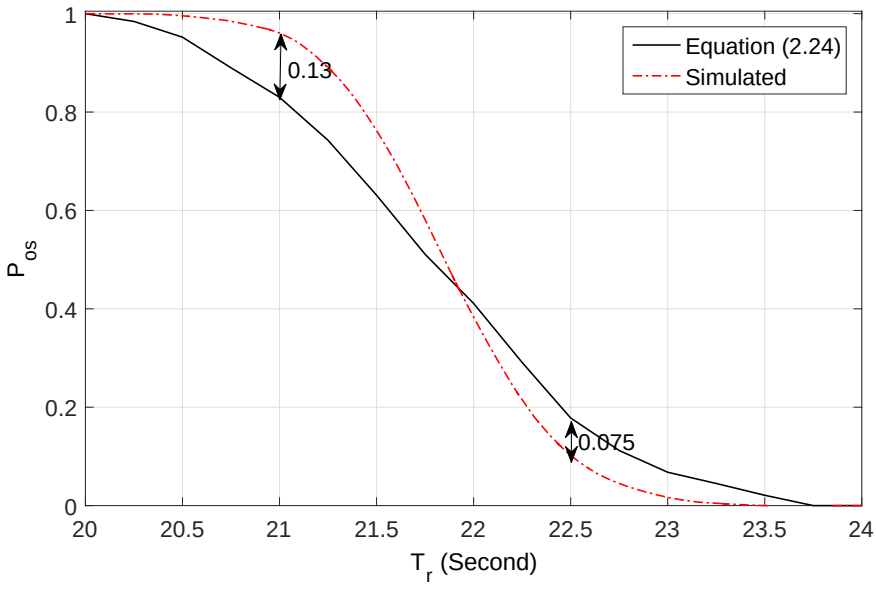

Figure 2.10: Probability of frequency overshoot versus average frequency recovery time.

Last, we investigate the trade-off between minimizing the average frequency recovery time versus the probability of frequency overshoot by setting different values of $\tilde{\lambda}_1$, but fixed $\tilde{\lambda}_2 = 0.1$Hz. As shown in Fig. 2.10, the simulated frequency overshoot probability and its approximation given in Proposition 2.5.5 follow the same decreasing trend as the average frequency recovery time increases, while they have some discrepancy. This is due to the fact that we use the average frequency recovery time $\overline{T}_r$ instead of its true distribution in evaluating P_{os} given in Proposition 2.5.5. With the approximated trade-off shown in Fig. 2.10, system operators can set response rates of SAPPs to achieve a balanced performance between the frequency recovery time and the probability of frequency overshoot.

2.6.2 Ireland Power System

In this section, we apply the aggregate model to the Ireland power system [25] and evaluate the performance of our proposed distributed frequency control algo-

rithm upon a contingency. The power system of the island of Ireland consists of both Northern Ireland Electricity (NIE) system and the Electricity Supply Board (ESB) system of the Republic of Ireland, which are tightly interconnected via multiple tie-lines and operated under a same electricity market, known as Single Electricity Market (SEM) [25]. The detailed information about the topology of transmission lines and power plants including both the fossil-fuel and renewable energy based generation units in the island of Ireland is given in [26]. The Ireland power system during the winter peak demand is characterized by the corresponding parameters given in Table 2.1, which are obtained based on the heuristic data provided in [25]. In this example, we assume that approximately 2% of the aggregated demand in the Ireland power system corresponds to the demand side controllable loads, i.e., the two classes of SAPPs as similarly assumed previously for the case of IEEE 9-Bus test system. We set $M_1 = 35000$ and $M_2 = 25000$. Table 2.2 provides more details of the assumed SAPPs in this system. We further assume that generation side frequency controllers are deactivated and the system frequency can solely be restored via SAPPs' responses.

First, we compare the performance of our demand frequency control with exponentially distributed inter-response time versus uniformly distributed inter-response time which has been used as response delay time in [43]. We consider a scenario that the Ireland power system experiences a generation power shortfall resulting in $A_e = -50$MW at $t = 0$. For the case of exponential distribution, we set SAPPs' response rates for the two classes as $(\tilde{\lambda}_1, \tilde{\lambda}_2) = (0.1, 0.2)$Hz. However, for the case of uniform distribution, we set the inter-response time of Classes 1 and 2 to be uniformly distributed as $\mathcal{U}(0, 20)$ and $\mathcal{U}(0, 10)$ in seconds, respectively. This setting results in the mean inter-response time of 10 seconds and 5 seconds for Classes 1 and 2, respectively, which is exactly same as the case of exponential inter-response time distribution. Fig. 2.11 shows the obtained experimental frequency mean for the two distribution cases, from which it is observed that the frequency recovery

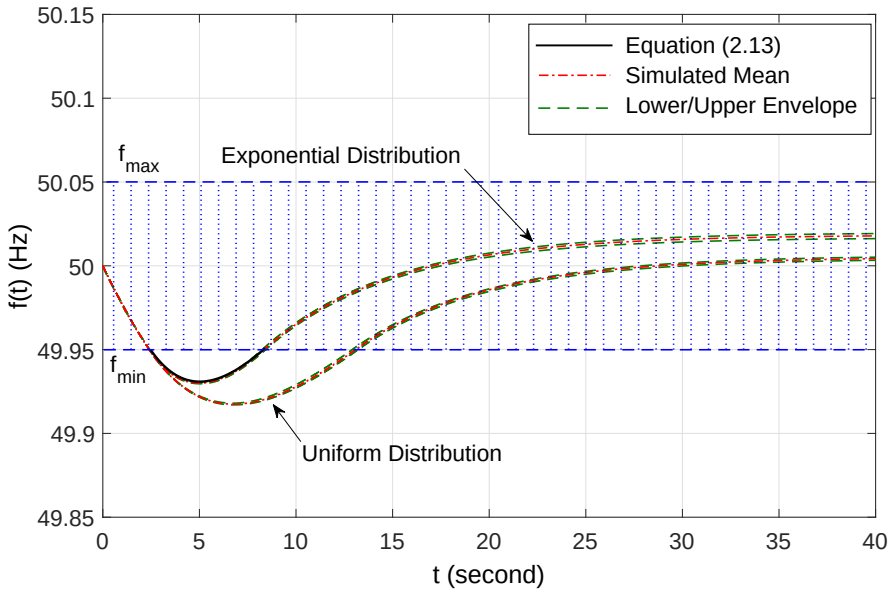

Figure 2.11: Comparison between exponentially and uniformly distributed inter-response time.

time is shorter in the case of exponential distributions. Note that the main advantage of considering the exponential distribution for inter-response time is to exploit its memoryless property, which helps us characterize the mean and variance of the system frequency over time in closed-form.

Next, we investigate the performance of our proposed demand frequency control under a scenario that the power imbalance follows $A_e = 58\cos(0.8\pi t) - 65\ \mathbf{1}_{\{t>0\}} + 115\ \mathbf{1}_{\{t>65\}} - 100\ \mathbf{1}_{\{t>115\}} + 80\ \mathbf{1}_{\{t>180\}}$ in MW, due to both the intermittent generation power of a large wind farm such as Gruig plant in Antrim, Ireland, as well as the aggregated demand power consumption variations over time. Note that the sinusoidal term in A_e models the rapid power imbalance changes over time due to e.g. fluctuations in the generation power of a wind farm due to variations in the wind velocity and/or the wind blowing direction. Furthermore, we assume that 50%(50%) of SAPPs from each of 2 classes are initially in the off(on) state at time $t = 0$. We set SAPPs' response rates as $(\tilde{\lambda}_1, \tilde{\lambda}_2) = (0.6, 0.6)$Hz, $(\tilde{\lambda}_1, \tilde{\lambda}_2) = (0.1, 0.1)$Hz. We simulate the system frequency for each of the two settings 100

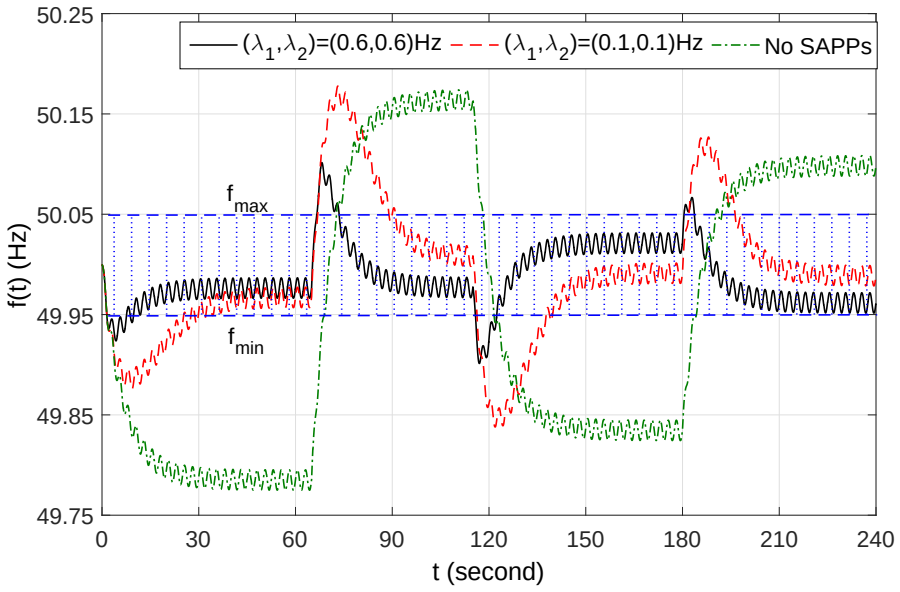

Figure 2.12: Frequency dynamics of Ireland power system.

times independently and plot the experimental mean frequency curves in Fig. 2.12. We also plot the system frequency dynamics for the case that the demand frequency control is totally deactivated. It is observed that for both settings, the system frequency by distributed frequency control is recovered back to the safe regime 49.95Hz to 50.05Hz following each of the power imbalances. However, the sinusoidal parts of the presumed A_e results in an undamped frequency oscillation with an amplitude ± 0.0057Hz over the mean system frequency, which is too small to further trigger the on/off frequency controller of SAPPs. By comparing the two curves, it is also revealed that in this particular example higher values of response rates $(\tilde{\lambda}_1, \tilde{\lambda}_2) = (0.6, 0.6)$Hz help reduce the frequency overshoot/undershoot peaks as compared to the case of smaller values of response rates $(\tilde{\lambda}_1, \tilde{\lambda}_2) = (0.1, 0.1)$Hz.

2.7 Chapter Summary

In this chapter, we investigated a new distributed frequency control algorithm to help stabilize the system frequency during a contingency of supply shortfall via

randomized on-off switching of distributed SAPPs. We derived the closed-form mean and variance of the system frequency over time as functions of the SAPPs' response rates and the given characteristics of power system. The average frequency recovery time and the average number of responded SAPPs over time were also derived in closed form. Accordingly, we revealed an interesting trade-off between minimizing the frequency recovery time and the probability of frequency overshoot for the proposed algorithm in setting different values of response rates for SAPPs. The analytical results were validated by extensive simulations based on the IEEE 9-Bus test system and the Ireland power system. It was shown by simulations that the deployment of 30MW SAPPs in the IEEE 9-Bus test system, each with the response rate of 10 to 20 seconds, can recover back the system frequency to a given safe range after a supply deficit of 20MW in less than 30 seconds while the maximum frequency drop does not exceed 0.7Hz. Moreover, it was shown that deployment of 117.5MW SAPPs in the Ireland power system recovers the system frequency after a generation power shortfall of 50MW in less than 15 seconds while the maximum frequency deviation does not exceed 0.1Hz. In conclusion, our proposed distributed frequency control algorithm via randomized responses of SAPPs is a promising low-cost alternative to the conventional primary reserve service provided by fast-ramping fossil-fuel based power plants.

Chapter 3

Frequency Control via Randomized Responses of Distributed EVs

3.1 Introduction

EVs have attracted great attention in the world due to the serious concern over environment, climate change, fossil-fuel reserve, energy cost, etc. Therefore, it is expected that the demand for EVs will increase remarkably in future [75]. As reported in [76], it is approximated that hybrid electric vehicles (HEVs) and plug-in hybrid electric vehicles (PHEVs) will share 60%, 72%, and 80% of the total vehicles in the new-car market of the USA by 2020, 2030, and 2050, respectively.

Although EVs are safer and greener means of transportation than the conventional internal combustion engine (CICE) vehicles, they will add significant load on the power system as they become more widespread. As an example, a typical EV that consumes 0.4–0.55kWh per one kilometer of driving can double the daily energy consumption of a residential user [77]. On the other hand, the flexible charging/discharging requirements of EVs can help the system operator implement DR successfully in practice, discussed as follows. Particularly, users connect their EVs to the power grid in the evening in order to be fully charged by the next morning; however, the charging time of a typical EV is much shorter than its connection time to the grid, e.g., 1–2 hours charging time versus 10–12 hours connection time. Moreover, upon a contingency of supply shortfall, the energy stored in the batteries of EVs can be injected into the power grid temporarily to help restore the power

system voltage and/or frequency to their nominal values. In summary, we can regard each EV as either an interruptible load, a power generation unit, or an ESS, under different system conditions.

According to the above discussions, controlling the power charging/discharging rates of grid-connected EVs is an appealing approach to implement DR in smart grid. This can help the system operator achieve various design objectives [66, 68, 77, 78, 82–87], discussed as follows. The optimal energy management of residential users including their deferrable loads as well as their EVs in order to maximize the social welfare or minimize users' individual electricity bills was investigated in [66, 68, 78, 82–84]. The charging coordination of a group of EVs subject to their given desired charging time periods to flatten the aggregate demand profile over time was studied in [77, 85, 86]. Specifically, it was shown in [85] that the charging cost of each individual EV reduces by nearly 40% due to the flattened demand profile achieved by coordinating the charging processes of EVs. Last, the charging scheduling for a set of EVs to minimize the power transmission losses subject to certain nodal voltage constraints, i.e., the power flow voltage constraints, was studied in [87]. It was shown in [87] that coordinated charging of EVs can reduce the power transmission loss (peak value) over the case of uncoordinated randomized charging up to 77%, 68%, and 48% when 63%, 47%, and, 32% of the total demand is due to the charging of EVs, respectively.

In contrast to the aforementioned studies [66, 68, 77, 78, 82–87], in this chapter we extend the randomized control algorithm proposed in Chapter 2 to regulate the system frequency via controlling operational modes of distributed EVs. Particularly, utilizing EVs' responses to control the system frequency can reduce the amount of conventional primary reserve service required in the system and thus the operational cost of grid reduces. Moreover, as compared to SAPPS, deploying EVs for frequency control has more flexibility due to both the charging and discharging control, which helps restore the system frequency more smoothly. A handful of centralized and

distributed algorithms under DLC and ILC schemes have been proposed in the literature for EV-enabled frequency control, which are discussed next.

3.2 Literature Review

Adopting centralized algorithms to jointly design power charging/discharging rates of EVs to provide a cost-efficient primary reserve service was investigated in [36–40]. However, it is difficult to implement these algorithms in practice, since the system operator needs to access a bidirectional communication system to collect large amount of information from all EVs, process the data and make a decision, and then command EVs in real time. The complexity of solving the required optimization problem for a large power system involving many decision variables is another barrier for using centralized frequency control algorithms. On the other hand, distributed algorithms to independently manage the power charging/discharging rates of EVs in response to their locally measured system frequency was investigated in [50–53]. As shown in Fig. 3.1, these works have adopted a similar policy for adjusting the power charging/discharging rates of each EV, which is a piecewise linear function over the system frequency; hence, it needs to be implemented continuously in time by varying over a wide range of power values. However, implementing the control policy reported in [50–53] is difficult due to two main reasons. First, designing rechargeable batteries that are highly efficient for such a wide operational power range is challenging. Second, the controlling mechanisms of EVs need to be upgraded to be enabled to adjust their power charging/discharging rates adaptively over time, which is costly.

Although the aforementioned prior works [36–40, 50–52] have shown promising aspects of utilizing EVs' responses to replace conventional reserve services for restoring the system frequency, there has been less effort to theoretically characterize the performance of their frequency control algorithms in large-scale dynamic

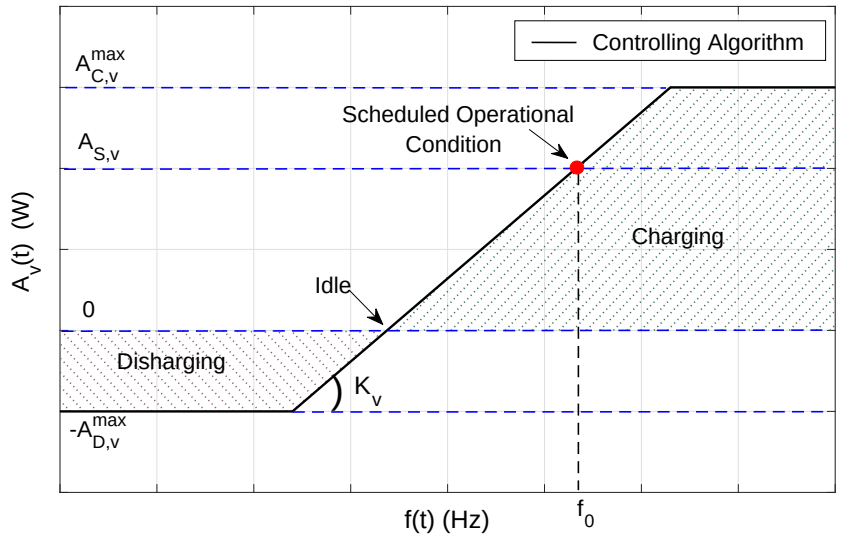

Figure 3.1: Piecewise linear frequency control algorithm in [50–53].[1]

power systems. This thus motivates our work to mathematically characterize the impacts of EVs' randomized responses on the system frequency, which helps the system operator design their control parameters more rigorously and effectively.

3.3 System Model

We consider the same power system as that considered in Section 2.3. We assume that a contingency of supply deficit with $A_e < 0$ occurs at time $t = 0$. In this chapter, we assume that EVs are solely utilized for DR-enabled frequency control, while generation side controllers and frequency responses of SAPPs are all deactivated. Specifically, we assume that $V \geq 1$ EVs are connected to the power grid, indexed by v, $v \in \mathcal{V} = \{1, \ldots, V\}$, where $A_{C,v} > 0$ and $A_{D,v} > 0$ denote the given fixed power charging and discharging rates of EV v. We assume that upon the contingency, the system operator will notify all EVs via sending a command

[1]Note that $K_v > 0$ is the response coefficient of EV v, $f(t)$ is the locally measured system frequency with the nominal value of f_0, and $A_v(t)$ is the power exchanged between the EV and the grid with the scheduled value of $-A^{\max}_{D,v} \leq A_{S,v} \leq A^{\max}_{C,v}$ under f_0. Moreover, $A^{\max}_{C,v} > 0$ and $A^{\max}_{D,v} > 0$ are the given charging and discharging power limits for the EV, respectively.

signal (e.g., bit '1') to activate their threshold based mode switching algorithms, as shown in Fig. 3.2. When the system frequency recovers back to its nominal range for a sufficient amount of time and the deficiency is compensated using alternative sources of energy, the system operator will send a clear signal (e.g., bit '0') to all EVs to deactivate their algorithms and resume their normal operation. In our work, the one-bit feedback signaling system is deployed to notify EVs to activate/deactivate their switching algorithms, while no other information will be shared between the system operator and EVs. This is in contrast to the bidirectional communication system assumed in [36, 38], under which larger amount of information between the system operator and EVs is shared in real time.

3.4 Frequency Control via Distributed EVs

In this section, we present the frequency control algorithm for EVs by extending the load control policy proposed for SAPPs in Chapter 2.

3.4.1 Frequency Threshold Based Mode Switching

Let $S_v(t) \in \{1, 0, -1\}$ denote the operational mode of EV v over time, where 1 indicates the charging mode when the EV draws $A_{C,v}$ amount of power from the power grid, 0 indicates the idle mode when the EV has no power exchange with the power grid, and -1 indicates the discharging mode when the EV injects $A_{D,v}$ amount of power to the grid. Our proposed threshold based switching policy for EV v with a given pair frequency thresholds, i.e., $(f_{\min}, f_{\max})$, is expressed as

$$S_v(t^+) = \begin{cases} 0, & \text{if } f(t) < f_{\min} \text{ and } S_v(t) = 1 \\ 0, & \text{if } f(t) > f_{\max} \text{ and } S_v(t) = -1 \\ -1, & \text{if } f(t) < f_{\min} \text{ and } S_v(t) = 0 \\ 1, & \text{if } f(t) > f_{\max} \text{ and } S_v(t) = 0 \\ S_v(t), & \text{otherwise,} \end{cases} \tag{3.1}$$

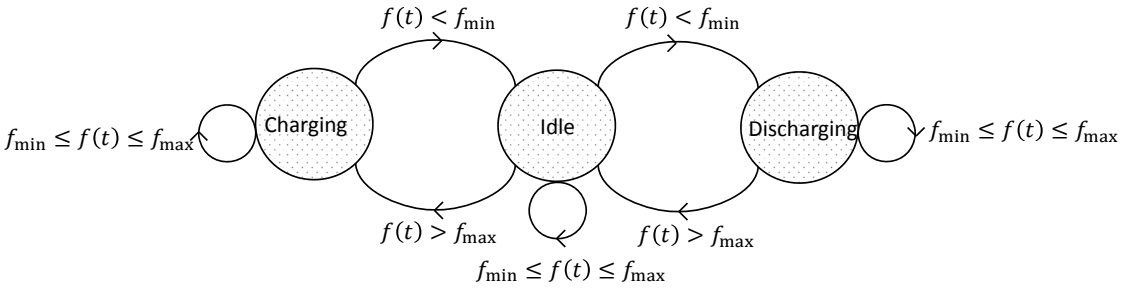

Figure 3.2: Threshold based mode switching policy for each EV.

where $t^+ = t + \Delta t$, with $\Delta t \to 0^+$. The control policy given in (3.1) is the extension of that proposed in (2.6) to switch on/off SAPPs in response to their locally measured system frequency. For simplicity of analysis, we assume that EV v can charge/discharge from/to the grid with given power rates $A_{C,v}$ and $A_{D,v}$, respectively, without the need of considering its battery level. This is justified due to the fact that contingencies of supply-demand imbalances that deviate the system frequency below $f_{\min}$ (or over $f_{\max}$) do not occur frequently and also each contingency lasts at most for a couple of minutes before the system frequency is permanently restored. Therefore, during the period of the contingency of our interest, the battery level of each EV changes marginally and thus is assumed to be a constant value.

Let $A_v(t)$ denote the power exchanged between EV v and the power system over time, which is defined as

$$A_v(t) = \begin{cases} A_{C,v}, & \text{if } S_v(t) = 1 \\ 0, & \text{if } S_v(t) = 0 \\ -A_{D,v}, & \text{if } S_v(t) = -1. \end{cases} \tag{3.2}$$

Accordingly, the power response of EV v over time is tracked by a stochastic process $X_v(t) = A_v(t) - A_v(t^+)$, which has five values in $\{\pm A_{C,v}, 0, \pm A_{D,v}\}$. Particularly, each EV can boost the system frequency by either discharging its battery to the power grid or stopping its ongoing power charging. It also can help reduce the system frequency by charging from the power grid or stopping its ongoing discharging. Last,

for a particular EV v whose battery is nearly empty (e.g., its state of charge is less than 5%), we assume that the *effective* power discharging rate of the EV is zero, i.e., we set $A_{D,v} = 0$. On the other hand, for EV v of which the battery is nearly full (e.g., more than 95% of the full capacity), we assume that the *effective* power charging rate of the EV is zero, i.e., we set $A_{C,v} = 0$.

3.4.2 Randomized Inter-Response Time

If all EVs monitor the system frequency continuously over time, they are likely to respond simultaneously by changing their operational modes when the system frequency reaches one of the two frequency thresholds $f_{\min}$ or $f_{\max}$. Hence, the system frequency will oscillate between $f_{\min}$ and $f_{\max}$ over time. To address this issue, we use the similar approach that has been used in Chapter 2 to desynchronize the responses of SAPPs. Specifically, we design EV v to monitor and respond to the system frequency in only discrete times, given in $\{t_{1,v}, t_{2,v}, \ldots\}$, where $t_{l,v}$ is the lth monitoring/response time of EV v. Denote $T_{l,v} = t_{l,v} - t_{l-1,v}$, $l = 1, 2, \ldots$, with $t_{0,v} = 0$ by default, as the lth inter-response time of EV v. To further desynchronize EVs' responses, we design $T_{l,v}$, $l = 1, 2, \ldots$, to follow independent exponentially distributed random variables with mean $1/\lambda_{C,v} \geq 0$ when $S_v(t) = 1$, $1/\lambda_{I,v} \geq 0$ when $S_v(t) = 0$, or $1/\lambda_{D,v} \geq 0$ when $S_v(t) = -1$. The number of responses of EV v over time $t \geq 0$ can be thus counted by a continuous-time counting process, defined as $C_v(t) = \sum_{l=1}^{\infty} \mathbf{1}_{\{t \geq t_{l,v}\}}$, which is a Poisson process with time-varying rate due to independent exponential inter-response times [81]. Note that $(\lambda_{C,v}, \lambda_{I,v}, \lambda_{D,v})$ are the controlling parameters of EV v, which can be designed by the system operator to achieve a certain design objective, e.g., minimizing the expected cost of employing EVs' frequency control for restoring the system frequency upon the contingency of supply-demand imbalance, as will be discussed later in Section 3.5.4.

Fig. 3.3 shows responses of a particular EV v that is initially in the charging mode at time $t = 0$ with the switching policy given in (3.1) applied, given the

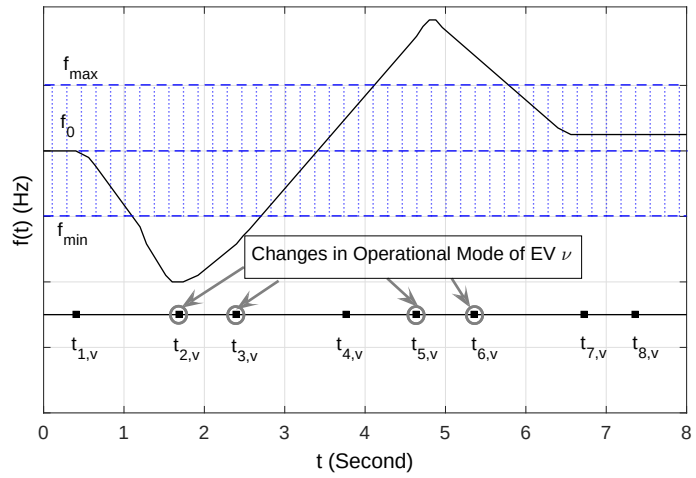

(a)

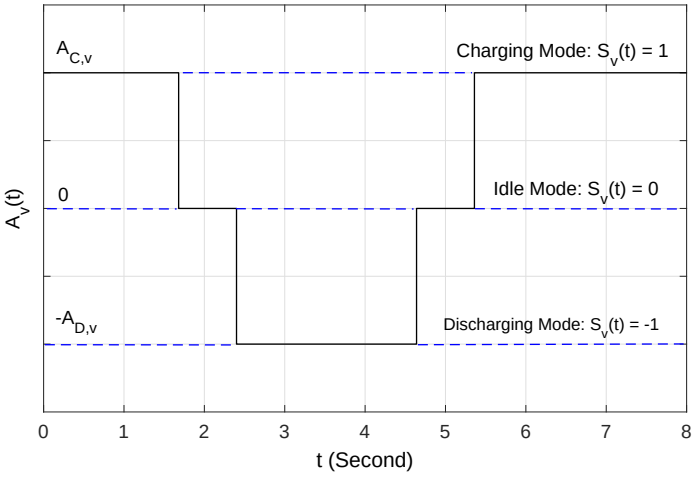

(b)

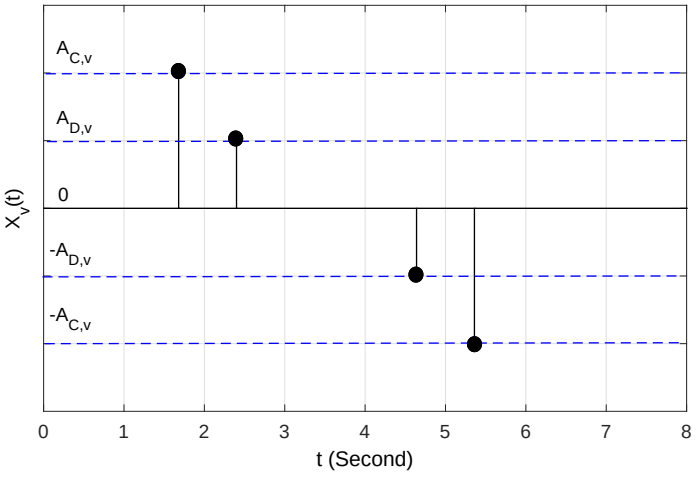

(c)

Figure 3.3: Illustration of EV responses by the proposed threshold based switching algorithm and the randomized monitoring/response times.

monitoring/response times and the system frequency $f(t)$ shown in Fig. 3.3 (a). It is observed that when the EV monitors the system frequency for the first time at $t = t_{1,v}$, it does not change its operational mode, since $f_{\max} \leq f(t_{1,v}) \leq f_{\min}$. However, the EV switches from the charging mode to the idle mode and then from the idle mode to the discharging mode when it monitors the system frequency for the second and third times at $t = t_{2,v}$ and $t = t_{3,v}$, respectively, since $f(t_{2,v}),\ f(t_{3,v}) < f_{\min}$. The EV remains in the discharging mode until its fifth monitoring time at $t = t_{5,v}$, after which it switches from the discharging mode to the idle mode, since $f(t_{5,v}) > f_{\max}$. It then switches from the idle mode to the charging mode at $t = t_{6,v}$, and remains in the charging mode for the rest of time, since $f_{\min} \leq f(t) \leq f_{\max}$ for $t > t_{7,v}$.

Let $A_a = \sum_{v\in\mathcal{V}_C}(A_{C,v} + A_{D,v}) + \sum_{v\in\mathcal{V}_I} A_{D,v}$ denote the aggregate power that can be shed and/or injected to the grid by all EVs after a contingency of supply deficit.[2] From (3.1), it follows that EVs in set $\mathcal{V}_D$ do not respond when $f(t) < f_0$. Hence, A_a does not involve any terms related to EVs in set $\mathcal{V}_D$. Since $A_a \ll A_0$ holds in practice, we can modify the aggregate demand model given in (2.1) to capture impacts of EVs' responses as

$$A_d(t) = A_0 + \left(\frac{f(t) - f_0}{f_0}\right) K_f A_0 - \sum_{v=1}^{V}\sum_{l=1}^{C_v(t)} X_v(t_{l,v})\mathbf{1}_{\{t\geq t_{l,v}\}}. \tag{3.3}$$

By substituting (3.3) into (2.3), and solving the obtained differential equation for A_e amount of supply deficit, the system frequency is obtained as

$$f(t) = f_0 + \frac{f_0}{K_f A_0}\Bigg(A_e\left(1 - e^{-\alpha t}\right) + \sum_{v=1}^{V}\sum_{l=1}^{C_v(t)} X_v(t_{l,v})\left(1 - e^{-\alpha(t-t_{l,v})^+}\right)\Bigg),\ t \geq 0. \tag{3.4}$$

[2]In Chapter 2, we defined $A_a = \sum_{i\in\mathcal{M}} A_i$ to represent the aggregate demand that can be shed by SAPPs upon a contingency of supply deficit. However, in this chapter, it is assumed that EVs control the system frequency solely. Hence, we re-express $A_a = \sum_{v\in\mathcal{V}_C}(A_{C,v}+A_{D,v})+\sum_{v\in\mathcal{V}_I} A_{D,v}$.

From (3.4), it follows that when a particular EV v switches from the charging mode to the idle mode or from the idle mode to the discharging mode at its lth monitoring event in $t = t_{l,v}$, we have $X_v(t_{l,v}) = A_{C,v}$ and $X_v(t_{l,v}) = A_{D,v}$, respectively, which can help increase the grid frequency given in (2.7) over $t \geq t_{l,v}$. The opposite is also true when EV v switches from the discharging mode to the idle mode or from the idle mode to the charging mode. Moreover, since $t_{l,v}$'s are random variables, the grid frequency given in (2.7) is a random process in general, for which the statistical characterizations such as the mean and variance over time will be investigated later in this chapter.

Let $\mathcal{V}_C$, $\mathcal{V}_I$, and $\mathcal{V}_D$ denote the subsets of EVs that are initially in charging, idle, and discharging modes at time $t = 0$, respectively, where $|\mathcal{V}_C| = V_C$, $|\mathcal{V}_I| = V_I$, and $|\mathcal{V}_D| = V_D$, with $V_C + V_I + V_D = V$. In the following, we discuss how the aggregate power response of all EVs A_a as well as EVs' response rates $(\lambda_{C,v}, \lambda_{I,v}, \lambda_{D,v})$'s can affect the system frequency. For convenience, we use the following power thresholds

$$A_{a,\min} = \frac{K_f A_0}{f_0}(f_{\min} - f_0) - A_e, \tag{3.5}$$

$$A_{a,\max} = \frac{K_f A_0}{f_0}(f_{\max} - f_0) - A_e, \tag{3.6}$$

where $A_{a,\min}$ is the minimum value of A_a that is required to recover the grid frequency to $f_{\min}$ in steady state after the contingency of supply deficit A_e, while $A_{a,\max}$ is the minimum amount of A_a required to recover the grid frequency to $f_{\max}$ in steady state. From (3.4), we discuss the following three cases assuming $A_e < A_{e,\min}$, with $A_{e,\min}$ given in (2.8), which ensures that the system frequency drops below $f_{\min}$ after the contingency and thus EVs can respond according to their frequency control algorithms. Case 1: $A_a < A_{a,\min}$, it follows that the system frequency $f(t)$ does not recover back to $f_{\min}$ even though all EVs respond after time $t > t_0$. Case 2: $A_{a,\min} \leq A_a \leq A_{a,\max}$, it follows that $f(t)$ recovers back to $f_{\min}$ at a certain time $T_r > t_0$ (see Fig. 2.3), while it will not overshoot $f_{\max}$. The frequency recovery time

T_r is rigorously defined as the smallest time $t > t_0$ that solves $f(t) = f_{\min}$, with $f(t)$ given in (3.4). Case 3: $A_a > A_{a,\max}$, it follows that $f(t)$ may overshoot $f_{\max}$ for $t > T_r$, when EVs' response rates are not well designed, e.g., response rates are set very large.

For the purpose of exposition, we study the Ireland power system [25] with the given parameters in Table 2.1 (in Section 2.6) under a contingency with $A_e = -100$MW that satisfies $A_e < A_{e,\min}$. For ease of explanation, we assume that all EVs in the system have the identical power charging/discharging rates as well as response rates. Specifically, we set $A_{C,v} = 11.2$kW, $A_{D,v} = 8.96$kW, $\lambda_{C,v} = \lambda_C$, $\lambda_{I,v} = \lambda_I$, and $\lambda_{D,v} = \lambda_D$, $v = 1, \ldots, V$. We also assume that all EVs are initially in the charging mode, i.e., $S_v(0) = 1$, $\forall v \in \mathcal{V}$. In addition, we set the frequency thresholds for all EVs as $f_{\min} = 49.8$Hz and $f_{\max} = 50.2$Hz, which yield $A_{e,\min} = -60.65$MW, $A_{a,\min} = 139.35$MW, and $A_{a,\max} = 260.65$MW.

Fig. 3.4 shows Cases 1 ($A_a < A_{a,\min}$), 2 ($A_{a,\min} \leq A_a \leq A_{a,\max}$), and 3 ($A_a > A_{a,\max}$) for the Ireland power system when the number of EVs is set as $V = 5000$, $V = 10000$, and $V = 35000$, respectively. It follows that the EVs' aggregate power response A_a is 100.8MW, 201.6MW, and 705.6MW. We consider two different sets of response rates for EVs. In the first set, we have $(\lambda_C, \lambda_I, \lambda_D) = (0.05, 0.05, 0.05)$Hz. In the second set, we have $(\lambda_C, \lambda_I, \lambda_D) = (0.5, 0.5, 0.5)$Hz, which are much larger than those in the first set. It is observed that for all cases, the second set of response rates results in smaller frequency recovery times as compared to the first set. This is reasonable since by increasing response rates, EVs monitor the system frequency more frequently and thus respond to any frequency deviations more quickly. However, the second set causes an undesired frequency overshoot in Case 3, as shown in Fig. 3.4 (c), due to over-responses of EVs. A simple rule of thumb for restoring the system frequency smoothly is to set $\lambda_{C,v}, \lambda_{I,v}, \lambda_{D,v} \ll \alpha$, $\forall v \in \mathcal{V}$. This helps prevent over-responses of EVs, since they will wait longer times (on average) before responding to the system frequency deviations, which however can increase the fre-

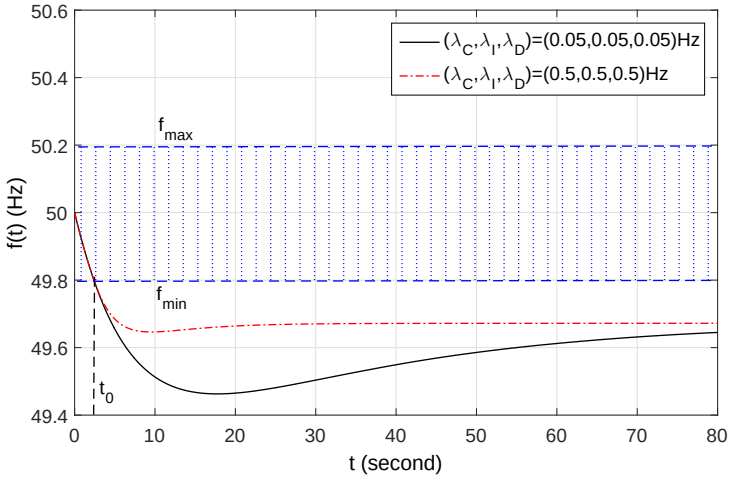

(a) Case 1

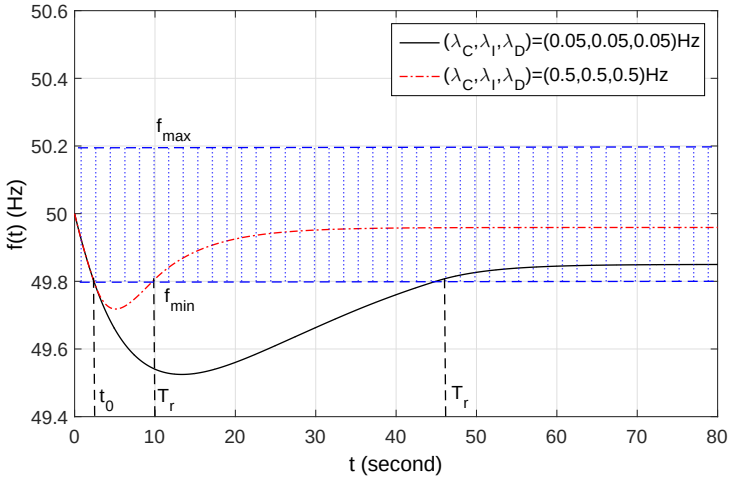

(b) Case 2

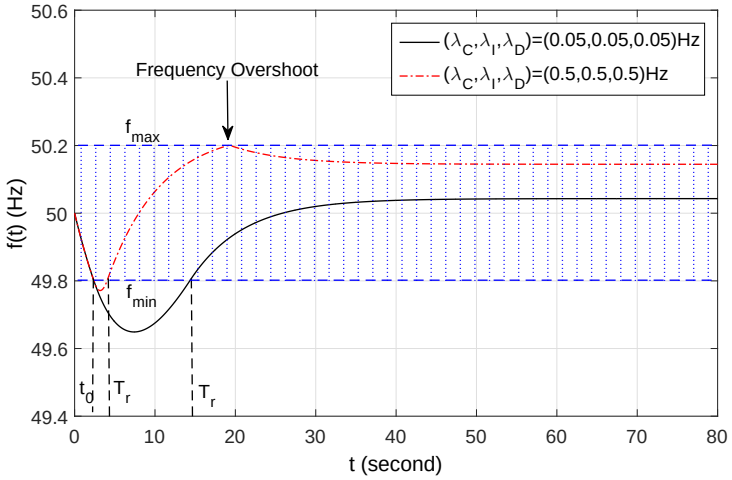

(c) Case 3

Figure 3.4: Simulated system frequency of Ireland power system for the case $A_e < A_{e,\min}$.

quency recovery time considerably. Specifically, there is a trade-off for minimizing the frequency recovery time and avoiding the frequency overshoot. The analysis on the mean frequency recovery time and the probability of frequency overshoot will be given later in Sections 3.5.2 and 3.5.4, respectively. At last, since Case 1 is not of our interest, we will focus on Cases 2 and 3, i.e., we assume $A_a \geq A_{a,\min}$.

In summary, as shown in Fig. 3.4, designing EVs' response rates, $(\lambda_{C,v}, \lambda_{I,v}, \lambda_{D,v})$, $\forall v \in \mathcal{V}$, is a challenging task that requires a rigorous understanding of the impact of each individual EV on the system frequency. Hence, we first provide theoretical results in Section 3.5 to characterize the performance of our EV-enabled frequency control algorithm. Based on the obtained analysis, we then design EVs' response rates in Section 3.6.

3.5 Analysis of System Frequency

In this section, we present our analysis on the impacts of randomized responses of EVs on the system frequency, including the mean and variance analysis, the average frequency recovery time, and the probability of frequency overshoot.

3.5.1 Mean and Variance of System Frequency

With the distributed frequency control algorithm discussed in Section 3.4, the system frequency $f(t)$ given in (3.4) is a random process in general. Particularly, we are interested to study the behavior of this random process over $t_0 \leq t \leq T_r$, under which the system frequency drops below $f_{\min}$ and thus EVs respond by switching from the charging mode to the idle mode and/or from the charging mode to the idle mode. Therefore, in the following two propositions, we analyze statistical properties of the system frequency by deriving its mean and variance over time in terms of EVs' response rates and given power system parameters.

In this chapter, we assume that the number of grid-connected EVs as well as

their initial operation modes are all known.

Proposition 3.5.1. Given $A_e < A_{e,\min}$ and $A_a \geq A_{a,\min}$, the mean of the system frequency over time $t_0 \leq t \leq T_r$ is given by

$$\mathbb{E}[f(t)] = f_0 + \frac{f_0}{K_f A_0}\Bigg(A_e\left(1-e^{-\alpha t}\right) + \sum_{v\in\mathcal{V}_C} h_\alpha(A_{C,v}, A_{D,v}, \lambda_{C,v}, \lambda_{I,v}, t-t_0) + \sum_{v\in\mathcal{V}_I} h_\alpha(A_{D,v}, 0, \lambda_{I,v}, 0, t-t_0)\Bigg), \tag{3.7}$$

where

$$h_\alpha(A_C, A_D, \lambda_C, \lambda_I, s) = A_C(1-u_\alpha(\lambda_C, s)) + A_D(1-\dot{u}_\alpha(\lambda_C, \lambda_I, s)), \tag{3.8}$$

with $u_\alpha(\lambda, s)$ given in (2.14) and $\dot{u}_\alpha(\lambda_C, \lambda_I, s)$ defined as

$$\dot{u}_\alpha(\lambda_C, \lambda_I, s) = \begin{cases} \dfrac{\lambda_I u_\alpha(\lambda_C, s) - \lambda_C u_\alpha(\lambda_I, s)}{\lambda_I - \lambda_C}, & \lambda_C \neq \lambda_I \\ u_\alpha(\lambda_I, s) - \dfrac{\partial u_\alpha(\lambda_I, s)}{\partial \lambda_I}, & \lambda_C = \lambda_I. \end{cases} \tag{3.9}$$

Proof. Please see Appendix E. □

From the frequency mean characterization function of EV v that is in the charging mode initially, i.e., $h_\alpha(A_{C,v}, A_{D,v}, \lambda_{C,v}, \lambda_{I,v}, s)$, it follows that the contribution of EV v on the mean system frequency is linearly proportional to its power charging rate $A_{C,v}$ and power discharging rate $A_{D,v}$. It also follows that the response rate $\lambda_{D,v}$ does not affect the contribution of EV v when $f(t) < f_{\min}$, as expected from Fig. 3.2. In addition, EVs in set $\mathcal{V}_D$ do not affect the mean system frequency over time $t_0 \leq t \leq T_r$, which is expected from (3.1). It can also be verified that $h_\alpha(A_{C,v}, A_{D,v}, \lambda_{C,v}, \lambda_{I,v}, s)$ is upper-bounded by $(A_{C,v} + A_{D,v})(1 - e^{-\alpha s})$ when $(\lambda_{C,v}, \lambda_{I,v}) \to (\infty, \infty)$, which corresponds to the case that EV v continuously monitors and responds to the system frequency and thus its resulting contribu-

tion is deterministic. Last, the result given in Proposition 3.5.1 can be simplified to that obtained in Proposition 2.5.1 by setting $A_{D,v} = 0$ and $\lambda_{I,v} = 0$ in $h_\alpha(A_{C,v}, A_{D,v}, \lambda_{C,v}, \lambda_{I,v}, s)$.

Fig. 3.5 plots $h_\alpha(A_{C,v}, A_{D,v}, \lambda_{C,v}, \lambda_{I,v}, s)$ for both the Ireland power system ($\alpha =$ 0.15Hz) and the IEEE 9-Bus test system ($\alpha = 0.1$Hz), by setting $A_{C,v} = 1$W and $A_{D,v} = 1$W. It is observed that the frequency mean function quickly reaches the first level $A_{C,v} = 1$W and then increases smoothly to the second level $A_{C,v} + A_{D,v} = 2$W. This is due to the fact that $\lambda_{I,v} \ll \lambda_{C,v}$ in our example. Hence, EV v quickly responds by switching from the charging mode to the idle mode as the system frequency drops below $f_{\min}$, while waits a much longer time before switching from the idle mode to the discharging mode. By setting $\lambda_{I,v} \ll \lambda_{C,v}$, we can avoid unnecessary discharging of EV v into the power grid (injecting power to the grid), since the EV will wait sufficiently long time before discharging to ensure that the system frequency is below $f_{\min}$. We use this rule for designing EVs' response rates later in Section 3.6.

Proposition 3.5.2. Given $A_e < A_{e,\min}$ and $A_a \geq A_{a,\min}$, the variance of the system frequency over time $t_0 \leq t \leq T_r$ is given by

$$\mathbb{V}\text{ar}[f(t)] = \left(\frac{f_0}{K_f A_0}\right)^2 \Bigg(\sum_{v\in\mathcal{V}_C} q_\alpha(A_{C,v}, A_{D,v}, \lambda_{C,v}, \lambda_{I,v}, t-t_0) + \sum_{v\in\mathcal{V}_I} q_\alpha(A_{D,v}, 0, \lambda_{I,v}, 0, t-t_0)\Bigg), \quad (3.10)$$

where $q_\alpha(A_C, A_D, \lambda_C, \lambda_I, s) = 2h_\alpha(A_C^2, A_D^2, \lambda_C, \lambda_I, s) - h_{2\alpha}(A_C^2, A_D^2, \lambda_C, \lambda_I, s) - (h_\alpha(A_C, 0, \lambda_C, \lambda_I, s))^2 - (h_\alpha(0, A_D, \lambda_C, \lambda_I, s))^2$, with $h_\alpha(A_c, A_D, \lambda_C, \lambda_I, s)$ given in (3.8).

Proof. Please see Appendix F. □

The result given in Proposition 3.5.2 can be simplified to that given in Proposition 2.5.2 for the case that the power system consists of SAPPs solely, by setting $A_{D,v} = 0$ and $\lambda_{I,v} = 0$.

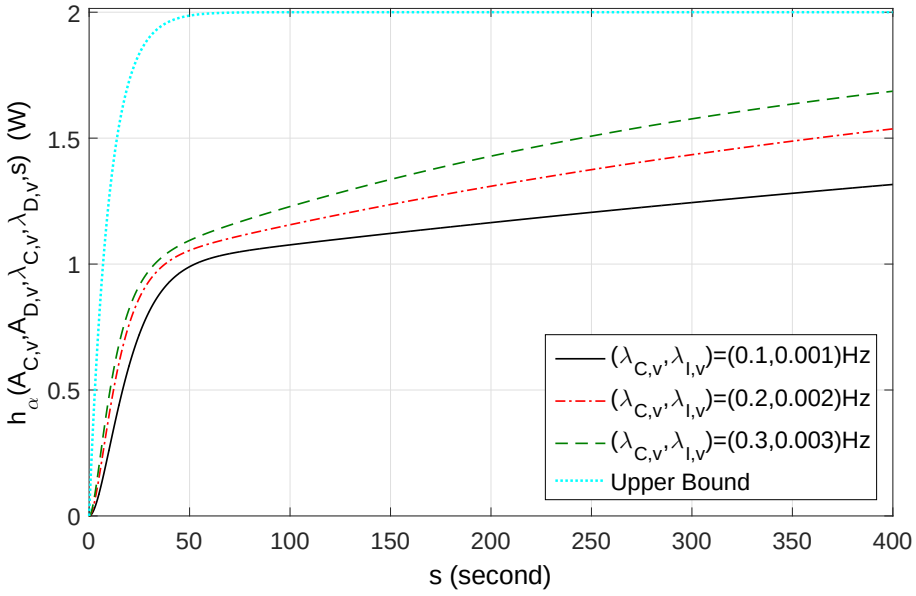

(a) IEEE 9-Bus test system with $\alpha = 0.1$Hz.

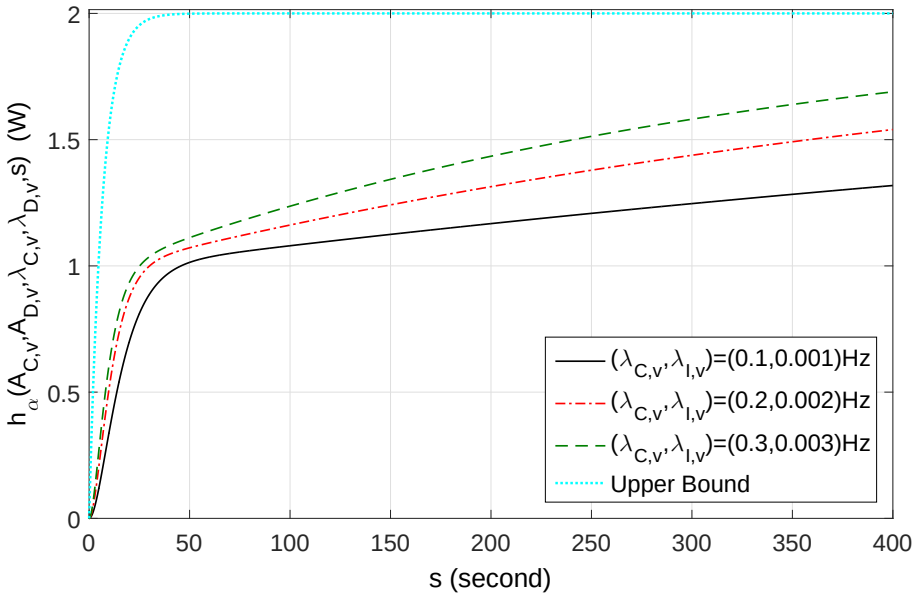

(b) Ireland power system with $\alpha = 0.15$Hz.

Figure 3.5: Frequency mean characterization function of EV v that is in the charging mode initially, $h_\alpha(A_{C,v}, A_{D,v}, \lambda_{C,v}, \lambda_{I,v}, s)$.

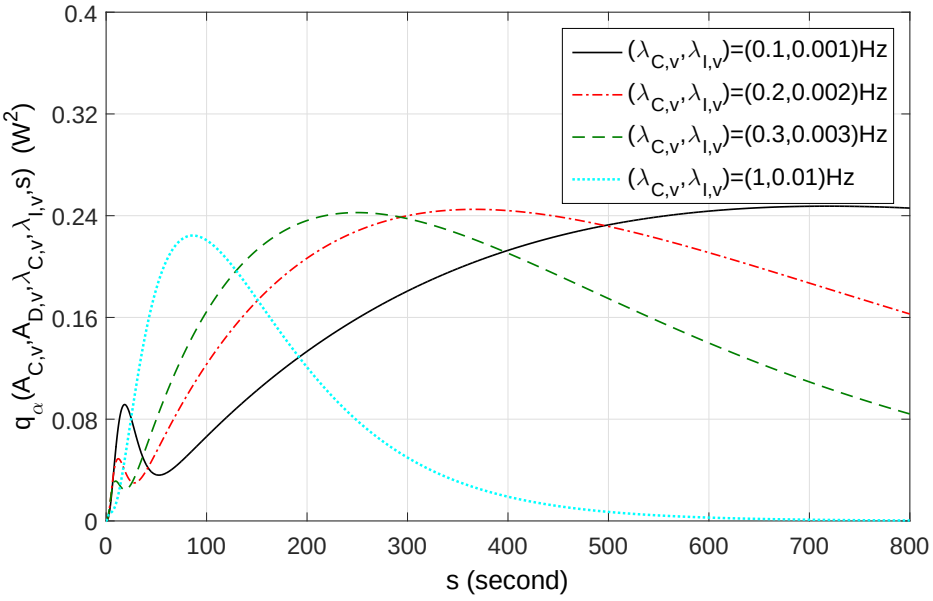

(a) IEEE 9-Bus test system with $\alpha = 0.1$Hz.

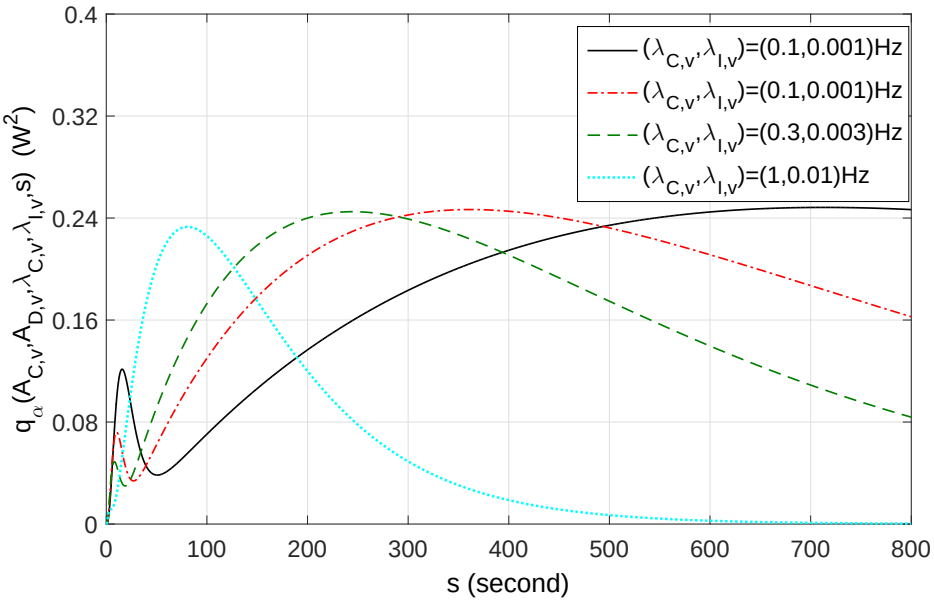

(b) Ireland power system with $\alpha = 0.15$Hz.

Figure 3.6: Frequency variance characterization function of EV v that is in the charging mode initially, $q_\alpha(A_{C,v}, A_{D,v}, \lambda_{C,v}, \lambda_{I,v}, s)$.

Fig. 3.6 plots $q_\alpha(A_{C,v}, A_{D,v}, \lambda_{C,v}, \lambda_{I,v}, s)$ for both the Ireland power system ($\alpha = 0.15$Hz) and the IEEE 9-Bus test system ($\alpha = 0.1$Hz), by setting $A_{C,v} = 1$W and $A_{D,v} = 1$W. It is observed that for a fixed pair of $(\lambda_{C,v}, \lambda_{I,v})$, the peak of the frequency variance characterization function is sharper in the Ireland power system as compared to the IEEE 9-Bus test system. It is also observed that $q_\alpha(A_{C,v}, A_{D,v}, \lambda_{C,v}, \lambda_{I,v}, s)$ has two peaks that are approximately located on $\lambda_{C,v}^{-1}$ and $\lambda_{C,v}^{-1} + \lambda_{I,v}^{-1}$ corresponding to the average waiting time before the first and second responses of EV v after t_0, respectively. The first response refers to the switching from the charging mode to the idle mode, while the second response refers to the switching from the idle mode to the discharging mode.

3.5.2 Average Frequency Recovery Time

Obtaining the distribution of T_r is not feasible because of large degree of randomness in $f(t)$ given in (3.4). Hence, we use the mean of the system frequency given in Proposition 3.5.1 to approximate the average frequency recovery time $\overline{T}_r$. This approximation is valid due to the fact that the variance of the system frequency given in Proposition 3.5.2 is very small in practice, since the power charging and discharging rates of individual EVs are much smaller than the aggregate demand, i.e., $(A_{C,v}/A_0)^2, (A_{D,v}/A_0)^2 \to 0,\ v = 1, \ldots, V$. We verify this approximation later via simulations (see Fig. 3.9). Thus, we have the following proposition.

Proposition 3.5.3. Given $A_e < A_{e,\min}$ and $A_a \geq A_{a,\min}$, the average frequency recovery time $\overline{T}_r$ can be approximated by the smallest time $t > t_0$ that solves $\mathbb{E}[f(t)] = f_{\min}$, where $\mathbb{E}[f(t)]$ is given in (3.7).

3.5.3 Expected Number of EVs in Each Operational Mode

Without loss of generality, we assume that the power system consists of $K \geq 1$ different classes of EVs, indexed by k, $k \in \mathcal{K} = \{1, \ldots, K\}$, where $\tilde{A}_{C,k} > 0$, $\tilde{A}_{D,k} > 0$, and $(\tilde{\lambda}_{C,k} \geq 0, \tilde{\lambda}_{I,k} \geq 0, \tilde{\lambda}_{D,k} \geq 0)$ are the power charging rate, power

discharging rate, and response rates of each EV from Class k, respectively. We define $N_{C,k}(t)$, $N_{I,k}(t)$, and $N_{D,k}(t)$ as random processes representing the numbers of EVs from Class k that are in the charging, idle, and discharging modes, respectively, over time $t \geq 0$. Obviously, we always have $N_{C,k}(t)+N_{I,k}(t)+N_{D,k}(t) = V_{C,k}+V_{I,k}+V_{D,k}$, where $V_{C,k} \geq 0$, $V_{I,k} \geq 0$, and $V_{D,k} \geq 0$ are the numbers of EVs from Class k that are initially in the charging, idle, and discharging modes at time $t = 0$, respectively. To be consistent with previous notations, we set $\sum_{k=1}^{K} V_{C,k} = V_C$, $\sum_{k=1}^{K} V_{I,k} = V_I$, and $\sum_{k=1}^{K} V_{D,k} = M_D$. We have the following proposition.

Proposition 3.5.4. Given $A_e < A_{e,\min}$ and $A_a \geq A_{a,\min}$, the expected number of EVs from Class k, $k \in \mathcal{K}$, that are in the charging, idle, or discharging modes over time $t_0 \leq t \leq T_r$ is given by

$$\mathbb{E}[N_{C,k}(t)] = V_{C,k}\, p_1(\tilde{\lambda}_{C,k}, \tilde{\lambda}_{I,k}, t - t_0), \tag{3.11}$$

$$\mathbb{E}[N_{I,k}(t)] = V_{C,k}\, p_2(\tilde{\lambda}_{C,k}, \tilde{\lambda}_{I,k}, t - t_0) + V_{I,k}\, p_1(\tilde{\lambda}_{I,k}, 0, t - t_0), \tag{3.12}$$

$$\mathbb{E}[N_{D,k}(t)] = V_{C,k}\, p_3(\tilde{\lambda}_{C,k}, \tilde{\lambda}_{I,k}, t - t_0) + V_{I,k}\, p_2(\tilde{\lambda}_{I,k}, 0, t - t_0) + V_{D,k}, \tag{3.13}$$

where $p_1(\lambda_C, \lambda_I, s) = 1 - p_2(\lambda_C, \lambda_I, s) - p_3(\lambda_C, \lambda_I, s)$, with $p_2(\lambda_C, \lambda_I, s)$ and $p_3(\lambda_C, \lambda_I, s)$ given by

$$p_2(\lambda_C, \lambda_I, s) = \begin{cases} \dfrac{\lambda_C \left(1 - e^{-\lambda_C s}\right) - \lambda_C \left(1 - e^{-\lambda_I s}\right)}{\lambda_C - \lambda_I}, & \text{if } \lambda_C \neq \lambda_I \text{ and } s > 0 \\ \lambda_C s e^{-\lambda_C s}, & \text{if } \lambda_C = \lambda_I \text{ and } s > 0 \\ 0, & \text{if } s = 0, \end{cases} \tag{3.14}$$

$$p_3(\lambda_C, \lambda_I, s) = \begin{cases} \dfrac{\lambda_I \left(1 - e^{-\lambda_C s}\right) - \lambda_C \left(1 - e^{-\lambda_I s}\right)}{\lambda_I - \lambda_C}, & \text{if } \lambda_C \neq \lambda_I \text{ and } s > 0 \\ 1 - (1 + \lambda_C s)\, e^{-\lambda_C s}, & \text{if } \lambda_C = \lambda_I \text{ and } s > 0 \\ 0, & \text{if } s = 0. \end{cases} \tag{3.15}$$

Proof. Please see Appendix G. □

In (3.12), $p_1(\tilde{\lambda}_{C,k}, \tilde{\lambda}_{I,k}, t-t_0)$ is the probability that an EV from Class k that is initially in the charging mode has remained in the charging mode by time t, $t_0 \leq t \leq T_1$; however, $p_2(\tilde{\lambda}_{C,k}, \tilde{\lambda}_{I,k}, t-t_0)$ and $p_3(\tilde{\lambda}_{C,k}, \tilde{\lambda}_{I,k}, t-t_0)$ are probabilities that this EV has switched to the idle and discharging modes, respectively. Similarly, in (3.13), $p_1(\tilde{\lambda}_{I,k}, 0, t-t_0)$ denotes the probability that an EV from Class k that is initially in the idle mode has remained in the idle mode by time t, $t_0 \leq t \leq T_r$; however, $p_2(\tilde{\lambda}_{I,k}, 0, t-t_0)$ is the probability that this EV has switched to the discharging mode. From the mode switching policy given in (3.1), it follows that an EV that is initially in the discharging mode (from any classes) cannot switch to other modes within an under-frequency event.

3.5.4 Probability of Frequency Overshoot

First, we specify the condition under which the system frequency will overshoot $f_{\max}$ assuming $A_a > A_{a,\max}$, as shown in Fig. 3.4 (c). Let $A_r(t)$ denote the total power that has been shed and/or injected to the grid by all EVs in different classes by time t, $t_0 \leq t \leq T_r$. Particularly, we can express

$$A_r(t) = \sum_{k=1}^{K} \left(\tilde{A}_{C,k} + \tilde{A}_{D,k}\right)\left(V_{C,k} - N_{C,k}(t)\right) + \tilde{A}_{D,k}\left(V_{I,k} - N_{I,k}(t)\right), \qquad (3.16)$$

where $A_r(t) \leq A_a$ always holds. We have the following proposition.

Proposition 3.5.5. Given $A_e < A_{e,\min}$ and $A_a > A_{a,\max}$, the system frequency will overshoot $f_{\max}$ at some time $t > T_r$, if and only if (iff) $A_r(T_r) > A_{a,\max}$.

The result given in Proposition 3.5.5 can be directly verified from (3.4). Using this result, the probability of frequency overshoot is then obtained as follows. Let $m_{C,k} = N_{C,k}(T_r)$, $m_{I,k} = N_{I,k}(T_r)$, $m_{D,k} = N_{D,k}(T_r)$, and $\boldsymbol{m}_k = [m_{C,k}, m_{I,k}, m_{D,k}]^T$, $\forall k \in \mathcal{K}$ ($m_{C,k}$ is a realization of the random variable $N_{D,k}(T_r)$). From (3.16)

and Proposition 3.5.5, all possible values of $\boldsymbol{M} = [\boldsymbol{m}_1, \ldots, \boldsymbol{m}_K]$ resulting in the frequency overshoot are given in the set $\mathcal{S} = \big\{\boldsymbol{M} \;\big|\; 0 \leq m_{C,k} \leq V_{C,k},\ 0 \leq m_{I,k} \leq V_{C,k} + V_{I,k},\ V_{D,k} \leq m_{D,k} \leq V_{C,k} + V_{I,k} + V_{D,k},\ m_{C,k} + m_{I,k} + m_{D,k} = V_{C,k} + V_{I,k} + V_{D,k},\ \forall k \in \mathcal{K},\ \sum_{k=1}^{K} (\tilde{A}_{C,k} + \tilde{A}_{D,k})(V_{C,k} - m_{C,k}) + \tilde{A}_{D,k}(V_{I,k} - m_{I,k}) > A_{a,\max}\big\}$. Since EVs respond independently, the conditional probability $P_k(\boldsymbol{m}_k, s) = \mathbb{P}\mathrm{r}\{[N_{C,k}(T_r), N_{I,k}(T_r), N_{D,k}(T_r)]^T = \boldsymbol{m}_k \mid T_r = s\}$, with $s > t_0$, can be derived as follows

$$\begin{aligned} P_k(\boldsymbol{m}_k, s) = \sum_{m=0}^{V_{C,k}-m_{C,k}} \beta_j(\boldsymbol{m}_j, m) \Bigg(& \Big(p_1(\tilde{\lambda}_{C,k}, \tilde{\lambda}_{I,k}, s - t_0)\Big)^{m_{C,k}} \\ & \Big(p_2(\tilde{\lambda}_{C,k}, \tilde{\lambda}_{I,k}, s - t_0)\Big)^{V_{C,k}-m_{C,k}-m} \Big(p_3(\tilde{\lambda}_{C,k}, \tilde{\lambda}_{I,k}, s - t_0)\Big)^{m} \\ & \Big(p_1(\tilde{\lambda}_{I,k}, 0, s - t_0)\Big)^{V_{I,k}-\dot{m}_{D,k}+m} \Big(p_2(\tilde{\lambda}_{I,k}, 0, s - t_0)\Big)^{\dot{m}_{D,k}-m} \Bigg), \end{aligned} \tag{3.17}$$

where $\beta_k(\boldsymbol{m}_k, m) = \binom{V_{C,k}}{m_{C,k}} \binom{V_{C,k}-m_{C,k}}{m} \binom{V_{I,k}}{\dot{m}_{D,k}-m}$ and $\dot{m}_{D,k} = m_{D,k} - V_{D,k}$. The probability that the system frequency overshoots $f_{\max}$ is thus derived as follows.

Proposition 3.5.6. Given $A_e < A_{e,\min}$ and $A_a > A_{a,\max}$, the probability of frequency overshooting the upper frequency threshold $f_{\max}$ is approximated as

$$P_{os} \approx \sum_{\mathbf{M} \in \mathcal{S}} \prod_{k=1}^{K} P_k(\boldsymbol{m}_k, \overline{T}_r), \tag{3.18}$$

where $\overline{T}_r$ is given in Proposition 3.5.3.

Proof. Please see Appendix H. □

Proposition 3.5.6 expresses the probability of frequency overshoot upon a contingency of supply deficit. On the other hand, the probability of frequency undershoot in the case of supply surplus, i.e., $A_e > 0$, can be studied using the same methodology.

Last, the results given in Propositions 3.5.1–3.5.6, their inter-relations, and

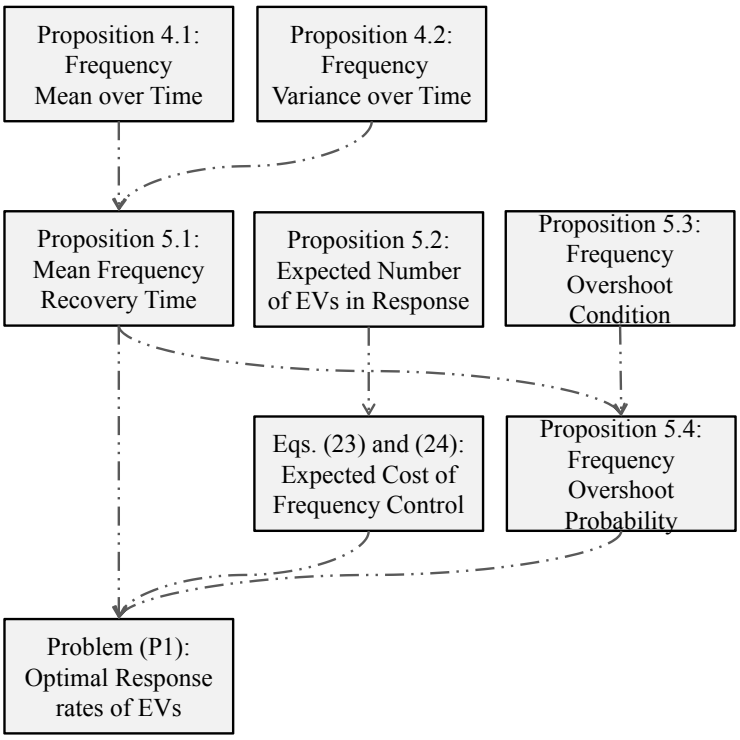

Figure 3.7: Summary of analytical results and their use in the optimal design of EVs' response rates.

their use in the optimal design of EVs' response rates (see Problem (P1) in the next section) are summarized in Fig. 3.7.

3.6 Optimal Response Rates for EVs

In the previous sections, we have provided theoretical results to characterize the performance of our frequency control algorithm via EVs. In this section, we discuss how to design EVs' response rates in different classes, i.e., $(\tilde{\lambda}_{C,k}, \tilde{\lambda}_{I,k}, \tilde{\lambda}_{D,k})$, $k = 1, \ldots, K$, so as to minimize the expected cost of implementing our frequency control algorithm subject to the EVs' requested incentive prices, EVs' practical constraints, and the given power grid performance requirements. The formulated problem can be solved offline and its solution is then be applied to set EVs' response rates in real time accordingly. For instance, the system operator can solve the

problem in a hourly/daily basis and then sends the optimal response rates to the users to set up their individual EVs. To have non-trivial cases, in this section, we assume $A_e < A_{e,\min}$ and $A_a > A_{a,\min}$.

3.6.1 Expected Frequency Control Cost

Denote $\omega_{CI,k} > 0$ and $\omega_{ID,k} > 0$ as incentive prices requested by the owner of each EV from Class k to switch its EV from the charging mode to the idle mode and from the idle mode to the discharging mode, respectively. Incentive prices requested by the owner of each EV to switch its EV from the discharging mode to the idle mode or from the idle mode to the charging mode are assumed to be zero. This is justified since the owner can charge the battery of its EV by absorbing the supply surplus or stop its ongoing discharging without any inconveniences and/or costs, which is a reasonable incentive for participating in the system frequency control. In practice, $\omega_{ID,k} \gg \omega_{CI,k}$, $\forall k \in \mathcal{K}$, since the cost/inconvenience of discharging to the power grid for each EV is much higher than that of the interrupting charging temporarily.

The expected cost of implementing our frequency control due to an EV from Class k that is initially in the charging mode given a desired frequency recovery time $T_{r,des} > t_0$ is derived as

$$G_C(\tilde{\lambda}_{C,k}, \tilde{\lambda}_{I,k}, T_{r,des}) = \omega_{CI,k} p_2(\tilde{\lambda}_{C,k}, \tilde{\lambda}_{I,k}, T_{r,des} - t_0) + (\omega_{CI,k} + \omega_{DI,k})\, p_3(\tilde{\lambda}_{C,k}, \tilde{\lambda}_{I,k}, T_{r,des} - t_0), \quad (3.19)$$

where $p_2(\lambda_C, \lambda_I, s)$ and $p_3(\lambda_C, \lambda_I, s)$ are given in (3.14) and (3.15), respectively. The first term on RHS of (3.19) shows the expected cost due to the switching from the charging mode to the idle mode, while the second term is due to the switching from the charging mode to the discharging mode. Similarly, the expected frequency control cost for an EV from Class k that is initially in the idle mode is derived as

follows

$$G_I(\tilde{\lambda}_{C,k}, \tilde{\lambda}_{I,k}, T_{r,des}) = \omega_{ID,k} p_2(\tilde{\lambda}_{I,k}, 0, T_{r,des} - t_0). \tag{3.20}$$

The results given in (3.19) and (3.20) reveal that there is a fundamental trade-off for utilizing EVs in different classes to control the system frequency, since their cost coefficients as well as their power charging/discharging rates are different in practice.

3.6.2 Problem Formulation and Solution

With cost functions obtained in the above subsection, we now proceed to optimize decision variables $\{(\tilde{\lambda}_{C,k}, \tilde{\lambda}_{I,k}, \tilde{\lambda}_{D,k})\}_{k\in\mathcal{K}}$ for minimizing the implementation cost given the desired frequency recovery time $T_{r,des}$. We impose an additional constraint to prevent the frequency overshoot (on average) based on the result given in Proposition 3.5.5. Thus, we consider the following optimization problem.

$$\begin{aligned}
(\text{P1}): \underset{\{(\tilde{\lambda}_{C,k},\tilde{\lambda}_{I,k},\tilde{\lambda}_{D,k})\}_{k\in\mathcal{K}}}{\texttt{min.}} \quad & \sum_{k=1}^{K} \Big(V_{C,k} G_C(\tilde{\lambda}_{C,k}, \tilde{\lambda}_{I,k}, T_{r,des}) \\
& \qquad + V_{I,k} G_I(\tilde{\lambda}_{C,k}, \tilde{\lambda}_{I,k}, T_{r,des}) \Big) && (3.21) \\
\texttt{s.t.} \ & \mathbb{E}\left[\, f(T_{r,des}) \,\right] \geq f_{\min}, && (3.22) \\
& \mathbb{E}\left[A_a(T_{r,des})\right] \leq A_{a,\max}, && (3.23) \\
& 0 \leq \tilde{\lambda}_{C,k} \leq \overline{\lambda}_{C,k},\ 0 \leq \tilde{\lambda}_{I,k} \leq \overline{\lambda}_{I,k},\ 0 \leq \tilde{\lambda}_{I,D} \leq \overline{\lambda}_{I,D},\ \forall k \in \mathcal{K}, && (3.24)
\end{aligned}$$

where $\overline{\lambda}_{C,k} > 0$, $\overline{\lambda}_{I,k} > 0$, and $\overline{\lambda}_{D,k} > 0$ are the maximum response rates of each EV from Class k in the charging, idle, and discharging modes, respectively. In (P1), the constraint (3.22) is for assuring that the mean of the system frequency will recover back to $f_{\min}$ by time $t = T_{r,des}$, while the constraint (3.23) is for recovering the system frequency smoothly without overshooting $f_{\max}$. In Section 3.7.1, we verify

that when constraint (3.23) holds, P_{os} is very small, i.e, the probability of frequency overshoot is negligible.

It can be verified that (P1) is a non-convex optimization problem and hence it cannot be solved globally optimally using standard convex optimization techniques such as the interior point method [90]. Consequently, we use following two assumptions to simplify (P1). First, we assume $\overline{\lambda}_{C,k} \ll \alpha$, $\forall k \in \mathcal{K}$. This assumption is valid since it is practically required to ensure that the system frequency is restored smoothly upon the contingency (see Figs. 3.4 (c)). Second, we assume $\overline{\lambda}_{I,k} \ll \overline{\lambda}_{C,k}$, $\forall k \in \mathcal{K}$. This assumption is also valid since we have $\omega_{ID,k} \gg \omega_{CI,k}$ for all classes; as a result, $\tilde{\lambda}_{I,k} \ll \tilde{\lambda}_{C,k}$, $\forall k \in \mathcal{K}$, always holds in practice to avoid unnecessary discharging of EVs. Using the aforementioned assumptions, the frequency mean characterization function can be approximated as $h_\alpha(\tilde{A}_{C,k}, \tilde{A}_{D,k}, \tilde{\lambda}_{C,k}, \tilde{\lambda}_{I,k}, s) \approx \tilde{A}_{C,k}(1 - e^{-\tilde{\lambda}_{C,k}s})$. Furthermore, we can approximate probability functions given in (3.14) and (3.15) as $p_2(\tilde{\lambda}_{C,k}, \tilde{\lambda}_{I,k}, s) \approx 1 - e^{-\tilde{\lambda}_{C,k}s}$ and $p_3(\tilde{\lambda}_{C,k}, \tilde{\lambda}_{I,k}, s) \approx 0$. Next, we make a change of variables as $(\tilde{\lambda}_{C,k}, \tilde{\lambda}_{I,k}, \tilde{\lambda}_{D,k}) \rightarrow (\phi_{C,k}, \phi_{I,k}, \phi_{D,k})$ with $\phi_{C,k} = 1 - e^{-\tilde{\lambda}_{C,k}(T_{r,des} - t_0)}$, $\phi_{I,k} = 1 - e^{-\tilde{\lambda}_{I,k}(T_{r,des} - t_0)}$, and $\phi_{D,k} = 1 - e^{-\tilde{\lambda}_{D,k}(T_{r,des} - t_0)}$, $\forall k \in \mathcal{K}$. From the above approximations and the given variable changes, we can reformulate (P1) as the following problem.

$$\text{(P2)}: \underset{\{(\phi_{C,k}, \phi_{I,k}, \phi_{D,k})\}_{k \in \mathcal{K}}}{\texttt{min.}} \quad \sum_{k=1}^{K} \left(\omega_{CI,k} V_{C,k} \phi_{C,k} + \omega_{ID,k} V_{I,k} \phi_{I,k} \right) \tag{3.25}$$

$$\texttt{s.t.} \ \sum_{k=1}^{K} V_{C,k} \tilde{A}_{C,k} \phi_{C,k} + V_{I,k} \tilde{A}_{D,k} \phi_{I,k} \geq A_{t,\min}, \tag{3.26}$$

$$\sum_{k=1}^{K} V_{C,k} \tilde{A}_{C,k} \phi_{C,k} + V_{I,k} \tilde{A}_{D,k} \phi_{I,k} \leq A_{t,\max}, \tag{3.27}$$

$$0 \leq \phi_{C,k} \leq \overline{\phi}_{C,k}, \ 0 \leq \phi_{I,k} \leq \overline{\phi}_{I,k}, \ 0 \leq \phi_{D,k} \leq \overline{\phi}_{D,k}, \ \forall k \in \mathcal{K}, \tag{3.28}$$

where $\overline{\phi}_{C,k} = 1 - e^{-\overline{\lambda}_{C,k}(T_{r,des} - t_0)}$, $\overline{\phi}_{I,k} = 1 - e^{-\overline{\lambda}_{I,k}(T_{r,des} - t_0)}$, and $\overline{\phi}_{D,k} = 1 - e^{-\overline{\lambda}_{D,k}(T_{r,des} - t_0)}$, $\forall k \in \mathcal{K}$. Note that (P2) is a LP; therefore, it can be solved efficiently using

standard optimization software, e.g., CVX [91]. From (3.26) and (3.28), it follows that (P2) is feasible iff $\sum_{k=1}^{K} V_{C,k}\tilde{A}_{C,k}\overline{\phi}_{C,k} + V_{I,k}\tilde{A}_{D,k}\overline{\phi}_{I,k} \geq A_{t,\min}$ holds, where $A_{a,\min}$ is given in (3.5). After solving (P2), we accordingly set the optimal response rates of EVs from different classes as $\tilde{\lambda}_{C,k} = -\log(1-\phi_{C,k})/(T_{r,des}-t_0)$, $\tilde{\lambda}_{I,k} = -\log(1-\phi_{I,k})/(T_{r,des}-t_0)$, and $\tilde{\lambda}_{D,k} = -\log(1-\phi_{D,k})/(T_{r,des}-t_0)$, $\forall k \in \mathcal{K}$, respectively.

Remark 3.6.1. In (P2), $\phi_{D,k}$'s do not appear neither in the objective function (3.25) nor in constraints (3.26) and (3.27). As a result, we can choose any $\phi_{D,k} \in [0,\ \overline{\phi}_{D,k}]$ as the optimal solution to (P2). By default, we set $\phi_{D,k} = \overline{\phi}_{D,k}$, $\forall k \in \mathcal{K}$, which yields $\tilde{\lambda}_{D,k} = \overline{\lambda}_{D,k}$, $\forall k \in \mathcal{K}$.

3.7 Simulation Results

To validate our analysis in Section 3.5, i.e., Propositions 3.5.1–3.5.6, we first simulate the grid frequency dynamics of IEEE 9-Bus test system [56] by setting the response rates of EVs in different classes based on the optimal solution to (P2). We then study the performance of our algorithm in the Ireland power system [25], which has a higher capacity.

3.7.1 IEEE 9-Bus Test System

We consider the IEEE 9-Bus test system [56], as shown in Fig. 3.8, where the wind farm connected to Bus 3 is planned to deliver 35MW to the power system. The aggregate model of this system is summarized in Table 2.1 (Chapter 2). We consider that there are $K = 2$ classes of EVs connected to the IEEE 9-Bus test system, where their respective parameters are given in Table 3.1, according to *SAE J1772* standard [92]. Consequently, we have $A_a = 44.64$MW. The rest of demand is non-frequency-responsive and hence does not respond to system frequency deviations.

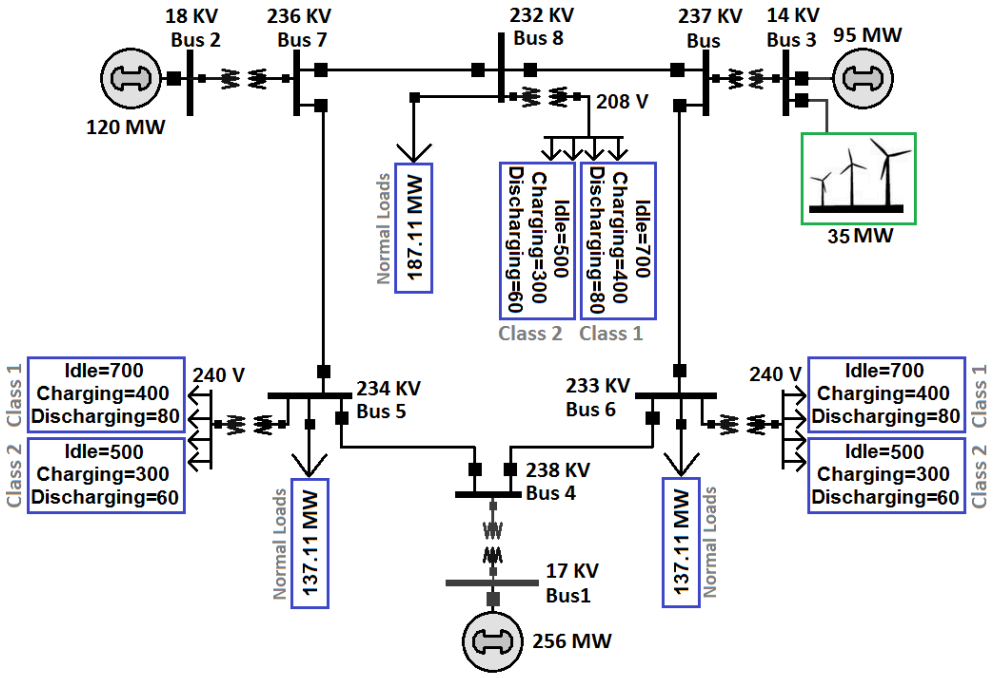

Figure 3.8: Schematic of IEEE 9-Bus test system.

We assume that EVs are equally distributed among Buses 5, 6, and 8 as shown in Fig. 3.8. We set frequency thresholds of the mode switching policies for all EVs as $(f_{\min}, f_{\max}) = (59.8, 60.2)$Hz. Let $(\omega_{CI,1}, \omega_{ID,1}) = (0.20, 1.35)$\$ and $(\omega_{CI,2}, \omega_{ID,2}) = (0.15, 1.10)$\$.[3] Assume $(\overline{\lambda}_{C,1}, \overline{\lambda}_{I,1}, \overline{\lambda}_{D,1}) = (\overline{\lambda}_{C,2}, \overline{\lambda}_{I,2}, \overline{\lambda}_{D,2}) = (0.05, 0.02, 0.05)$Hz. In the following, we study the system frequency upon a contingency of supply-demand imbalance with $A_e = -25$MW, e.g., due to the deficit in power generation of the wind farm connected to Bus 3.

First, let $T_{r,des} = 60$ seconds, which is practically valid when the power imbalance is large [72]. By solving (P2) given the above system setting, we obtain $(\tilde{\lambda}_{C,1}, \tilde{\lambda}_{I,1}, \tilde{\lambda}_{D,1}) = (0.05, 0.019, 0.05)$Hz and $(\tilde{\lambda}_{C,2}, \tilde{\lambda}_{I,2}, \tilde{\lambda}_{D,2}) = (0.05, 0, 0.05)$Hz,

[3]Note that the incentive prices $(\omega_{CI,k}, \omega_{ID,k})$'s are chosen randomly subject to the following practical constraints: i) $\omega_{CI,k} < \omega_{ID,k}$; and ii) $\omega_{ID,k} > \omega_{k,\min}$, where $\omega_{k,\min}$ denotes the minimum incentive that the owner of an EV from Class k needs to receive from the grid operator so as to recharge its EVs' battery to the same level as that before injecting power to the grid within the contingency. By assuming that the contingency of supply-demand power imbalance remains for approximately 10 minutes and the electricity tariff is 25cents/kWh, we have $\omega_{k,\min} = 0.042 A_{D,k}$\$, with $A_{D,k}$ given in kW.

Table 3.1: Parameters of EVs in IEEE-9 Bus test system.

Class (k)	Parameters					
	Supply Voltage (V)	$\tilde{A}_{C,k}$ (kW)	$\tilde{A}_{D,k}$ (kW)	$V_{C,k}$	$V_{I,k}$	$V_{D,k}$
1	208-240 AC	3.4	2.72	1200	2100	240
2	208-240 AC	11.2	8.96	900	1500	180

where these optimal response rates are used in all simulations presented in the rest of this subsection. Given the obtained optimal response rates, we compare the system frequency dynamics obtained by simulating the IEEE 9-Bus test system using Power World simulator [74] with that obtained in Proposition 3.5.1 based on the aggregate power system model. We simulate the system frequency under the above setting 100 times. The simulated system frequency mean together with its upper and lower envelopes over time are then plotted in Fig. 3.9. It is observed that the system frequency is recovered back to $f_{\min}$, without any overshoot, in about 55 seconds on average (less than the target frequency recovery time), as expected from (P2). It is also observed that the theoretical mean given in (3.7) fits very well to the simulated mean. Moreover, it is observed that the variance of the system frequency is very small, which is in accordance with our assumption made in Proposition 3.5.3. Last, from (3.4), it follows that when EVs' responses are deactivated, the system frequency drops to the steady state level 58.334Hz eventually. On the other hand, from Fig. 3.9, it is observed that when EVs' responses are active, the system frequency never drops below 58.85Hz and also returns back to the steady state level 60.01Hz quickly, which is desired for the reliable operation of the power system.

Second, we show how EVs in the same class respond in different time instants under our proposed randomized control algorithm. We consider 4 different EVs from Class 1 that are all in the charging mode initially at time $t = 0$. The states of the considered EVs over time are plotted in Fig. 3.10. From Fig. 2.7, it is observed that the grid frequency drops below $f_{\min}$ after $t_0 = 1.1$ seconds. Accordingly, EVs 1, 2, 3,

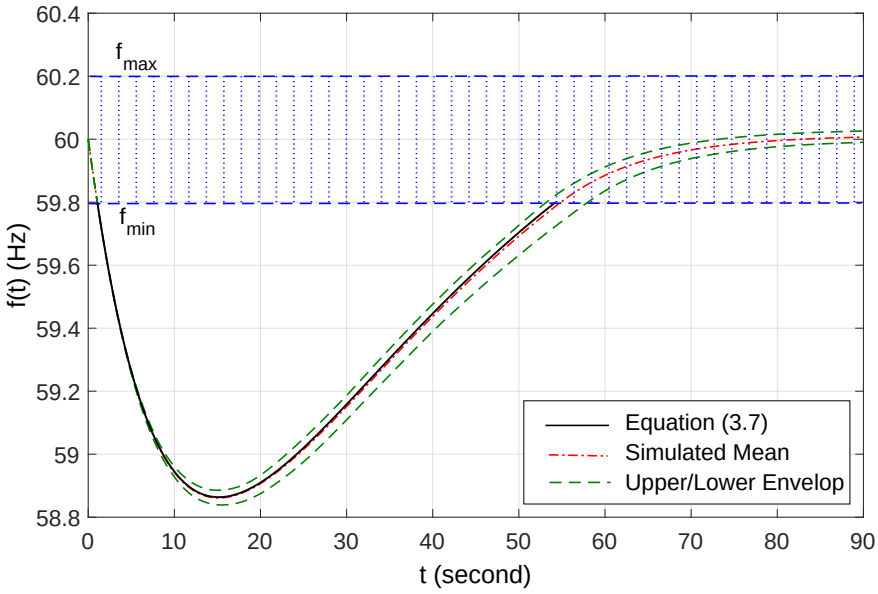

Figure 3.9: Simulated frequency dynamics of IEEE 9-Bus test system.

and 4 respond by switching from the charging mode to the idle mode at $t = 11.39$, $t = 29.72$, $t = 24.51$, and $t = 18.18$ seconds, respectively, as shown in Fig. 3.10. This is expected since due to the memoryless property of the exponential distribution, the waiting time to the first monitoring event after t_0 for an EV from Class 1 that is initially in the charging mode follows an exponential distribution with the mean $1/\tilde{\lambda}_{C,1} = 20$ seconds. Accordingly, for the four considered EVs, the mean waiting time to their first responses after t_0 is obtained as 19.85 seconds. Furthermore, it is observed from Fig. 3.10 that EVs 1 and 4 respond by switching from the idle mode to the discharging mode at $t = 49.71$ and $t = 52.24$ seconds, respectively, while EVs 2 and 3 remain in the idle mode. This is also reasonable since given $(\tilde{\lambda}_{C,1}, \tilde{\lambda}_{I,1}, \tilde{\lambda}_{D,1}) = (0.05, 0.019, 0.05)$Hz, from (3.15) it follows that a particular EV from Class 1 that is initially in the charging mode will switch to the discharging mode given the frequency recovery time $T_r \approx \overline{T}_r = 55$ seconds with the probability 0.46, i.e., it is expected that approximately 1 from every 2 EVs in Class 5 switches from the charging mode to the discharging mode by the given frequency recovery

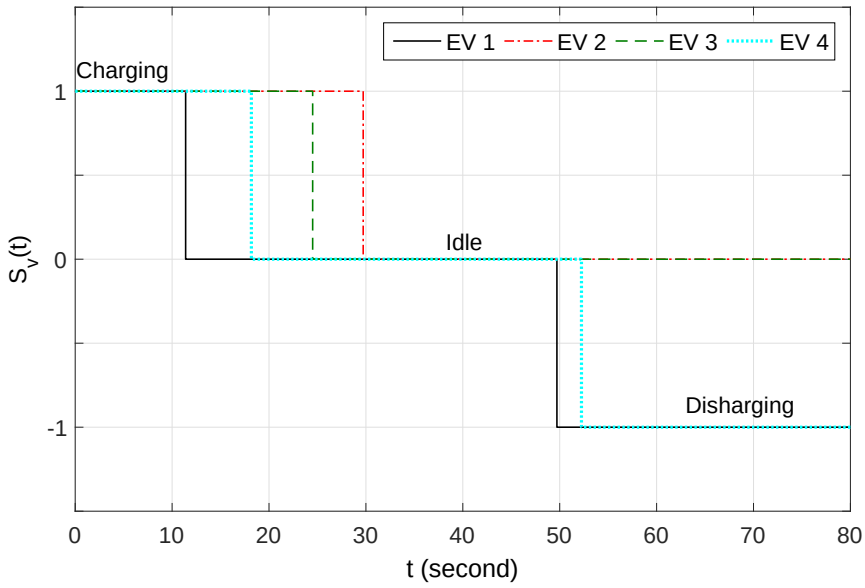

Figure 3.10: Response trajectories of four different EVs from Class 1.

time.

Third, under the above system setup, we compare the simulated and theoretical results for the frequency recovery time and the expected number of EVs from Class 1 that are in each of the three operation modes over time in Fig. 3.11. It is observed that within time $t_0 < t < T_r$, EVs from Class 1 respond by switching from the charging and idle modes to the discharging mode to boost the system frequency. Specifically, since $\tilde{\lambda}_{C,1} > \tilde{\lambda}_{I,1}$, the number of EVs from Class 1 that are in the idle mode, i.e., $N_{I,1}(t)$, increases initially until $t = 12$ seconds. It is also observed that the simulated results match our analysis given in Propositions 3.5.3 and 3.5.4 perfectly.

Fourth, we compare the probability of frequency overshoot obtained by the simulation versus the approximation given in (3.18). As shown in Fig. 3.11, the theoretical recovery time derived from Proposition 2.5.3 is $\overline{T}_r = 54.26$ seconds. By substituting this value in (3.18), we obtain $P_{os} = 10^{-8} \approx 0$. On the other hand, as shown in Fig. 3.9, the upper envelope of simulated system frequency is always

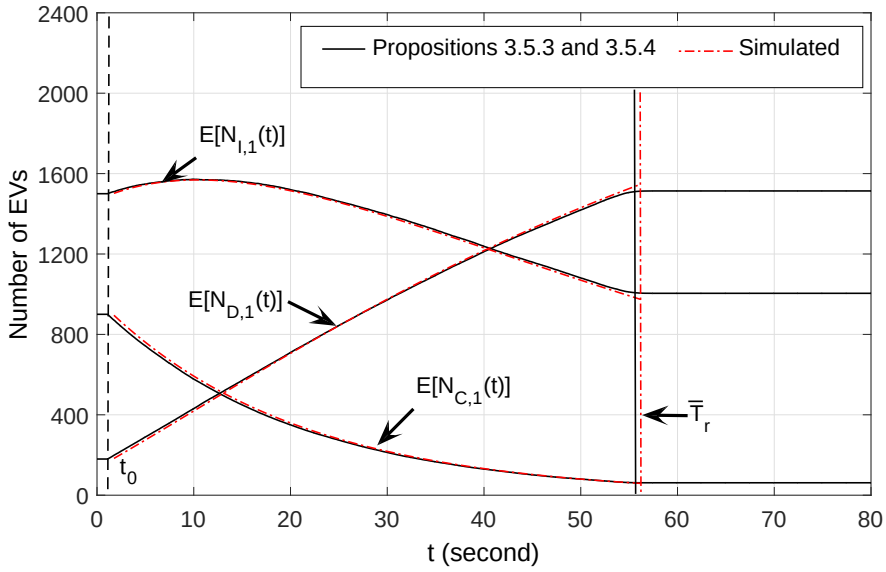

Figure 3.11: Average frequency recovery time and the expected number of EVs from Class 1 in each operational mode over time.

below $f_{\max}$, which shows that the probability of frequency overshoot is almost zero. As a result, the experimental result matches our derived theoretical approximation accurately.

Last, we evaluate the optimal frequency control solution to (P2) over $T_{r,des} \geq 40.5$, where (P2) is feasible in this range. Fig. 3.12 (a) shows the optimal (minimum) expected cost for implementing our frequency control scheme as a function of $T_{r,des}$, from which it is observed that the expected cost increases as the desired frequency recovery time reduces. This is due to the fact that for lowering the frequency recovery time, we need to set higher values for EVs' response rates and hence more EVs respond by switching their operational modes. As a result, the expected cost increases. Fig. 3.12 (b) also show the corresponding optimal response rates of EVs over $T_{r,des}$. It is observed that both $\lambda_{I,2}$ and $\lambda_{I,1}$ reduce when $T_{r,des}$ increases, since $\omega_{ID,1} > w_{CI,1}$ and $w_{ID,2} > w_{CI,1}$. Moreover, it is observed that $\lambda_{I,2}$ declines faster than $\lambda_{I,1}$ over $T_{r,des}$. This is due to the fact that $w_{ID,2} > w_{ID,1}$.

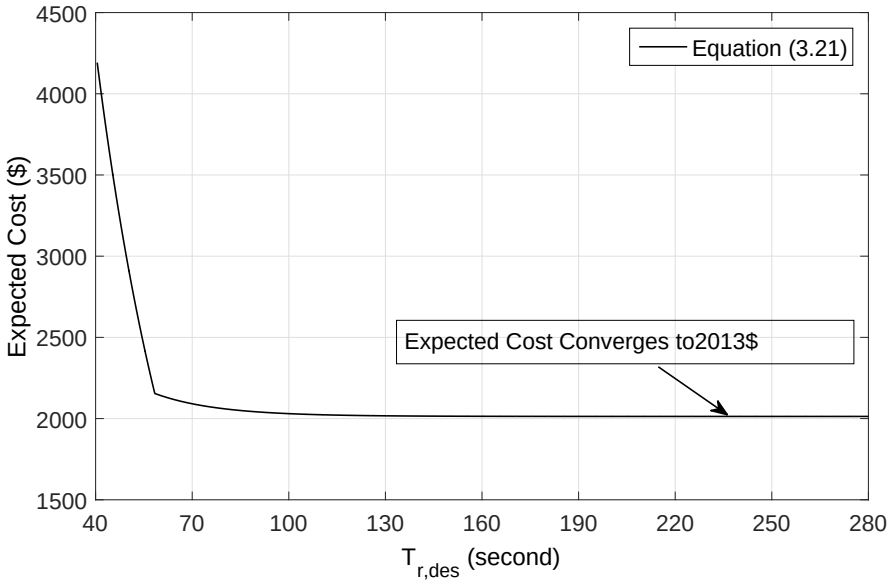

(a)

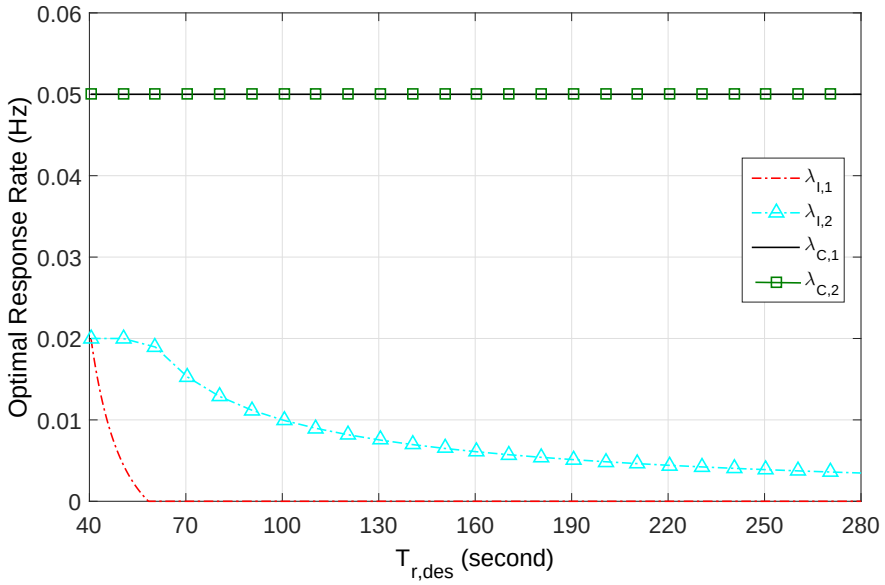

(b)

Figure 3.12: Minimum expected frequency control cost and response rates of EVs versus the desired frequency recovery time.

Table 3.2: Parameters of electric vehicles in Ireland power systrem.

Class (k)	Parameters					
	Supply Voltage (V)	$\tilde{A}_{C,k}$ (kW)	$\tilde{A}_{D,k}$ (kW)	$V_{C,k}$	$V_{I,k}$	$V_{D,k}$
1	120 AC	1.7	1.36	4000	3500	1050
2	208-240 AC	3.4	2.72	2500	1400	400
3	208-240 AC	11.2	8.96	5500	1500	1200
4	600 DC	40	32	200	1200	300
5	600 DC	100	80	100	350	200

3.7.2 Ireland Power System

In this subsection, we evaluate the performance of our EV-based frequency control algorithm upon a large-scale contingency in the Ireland power system, where parameters of the aggregate model of the Ireland power system during the winter peak demand are summarized in Table 2.1 (see Section 2.6.2 for detailed information about the Ireland power grid), which are derived based on the realistic data given in [25]. In this example, we consider that there are five different classes of EVs connected to the Ireland power system, where their corresponding parameters are given in Table 3.2, according to *SAE J1772* standard [92]. Thus, we have $A_a = 258.14$MW. We assume that EVs are distributed evenly in the whole power grid. We set the frequency thresholds for all EVs as $(f_{\min}, f_{\max}) = (49.8, 50.2)$Hz. Let $(\omega_{CI,1}, \omega_{ID,1}) = (0.12, 0.55)$\$, $(\omega_{CI,2}, \omega_{ID,2}) = (0.20, 1.35)$\$, $(\omega_{CI,3}, \omega_{ID,3}) = (0.15, 1.10)$\$, $(\omega_{CI,4}, \omega_{ID,4}) = (0.35, 2.35)$\$, and $(\omega_{CI,5}, \omega_{ID,5}) = (0.75, 3.65)$\$. Assume $(\overline{\lambda}_{C,k}, \overline{\lambda}_{I,k}, \overline{\lambda}_{D,k}) = (0.05, 0.02, 0.05)$Hz, $k = 1, \ldots, 5$. In the following, we study the system frequency upon a contingency of supply-demand imbalance with $A_e = 12.5\cos(0.3\pi t) + 3.15\cos(5.5\pi t) - 105\,\mathbf{1}_{\{t\geq 0\}} + 190\,\mathbf{1}_{\{t\geq 60\}} - 165\,\mathbf{1}_{\{t\geq 155\}} - 55\,\mathbf{1}_{\{t\geq 210\}}$ in MW, resulting from the intermittent generation power of the Slieve-Divena wind farm (30MW) in Londonderry, North Ireland, the Knockacummer wind farm (87.5 MW) in Cork and the Mount Lucas wind far (84 MW) in Offaly, Republic of Ireland,

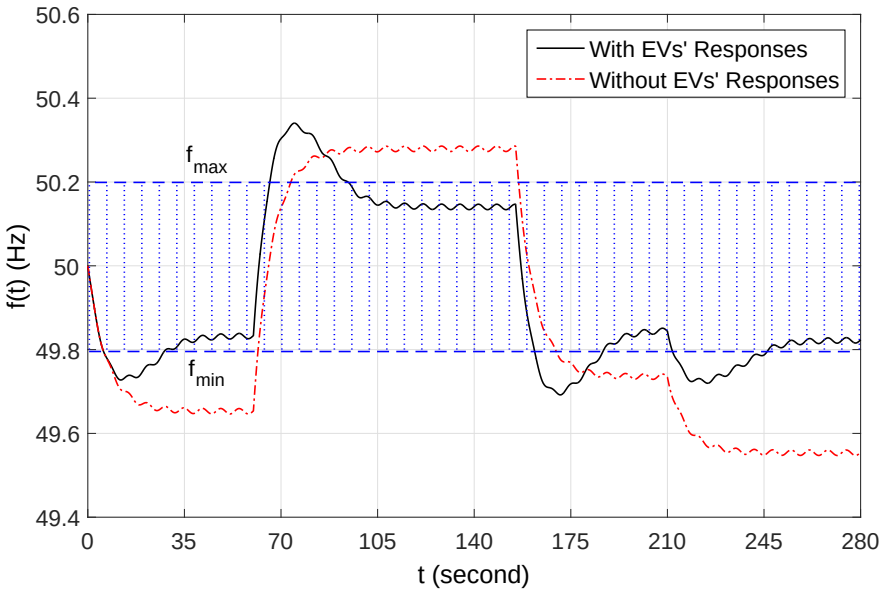

Figure 3.13: System frequency with/without EVs' responses.

as well as fluctuation of the demand over time, while $|\Delta A_g| \leq 201.5$MW.

By solving (P2) for the worst case scenario, i.e., $A_e = -201.5$MW, with the given $T_{r,des} = 60$ seconds, we obtain EVs' response rates as $(\tilde{\lambda}_{C,1}, \tilde{\lambda}_{I,1}, \tilde{\lambda}_{D,1}) = (\tilde{\lambda}_{C,2}, \tilde{\lambda}_{I,2}, \tilde{\lambda}_{D,2}) = (0.05, 0, 0.05)$Hz, $(\tilde{\lambda}_{C,3}, \tilde{\lambda}_{I,3}, \tilde{\lambda}_{D,3}) = (0.05, 0.0087, 0.05)$Hz, and $(\tilde{\lambda}_{C,4}, \tilde{\lambda}_{I,4}, \tilde{\lambda}_{D,4}) = (\tilde{\lambda}_{C,5}, \tilde{\lambda}_{I,5}, \tilde{\lambda}_{D,5}) = (0.05, 0.02, 0.05)$Hz. Given the obtained optimal response rates, we then plot the system frequency dynamics for both cases that EVs' responses are active versus deactivate in Fig. 3.13. It is observed that EVs' responses help recover the system frequency to its safe region [49.8, 50.2]Hz following each of the major power imbalances at $t = 0,\ 60,\ 155,\ 210$ seconds. However, each sinusoidal part of A_e yields an undamped frequency oscillation with a very small amplitude over the system frequency, which cannot further trigger EVs' controllers.

Second, we plot the number of EVs from Class 2 that are in each of the three operation modes over time in Fig. 3.14. It is observed that the number of EVs from this class which are in the idle mode increases over time, while the number of EVs that are in each of the charging and discharging modes decreases. This is due to the

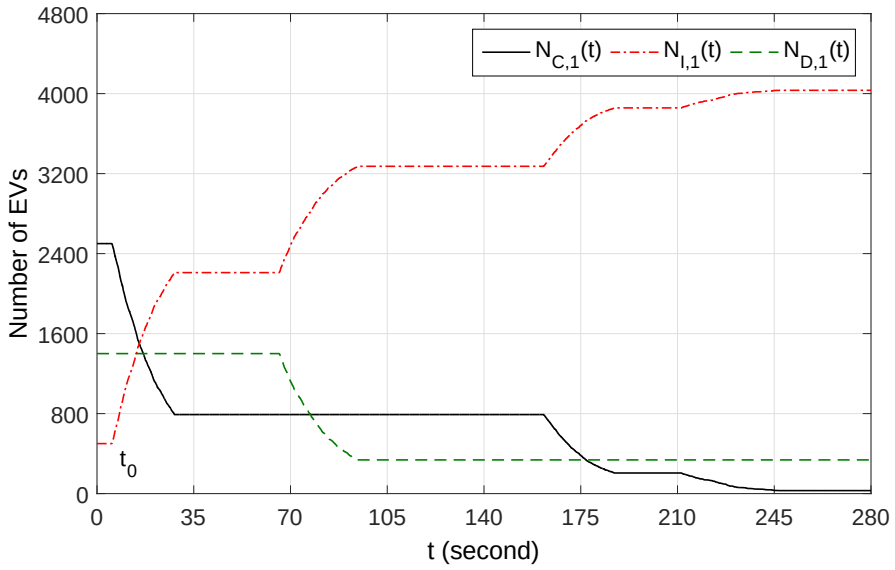

Figure 3.14: Responses of EVs in the Ireland power system.

fact that $\tilde{\lambda}_{I,2} = 0$, while $\tilde{\lambda}_{C,2} = \tilde{\lambda}_{D,2} = 0.05$Hz. This means that EVs from Class 2 can switch from the charging and discharging modes to the idle mode, while they cannot switch out of the idle mode. Hence, the number of EVs in the idle mode increases over time, while those for the other two modes decrease.

Last, we discuss how responses of EVs from different classes can affect the expected cost of implementing our frequency control algorithm. We consider five different scenarios, where for the lth scenario, $l = 1, \ldots, 5$, it is assumed that responses of EVs from Class $k = l$ are deactivated, i.e., $V_{C,l} = V_{I,l} = V_{D,l} = 0$. Accordingly, given $A_e = -200$MW ($A_e = -150$MW and $A_e = -100$MW) and $T_{r,des} = 60$ seconds, we solve (P2) for each scenario and the resulting objective value, i.e., the expected implementation cost, is given in Table 3.3. Moreover, we solve (P2) for the case that responses of EVs from all the five classes are active, where the resulting expected implementation cost is 438.56\$, 1780\$, and 8153.2\$, given $A_e = -100$MW, $A_e = -150$MW, and $A_e = -200$MW, respectively. It is observed that for each A_e, the lowest cost is achieved when responses of EVs from all classes are active. This

Table 3.3: Impacts of different active EV classes on the expected cost.

Scenario (l)	Cost ($)		
	$A_e = -100$MW	$A_e = -150$MW	$A_e = -200$MW
1	438.56	1780.58	13401.12
2	438.56	1780.58	Infeasible
3	1470.51	Infeasible	Infeasible
4	472.757	2154.72	Infeasible
5	492.81	2604.54	Infeasible

show that the diversity of EVs in response rate provide extra degree of freedom for the system operator to further minimize the cost. It is also observed that given $A_e = -200$MW, (P2) is infeasible under scenarios l, $l = 2, \ldots, 5$. Similarly, given $A_e = -150$MW, (P2) is infeasible under the third scenario. These are due to the fact that there are not enough EVs available in the system to respond and restore the system frequency to $f_{\min}$ in $T_{r,des} = 60$ seconds.

3.8 Chapter Summary

In this chapter, we proposed a new DR-enabled frequency control algorithm by utilizing randomized responses of distributed EVs. We analyzed the performance of our proposed algorithm upon a contingency of supply shortfall from various perspectives, including the mean and variance of the resulting system frequency over time, the average frequency recovery time, the expected number of EVs responded in different operational modes, and the probability of frequency overshoot due to the responses of EVs. Accordingly, we jointly designed the response rates of EVs to minimize the expected cost for implementing our proposed frequency control subject to the power grid performance requirements. It was shown via extensive simulations that the randomized responses of EVs can restore the system frequency cost-efficiently and smoothly when their response rates are appropriately designed.

Chapter 4

Frequency Control via Demand Rescheduling of Aggregators

4.1 Introduction

Price based demand response (PDR) is a commonly adopted ILC method, which adjusts the electricity prices in either day-ahead [16, 94] or real-time [95, 96] to shape the power consumption of users over time so as to achieve a certain goal. For instance, the system operator can motivate users to shift portions of their loads from the peak-demand period to the off-peak-demand period by lowering the electricity price during the off-peak-demand period. Although PDR has been successfully implemented for industrial and/or commercial users, it is challenging to utilize PDR for residential users in general due to their large population. Furthermore, each residential user has a very small amount of power consumption as compared to the aggregate demand; therefore, its contribution on the power system is insignificant. Hence, the user cannot negotiate with the system operator effectively. In this case, deploying aggregators [97] as coordinating agents between the system operator and preassigned groups of residential (and/or commercial, industrial) users can facilitate the implementation of PDR. Due to the fact that each aggregator controls a larger amount of load demand, it can effectively take part in the electricity market on behalf of its users and negotiate with the system operator, based on the agreements with both parties.

In this chapter, we investigate real-time pricing for a power system operator that sells electricity to a group of self-interested aggregators within a particular day,

named *actual day*, to achieve balanced demand and supply in long term, after a contingency of supply shortfall.[1] Under our scheme, the system operator offers real-time discounted electricity prices, which are cheaper than the day-ahead prices, to aggregators in order to incentivize them to reschedule their day-ahead demand over time; while the day-ahead values of electricity prices and demand are assumed to be given by the day-ahead electricity market before the beginning of the actual day. Since aggregators are regarded as self-interested entities, given discounted electricity prices, each aggregator reschedules its day-ahead demand over time to maximize its own utility. If discounted electricity prices are designed appropriately, aggregators will shift portions of their instantaneous demand (which are planned in the day-ahead electricity market to be consumed at this particular time) to future time periods. This can decrease the need for deploying conventional secondary/tertiary reserve services to address the supply deficit; thus, the overall cost of the power system reduces.

By assuming that the system operator has full knowledge about the behavior of aggregators, i.e., aggregators convey all data about their rescheduling problems to the system operator, we formulate a bilevel optimization problem, named *bilevel discount pricing problem* (BDPP), to design discounted electricity prices in order to minimize the system operator's *residual cost*, defined as the sum of operational costs (including the frequency control cost) from the contingency up to the end of the actual day.[2] Note that our proposed formulation is practically valid, since aggregators are rewarded by receiving cheaper electricity prices when they share the data about their rescheduling problems with the system operator. We then derive the equivalent one-level optimization problem of BDPP, named *one-level discount pricing problem* (ODPP), to solve the proposed problem efficiently.

[1]The real-time pricing scheme proposed in this paper exploits DR for providing a secondary/tertiary reserve service. Hence, it is assumed that the contingency holds for a long-time, e.g., couples of ten minutes up to hours.

[2]The results of this chapter can be extended to optimize other objective functions of the system operator, e.g., maximizing the profit or revenue of selling electric power to aggregators.

Solving BDPP and ODPP optimally is difficult, since both the problems are non-convex in general. Furthermore, the problems need to be solved efficiently to alleviate the power imbalance resulted from the contingency quickly; otherwise, the power system may experience catastrophic damages such as wide-area blackouts. Hence, we develop an efficient algorithm based on the sequential convex programming (SCP) method [99] to solve ODPP locally optimally. We also propose a randomized search (RS) based algorithm to solve heuristically BDPP, where by relying over a bidirectional communication system, this algorithm can be used to solve BDPP iteratively even without any presumed information about behavior of the aggregators.

Last, we show via a numerical example based on the Singapore power grid data [102] that the demand rescheduling of aggregators can function similarly as the conventional secondary/tertiary reserve services provided by generation units, but in a more cost-efficient manner.

4.2 Literature Review

There have been related studies reported in the literature on day-ahead or real-time pricing for managing DR [61–71]. The real-time pricing was utilized in [61–65] as a tool to motivate users to schedule their loads over time so as to achieve the maximum social welfare. Particularly, Meng *et al.* [65] solved a bilevel optimization problem to maximize the social welfare subject to reducing the electricity bills of individual users as compared to the case without DR. The real-time pricing for maximizing the net revenue of a retailer selling electric power to a group of price-responsive users was investigated in [66], where a simulated annealing based algorithm was adopted to design electricity prices offered to different users. On the other hand, the day-ahead pricing for maximizing the system operator's profit under a non-cooperative market structure was discussed in [67], where a greedy algorithm

was developed to solve the pricing problem approximately. The demand scheduling problem for a set of selfish users in a non-collaborative scenario was studied in [68], where a strategic game was adopted to solve the problem under a tiered proportional billing scheme. However, Kim *et al.* [68] did not provide any justification to show that the tiered proportional billing scheme can either minimize the total cost of the system operator or maximize its profit. Samadi *et al.* [69] studied real-time pricing for minimizing the peak-to-average ratio of the aggregate demand in a smart power grid, where the stochastic approximation approach was used to develop an efficient algorithm to design electricity prices sub-optimally. Recently, Vivekananthan *et al.* [70] introduced a reward based DR mechanism in order to shave the peak power consumption of residential users, for which the reward received by each particular user was set to be proportional to the total load deferred to the off-peak-demand period by this user as well as the impact of load adjustment of this user on improving the power grid voltage stability.

In summary, [61–70] proposed algorithms to design electricity prices/rewards for the system operator assuming that the power grid is operated under its normal condition. However, there has been less effort to investigate real-time pricing for contingency management. This is a more challenging scenario, since the proposed pricing algorithms need to converge quickly (say, in less than 5-10 minutes); otherwise, the system reliability will be jeopardized. Recently, a real-time balancing market with elastic demand was studied in [71], while the optimal bidding strategies of users in response the real-time electricity prices offered by the suppliers were unaddressed for simplicity of analysis. In contrast, in this chapter we propose a real-time pricing scheme for the system operator to manage DR in a group of self-interested aggregators to provide cost-efficient secondary/tertiary reserve services. Last, note that our formulated pricing problem in this chapter substantially differs from that investigated in [9,36,71], since we take the selfish behavior of aggregators into account.

4.3 System Model

We consider a power system consisting of $H \geq 1$ aggregators, indexed by h, $h \in \mathcal{H} = \{1, \ldots, H\}$, each of which purchases electric power from the system operator to satisfy demand of its residential, commercial, and/or industrial users within the actual day. We consider a time-slotted system with index $n, n \in \mathcal{N} = \{1, \ldots, N\}$, where $N \geq 1$ (typical values are 24 or 48) is the total number of time slots in the actual day that have even durations of $24/N$ hours. We further consider a quasi-static time-varying model for demand of aggregators, where the demand of each aggregator is constant during each time slot, but it may change from one time slot to another time slot.

We assume that the day-ahead electricity market is held before the beginning of the actual day, where $\dot{\boldsymbol{x}}_h = [\dot{x}_{h,1}, \ldots, \dot{x}_{h,N}]^T$ and $\dot{\boldsymbol{y}}_h = [\dot{y}_{h,1}, \ldots, \dot{y}_{h,N}]^T$ are given as the day-ahead electricity price and the day-ahead demand (i.e., the sum of its users' demand) for each aggregator h, respectively. Note that $\dot{\boldsymbol{y}}_h$ and $\dot{\boldsymbol{x}}_h$ are the scheduled/planned values of demand and price for aggregator h within the actual day, respectively. By default, we assume $\sum_{n=1}^{N} \dot{y}_{h,n} = y_{h,tot}$, $\underline{y}_{h,n} \leq \dot{y}_{h,n} \leq \overline{y}_{h,n}$, $x_{h,n} \geq \underline{x}_n$, $\forall h \in \mathcal{H}$, $\forall n \in \mathcal{N}$, hold, where $\underline{x}_n > 0$'s are the marginal electricity prices over time and $y_{h,tot}$, $\sum_{n=1}^{N} \underline{y}_{h,n} \leq y_{h,tot} \leq \sum_{n=1}^{N} \overline{y}_{h,n}$, is the total demand of aggregator h in the actual day, which should be fully satisfied by the end of time slot N. However, $\underline{y}_{h,n} > 0$ and $\overline{y}_{h,n} > \underline{y}_{h,n}$ represent the minimum and maximum limits for the demand of aggregator h at time slot n, respectively, which should be held to meet time-inflexible demand of its users.

In the actual day, we assume that an emergency event occurs at the beginning of time slot n_0, $1 \leq n_0 < N$, which results in $A_e < 0$ amount of supply-demand power imbalance (supply deficit) over time slots $n_0 \leq n \leq n_1$, where $n_1 \in \mathcal{N}_0 = \{n_0, \ldots, N\}$. In this cases, the system operator holds the real-time electricity market and negotiates with the aggregators to reschedule their demand to alleviate the

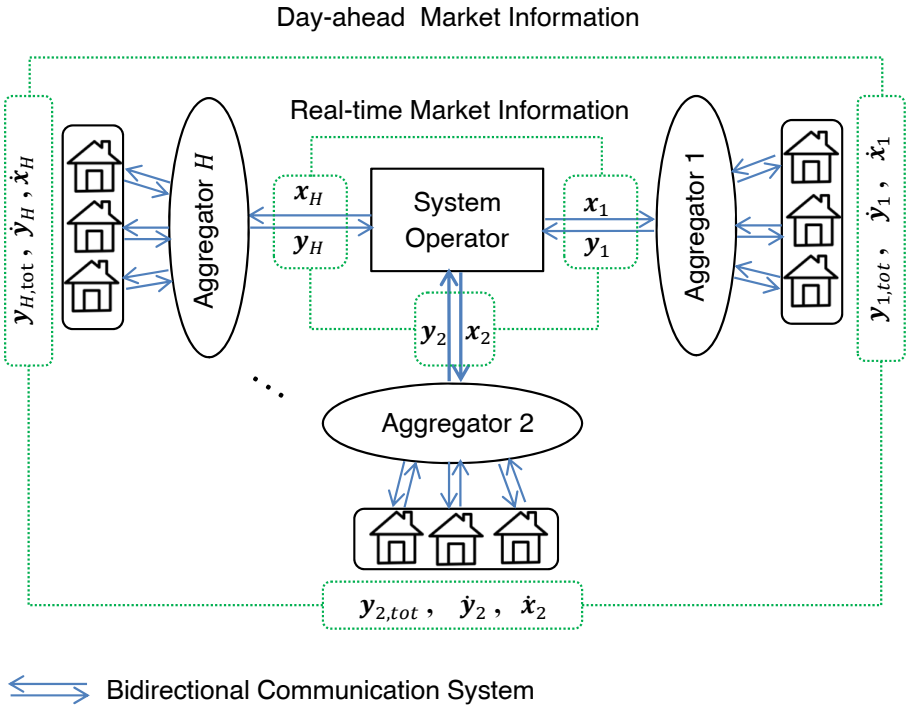

Figure 4.1: Real-time versus day-ahead market information sharing.

power imbalance in long term, which is in contrast to the short term responses of SAPPs/EVs that have been discussed previously in Chapters 2 and 3.

4.4 Proposed Real-Time Pricing Scheme

Fig. 4.1 shows the schematic of the power system considered in this paper. We assume that the system operator offers the real-time discounted electricity price $\boldsymbol{x}_h = [x_{h,n_0}, \ldots, x_{h,N}]^T$, $\underline{x}_n \leq x_{h,n} \leq \dot{x}_{h,n}$, $\forall n \in \mathcal{N}_0$, to each aggregator h in order to incentivize this aggregator to reschedule its day-ahead demand over time slots $n_0 \leq n \leq N$. Typically, the real-time price $x_{h,n}$ is more attractive (lower as compared to the day-ahead price $\dot{x}_{h,n}$) after the contingency, i.e., $n_1 < n \leq N$, versus during the contingency, i.e., $n_0 \leq n \leq n_1$, to motivate aggregator h to shift more loads to future time slots after the contingency. Let $\boldsymbol{y}_h = [y_{h,n_0}, \ldots, y_{h,N}]^T$, where $\sum_{n=n_0}^{N} y_{h,n} = y_{h,tot} - \sum_{n=1}^{n_0-1} \dot{y}_{h,n}$ and $\underline{y}_{h,n} \leq y_{h,n} \leq \overline{y}_{h,n}$, $\forall n \in \mathcal{N}_0$, be the rescheduled demand of

aggregator h. Since aggregators are regarded as self-interested entities, given the discounted electricity price $\boldsymbol{x}_h$, each aggregator h designs its rescheduled demand $\boldsymbol{y}_h$ to maximize its utility. On the other hand, the system operator designs $\boldsymbol{x}_h$, $\forall h \in \mathcal{H}$, so as to minimize its residual cost, i.e., the sum of operational costs of the power system over time slots $n = n_0, \ldots, N$ (time slots $n = 1, \ldots, n_0 - 1$ are past and no changes can be applied for these slots). Note that this approach can help the system operator to reduce its total operational cost, while aggregators also have the opportunity to reduce their total electricity bills by responding to the offered discounted electricity prices.

4.5 Problem Formulation

In this section, we first formulate the demand rescheduling problem for each aggregator h, given the offered discounted electricity price $\boldsymbol{x}_h$. Next, we formulate BDPP for the system operator to design $\boldsymbol{x}_h$, $h = 1, \ldots, H$. Moreover, we derive ODPP, i.e., the equivalent one-level optimization problem of BDPP, to derive our solution based on it.

4.5.1 Demand Rescheduling Problem

Each aggregator h designs its rescheduled demand $\boldsymbol{y}_h$ to maximize its utility, where the utility is defined as the weighted sum of the negative of its residual bill for purchasing electric power from the system operator, $B_h(\boldsymbol{x}_h, \boldsymbol{y}_h) = \sum_{n=n_0}^{N} x_{h,n}\ y_{h,n}$, and its service quality index that interprets the satisfaction of its users given the rescheduled demand. Specifically, we model the service quality index of aggregator h by a predefined function $Q_h(\boldsymbol{y}_h)$, which is assumed to be concave and differentiable over $\boldsymbol{y_h} \geq 0$. We also assume that $Q_h(\boldsymbol{y}_h)$ achieves its maximum value equal to unity iff $y_{h,n} = \dot{y}_{h,n}$, $\forall n \in \mathcal{N}_0$, i.e., the planned demand of aggregator in the day-ahead electricity market remains unchanged.

Given the discounted electricity price $\boldsymbol{x}_h$, we present the rescheduling problem for each aggregator h, as follows

$$(\text{DR}-h): \quad \underset{\boldsymbol{y}_h}{\texttt{max.}} \; Q_h(\boldsymbol{y}_h) - \theta_h B_h(\boldsymbol{x}_h, \boldsymbol{y}_h) \tag{4.1}$$

$$\texttt{s.t.} \; \underline{y}_{h,n} \leq y_{h,n} \leq \overline{y}_{h,n}, \; \forall n \in \mathcal{N}_0, \tag{4.2}$$

$$\sum_{n=n_0}^{N} y_{h,n} = y_{h,tot} - \sum_{n=1}^{n_0-1} \dot{y}_{h,n}, \tag{4.3}$$

where $\theta_h \geq 0$ is a constant weight for aggregator h, which can be used to adjust the trade-off between its service quality index and its residual electricity bill. It can be readily verified that with given $\boldsymbol{x}_h$, (DR$-h$) is a convex optimization problem. For convenience, we define $U_h(\boldsymbol{y}_h, \boldsymbol{x}_h) = Q_h(\boldsymbol{y}_h) - \theta_h B_h(\boldsymbol{x}_h, \boldsymbol{y}_h)$ and Ω_h as the utility function of aggregator h and the convex set specified by the constraints given in (4.2) and (4.3) over $\boldsymbol{y}_h$, respectively.

4.5.2 Bilevel Discount Pricing Problem (BDPP)

The system operator designs discounted electricity prices $\boldsymbol{x}_h$, $\forall h \in \mathcal{H}$, so as to minimize its total operational cost till the end of actual day. We model the operational costs (including the costs of power generation, transmission, ramping up/down reserve services, etc.) of the system operator over time by a sequence of time-variant functions $C_n(g_n)$, $\forall n \in \mathcal{N}$, where $g_n \geq 0$ is the total electric power generated at time slot n. Specifically, we assume that each $C_n(g_n)$ is a convex non-decreasing function with a finite value over $g_n \leq \overline{g}_n$, where $\overline{g}_n \gg \sum_{h=1}^{H} \overline{y}_{h,n}$. This is justified by considering that fact that the power system has adequate generation resources to meet the maximum demand of all aggregators, while the generation cost may increase drastically.

From (DR$-h$), it has been revealed that the rescheduled demand of aggregator h is an implicit function of the discounted electricity price $\boldsymbol{x}_h$. Hence, there is a

hierarchical relationship between demand rescheduling problems of aggregators and the discount pricing problem of the system operator. Assume that the system operator has full knowledge about behavior of all aggregators, i.e., the system operator knows (DR$-h$), $\forall h \in \mathcal{H}$. We thus formulate BDPP to minimize the residual cost of the power system as

$$\text{(G1)}: \min_{\{\boldsymbol{x}_h\}_{h\in\mathcal{H}},\{\boldsymbol{y}_h\}_{h\in\mathcal{H}}} \sum_{n=n_0}^{n_1} C_n(\sum_{h=1}^{H} y_{h,n} - A_e) + \sum_{n=n_1+1}^{N} C_n(\sum_{h=1}^{H} y_{h,n}) \tag{4.4}$$

$$\text{s.t. } \underline{x}_n \leq x_{h,n} \leq \dot{x}_{h,n},\ \forall n \in \mathcal{N}_0,\ \forall h \in \mathcal{H}, \tag{4.5}$$

$$\boldsymbol{y}_h \in \arg\max_{\boldsymbol{z}_h\in\Omega_h} U_h(\boldsymbol{z}_h, \boldsymbol{x}_h),\ \forall h \in \mathcal{H}, \tag{4.6}$$

where $\boldsymbol{z}_h = [z_{h,n_0}, \ldots, z_{h,N}]^T$, $\forall h \in \mathcal{H}$, are dummy variables. Alternatively, interactions among the system operator and aggregators can be captured by Stackelberg game (see Appendix I for more information), where the solution to (G1) returns the Stackelberg equilibrium point. It is also worth noting that [104, 105] have recently proposed mathematical models to approximately express the behavior of each aggregator (or user) in response to the electricity prices offered by the system operator, where the coefficients of the models are all tuned based on the historical data of the electricity market. In this case, we can replace the constraints given in (4.6) by the models proposed in [104, 105] to approximately design electricity prices for the system operator.

In (G1), the electric power generated at each time slot n, $n_0 \leq n \leq n_1$, is offset by $-A_e$ ($A_e < 0$), which means that the system operator generates $-A_e$ amount of electric power more than that requested by all aggregators to compensate the supply shortfall. From the hierarchical point of view, we term the minimization problem resulted from (G1) by ignoring the constraints in (4.6) as the *upper level problem*, while we term (DR$-h$), $\forall h \in \mathcal{H}$, as *lower level problems*, which appear in (4.6) to interpret the impacts of aggregators' demand rescheduling problems on the pricing

problem of system operator.

For convenience, we define $C_{res}(\boldsymbol{y}_1, \ldots, \boldsymbol{y}_H) = \sum_{n=n_0}^{n_1} C_n(\sum_{h=1}^{H} y_{h,n} - A_e) + \sum_{n=n_1+1}^{N} C_n(\sum_{h=1}^{H} y_{h,n})$. Although $C_{res}(\cdot)$ is a convex function over $\boldsymbol{y}_h$'s and the constraints given in (4.5) specify a convex set over $\boldsymbol{x}_h$'s, (G1) is in general a non-convex optimization problem. This is due to the coupling between $\boldsymbol{x}_h$ and $\boldsymbol{y}_h$ for each $h \in \mathcal{H}$ as expressed in (4.6), together with the fact that $U_h(\boldsymbol{y}_h, \boldsymbol{x}_h)$ is neither a convex nor concave function over $\boldsymbol{y}_h$ and $\boldsymbol{x}_h$. As a result, (G1) cannot be solved optimally globally via standard convex optimization techniques such as interior point method. In the following, we reformulate (G1) into a simplified form by exploiting the dual problem of (DR$-h$), $\forall h \in \mathcal{H}$, to obtain a locally optimal solution to the resulting problem.

4.5.3 One-level Discount Pricing Problem (ODPP)

For (DR$-h$), we denote $\underline{v}_{h,n}$ and $\overline{v}_{h,n}$, $\forall n \in \mathcal{N}_0$, as the Lagrange dual variables associated with constraints $\underline{y}_{h,n} \leq y_{h,n}$ and $y_{h,n} \leq \overline{y}_{h,n}$, respectively, given in (4.2). We also denote w_h, $h = 1, \ldots, H$, as the Lagrange dual variables associated with the constraints given in (4.3). For convenience, we define $\underline{\boldsymbol{v}}_h = [\underline{v}_{h,n_0}, \ldots, \underline{v}_{h,N}]^T$ and $\overline{\boldsymbol{v}}_h = [\overline{v}_{h,n_0}, \ldots, \overline{v}_{h,N}]^T$. Accordingly, we can derive the Lagrangian of problem (DR$-h$) as

$$\mathcal{L}_h = Q_h(\boldsymbol{y}_h) - \theta_h B_h(\boldsymbol{x}_h, \boldsymbol{y}_h) + \sum_{n=n_0}^{N} \underline{v}_{h,n}(y_{h,n} - \underline{y}_{h,n}) + \sum_{n=n_0}^{N} \overline{v}_{h,n}(\overline{y}_{h,n} - y_{h,n}) - w_h\Bigg(\sum_{n=n_0}^{N} y_{h,n} - y_{h,tot} + \sum_{n=1}^{n_0-1} \dot{y}_{h,n}\Bigg). \quad (4.7)$$

Since (DR$-h$) is a convex optimization problem and holds the Slater's condition (linear constraints), any set of primal and dual points, i.e., $(\boldsymbol{y}_h, \underline{\boldsymbol{v}}_h, \overline{\boldsymbol{v}}_h, w_h)$, which satisfies the Karush-Kuhn-Tucker (KKT) conditions of (DR$-h$), will be its primal and dual optimal solutions [90]. Specifically, the KKT conditions of (DR$-h$) are

listed below

$$q_{h,n}(\boldsymbol{y_h}) - \theta_h x_{h,n} + \underline{v}_{h,n} - \overline{v}_{h,n} - w_h = 0,\ \forall n \in \mathcal{N}_0, \tag{4.8}$$

$$\underline{v}_{h,n}(y_{h,n} - \underline{y}_{h,n}) = 0,\ \forall n \in \mathcal{N}_0, \tag{4.9}$$

$$\overline{v}_{h,n}(\overline{y}_{h,n} - y_{h,n}) = 0,\ \forall n \in \mathcal{N}_0, \tag{4.10}$$

$$\underline{y}_{h,n} \leq y_{h,n} \leq \overline{y}_{h,n},\ \forall n \in \mathcal{N}_0, \tag{4.11}$$

$$\sum_{n=n_0}^{N} y_{h,n} = y_{h,tot} - \sum_{n=1}^{n_0-1} y_{h,n}, \tag{4.12}$$

$$\underline{v}_{h,n} \geq 0,\ \overline{v}_{h,n} \geq 0,\ \forall n \in \mathcal{N}_0, \tag{4.13}$$

where $q_{h,n}(\boldsymbol{y_h}) = \partial Q_h(\boldsymbol{y}_h)/\partial y_{h,n}$. Note that (4.8) follows due to the fact that the gradient of the Lagrangian with respect to $\boldsymbol{y}_h$ must vanish, (4.9) and (4.10) stand for the complimentary slackness, and (4.11)–(4.13) represent the primal and dual feasibility constraints. Let $\boldsymbol{w} = [w_1, \ldots, w_H]^T$. Based on the KKT conditions listed above, we can rewrite (G1) as a one-level optimization problem, named ODPP, as follows

$$\text{(G2)}: \underset{\{\boldsymbol{x}_h\}_{h\in\mathcal{H}},\{\boldsymbol{y}_h\}_{h\in\mathcal{H}},\{\underline{\boldsymbol{v}}_h\}_{h\in\mathcal{H}},\{\overline{\boldsymbol{v}}_h\}_{h\in\mathcal{H}},\boldsymbol{w}}{\texttt{min.}} C_{res}(\boldsymbol{y}_1, \ldots, \boldsymbol{y}_H)$$
$$\texttt{s.t.}\ (4.5) \text{ and } (4.8) - (4.13), \forall h \in \mathcal{H}.$$

It can be verified that (G2) is a non-convex optimization problem due to the constraints given in (4.8)–(4.10), $\forall h \in \mathcal{H}$. However, we can solve (G2) at least locally optimally, as will be shown in the next section.

4.6 Proposed Solution

Herein, we develop an SCP based algorithm [99] to solve ODPP, i.e., (G2). We also propose an RS based algorithm to solve BDPP, i.e., (G1).

4.6.1 SCP Based Algorithm

SCP is an iterative method to solve non-convex problems locally optimally, by leveraging convex optimization techniques shown as follows. At each iteration itr, $itr = 1, 2, \ldots$, we approximate non-convex constraints and/or objective function of the considered optimization problem, i.e., the constraints (4.8)–(4.10), $\forall h \in \mathcal{H}$, in problem (G2), by a set of convex functions (linear or quadratic function) over a certain convex *trust region* $\mathcal{R}^{(itr)}$ to form a convex *approximate* optimization problem. Next, we set the decision variables for iteration itr as the optimal solution to the approximate problem at iteration itr. The algorithm continues until a presumed stopping criterion is satisfied. In the following, we provide details of our SCP based algorithm to solve (G2).

Let $\pi_{SCP}^{(itr-1)} = (\{\boldsymbol{x}_{h,SCP}^{(itr-1)}\}_{h\in\mathcal{H}}, \{\boldsymbol{y}_{h,SCP}^{(itr-1)}\}_{h\in\mathcal{H}}, \{\underline{\boldsymbol{v}}_{h,SCP}^{(itr-1)}\}_{h\in\mathcal{H}}, \{\overline{\boldsymbol{v}}_{h,SCP}^{(itr-1)}\}_{h\in\mathcal{H}}, \boldsymbol{w}_{SCP}^{(itr-1)})$ denote the values of decision variables of (G2) at the beginning of iteration each itr, where $\pi_{SCP}^{(0)}$ is a given initial point at iteration 1. For each $h \in \mathcal{H}$, $n \in \mathcal{N}_0$, we approximate its corresponding constrain in (4.8) using its first-order Taylor series around $\pi_{SCP}^{(itr-1)}$ as follows

$$q_{h,n}(\boldsymbol{y}_{h,SCP}^{(itr-1)}) + \nabla q_{h,n}(\boldsymbol{y}_{h,SCP}^{(itr-1)})^T(\boldsymbol{y}_h - \boldsymbol{y}_{h,SCP}^{(itr-1)}) - \theta_h x_{h,n} + \underline{v}_{h,n} - \overline{v}_{h,n} - w_h = 0, \tag{4.14}$$

with $\nabla q_{h,n}(\boldsymbol{y}_h) = [\partial q_{h,n}(\boldsymbol{y}_h)/\partial y_{h,n_0}, \ldots, \partial q_{h,n}(\boldsymbol{y}_h)/\partial y_{h,N}]^T$. Similarly, for each $h \in \mathcal{H}$, $n \in \mathcal{N}_0$, we approximate its corresponding constrains in (4.9) and (4.10) using their first-order Taylor series around $\pi_{SCP}^{(itr-1)}$ as

$$\underline{v}_{h,n}(y_{h,n,SCP}^{(itr-1)} - \underline{y}_{h,n}) + \underline{v}_{h,n,SCP}^{(itr-1)}(y_{h,n} - y_{h,n,SCP}^{(itr-1)}) = 0, \tag{4.15}$$

$$\overline{v}_{h,n}(\overline{y}_{h,n} - y_{h,n,SCP}^{(itr-1)}) - \overline{v}_{h,n,SCP}^{(itr-1)}(y_{h,n} - y_{h,n,SCP}^{(itr-1)}) = 0, \tag{4.16}$$

respectively. Since approximations given in (4.14)–(4.16) are accurate in the vicinity

of $(\{\boldsymbol{y}_{h,SCP}^{(itr-1)}\}_{h\in\mathcal{H}}, \{\underline{\boldsymbol{v}}_{h,SCP}^{(itr-1)}\}_{h\in\mathcal{H}}, \{\overline{\boldsymbol{v}}_{h,SCP}^{(itr-1)}\}_{h\in\mathcal{H}})$, we define a convex trust region $\mathcal{R}^{(itr)}$ to restrict the space of searching for $\pi_{SCP}^{(itr)}$ with better accuracy. In particular, at iteration itr, we define

$$\begin{aligned}\mathcal{R}^{(itr)} \quad = \quad \Big\{ & (\{\boldsymbol{y}_h\}_{h\in\mathcal{H}}, \{\underline{\boldsymbol{v}}_h\}_{h\in\mathcal{H}}, \{\overline{\boldsymbol{v}}_h\}_{h\in\mathcal{H}}) \;\Big|\; \|\boldsymbol{y}_h - \boldsymbol{y}_{h,SCP}^{(itr-1)}\|_\infty \le \rho, \\ & \|\underline{\boldsymbol{v}}_h - \underline{\boldsymbol{v}}_{h,SCP}^{(itr-1)}\|_\infty \le \rho, \|\overline{\boldsymbol{v}}_h - \overline{\boldsymbol{v}}_{h,SCP}^{(itr-1)}\|_\infty \le \rho,\ \forall h \in \mathcal{H} \Big\}, \end{aligned} \tag{4.17}$$

where $\rho > 0$ is a constant that controls the size of the trust region. We set ρ to be a small value (as compared to the range of decision variables) to have accurate approximations. Note that for $\mathcal{R}^{(itr)}$, we do not impose any limits on $\boldsymbol{x}_h$'s and $\boldsymbol{w}$ since the non-linear terms of constraints (4.8)–(4.10) do not involve these decision variables.

Although for each h we can replace the constraints given in (4.8)–(4.10) by the approximated expressions derived in (4.14)–(4.16) to form the approximate problem of (G2), the resulting problem may or may not be feasible given any arbitrary chosen initial point $\pi_{SCP}^{(0)}$. To alleviate this issue, we add a penalty function associated with the constraints in (4.14)–(4.16) into the objective of the approximate problem of (G2) instead of applying them as explicit constraints [99]. For each $h \in \mathcal{H}$, we define the penalty function at iteration itr as follows

$$\begin{aligned}&\phi_h^{(itr)}(\boldsymbol{x}_h, \boldsymbol{y}_h, \underline{\boldsymbol{v}}_h, \overline{\boldsymbol{v}}_h, w_h) = \\ &\xi\Bigg(\sum_{n=n_0}^{N} \Big| q_{h,n}(\boldsymbol{y}_{h,SCP}^{(itr-1)}) + \nabla q_{h,n}(\boldsymbol{y}_{h,SCP}^{(itr-1)})^T(\boldsymbol{y}_h - \boldsymbol{y}_{h,SCP}^{(itr-1)}) - \theta_h x_{h,n} + \underline{v}_{h,n} - \overline{v}_{h,n} - w_h \Big| \\ &+ \sum_{n=n_0}^{N} \Big| \underline{v}_{h,n}(y_{h,n,SCP}^{(itr)} - \underline{y}_{h,n}) + \underline{v}_{h,n,SCP}^{(itr-1)}(y_{h,n} - y_{h,n,SCP}^{(itr-1)}) \Big| \\ &+ \sum_{n=n_0}^{N} \Big| \overline{v}_{h,n}(\overline{y}_{h,n} - y_{h,n,SCP}^{(itr-1)}) - \overline{v}_{h,n,SCP}^{(itr-1)}(y_{h,n} - y_{h,n,SCP}^{(itr-1)}) \Big| \Bigg), \end{aligned} \tag{4.18}$$

where $\xi \gg 1$ (a large constant) is a given penalty coefficient. Accordingly, we can

express the approximate problem of (G2) for each iteration itr, $it = 1, 2, \ldots$, as follows

$$(\text{G2} - itr): \underset{\{\boldsymbol{x}_h\}_{h\in\mathcal{H}},\{\boldsymbol{y}_h\}_{h\in\mathcal{H}},\{\underline{\boldsymbol{v}}_h\}_{h\in\mathcal{H}},\{\overline{\boldsymbol{v}}_h\}_{h\in\mathcal{H}},\boldsymbol{w}}{\texttt{min.}} C_{res}(\cdot) + \sum_{h=1}^{H} \phi_h^{(itr)}(\cdot)$$
$$\texttt{s.t. } (4.5) \text{ and } (4.11) - (4.13), \forall h \in \mathcal{H},$$
$$(\{\boldsymbol{y}_h\}_{h\in\mathcal{H}}, \{\underline{\boldsymbol{v}}_h\}_{h\in\mathcal{H}}, \{\overline{\boldsymbol{v}}_h\}_{h\in\mathcal{H}}) \in \mathcal{R}^{(itr)}.$$

It can be verified that (G2$-itr$) is a convex optimization problem and thus it can be solved efficiently by, e.g., the interior-point method [90]. After solving (G2$-itr$), we then set $\pi_{SCP}^{(itr)}$ to be the obtained optimal solution.

In order to stop the algorithm, we first derive the Euclidean distance between $\pi_{SCP}^{(itr-1)}$ and $\pi_{SCP}^{(itr)}$ as

$$ED(\pi_{SCP}^{(itr-1)}, \pi_{SCP}^{(itr)}) = \Bigg(\|\boldsymbol{r}_{SCP}^{(itr-1)} - \boldsymbol{r}_{SCP}^{(itr)}\|_2^2 + \sum_{h=1}^{H} \Bigg(\|\boldsymbol{x}_{h,SCP}^{(itr-1)} - \boldsymbol{x}_{h,SCP}^{(itr)}\|_2^2 + \|\boldsymbol{y}_{h,SCP}^{(itr-1)} - \boldsymbol{y}_{h,SCP}^{(itr)}\|_2^2 + \|\underline{\boldsymbol{v}}_{h,SCP}^{(itr-1)} - \underline{\boldsymbol{v}}_{h,SCP}^{(itr)}\|_2^2 + \|\overline{\boldsymbol{v}}_{h,SCP}^{(itr-1)} - \overline{\boldsymbol{v}}_{h,SCP}^{(itr)}\|_2^2 \Bigg) \Bigg)^{1/2}. \tag{4.19}$$

Accordingly, we evaluate

$$\mathcal{E} = \max \Bigg\{ \frac{1}{\xi} \sum_{h=1}^{H} \phi_h^{(itr)}(\boldsymbol{x}_{h,SCP}^{(itr)}, \boldsymbol{y}_{h,SCP}^{(itr)}, \underline{\boldsymbol{v}}_{h,SCP}^{(itr)}, \overline{\boldsymbol{v}}_{h,SCP}^{(itr)}, w_{h,SCP}^{(itr)}), ED(\pi_{SCP}^{(itr-1)}, \pi_{SCP}^{(itr)}) \Bigg\}. \tag{4.20}$$

Let $\epsilon > 0$ be a given stopping threshold for the algorithm. If $\mathcal{E} \leq \epsilon$, then the algorithm terminates. Otherwise, if $\mathcal{E} > \epsilon$, then the algorithm continues to the next iteration. Our SCP based algorithm is summarized in Table 4.1. Last, note that since (G2-itr) is decreasing over the iteration, the convergence of the SCP based algorithm is guaranteed.

Table 4.1: SCP based algorithm for (G2).

a) Initialize $itr \leftarrow 0$, $\rho > 0$, $\xi \gg 1$, $\epsilon > 0$, $\mathcal{E} > \epsilon$, and choose any initial point $\pi_{SCP}^{(0)}$ satisfying the linear constraints given in (4.5) and (4.11)–(4.13).

b) **While** Err $< \epsilon$ **do**:

   1) Set $itr \leftarrow itr + 1$.
   2) Specify the trust region $\mathcal{R}^{(itr)}$ given in (4.17).
   3) Form $\phi_h^{(itr)}(\boldsymbol{x}_h, \boldsymbol{y}_h, \underline{\boldsymbol{v}}_h, \overline{\boldsymbol{v}}_h, w_h)$, $\forall h \in \mathcal{H}$, as given in (4.18).
   4) Solve (G2$-itr$) and save its optimal solution as $\pi_{SCP}^{(itr)}$.
   5) Update $\mathcal{E}$ based on (4.20).

c) Return $\pi_{SCP}^{(itr)}$ as the solution to (G2).

Proposition 4.6.1. Given $\epsilon \to 0$, the solution returned by the SCP based algorithm given in Table 4.1 locally minimizes (G2).

Proof. See Appendix J. □

4.6.2 RS Based Algorithm

In this subsection, we propose an alternative algorithm, which is in similar spirit of the well-know simulated annealing algorithm [100], in order to solve (G1) directly by the approach of randomized search over the set of all possible values of decision variables, discussed as follows. At each iteration itr, $itr = 1, 2, \ldots$, we replace each decision variable of (G1), one by one, by a randomly generated feasible point. Accordingly, we evaluate the change in the objective value of (G1). Since (G1) is a minimization problem, if the change in the objective value is negative, i.e., the objective value decreases as compared to the previous iteration, then we set this particular decision variable for iteration $itr - 1$ as the given randomly generated point with probability $1/2 < \varrho_1 \leq 1$ or we set it the same as its value at iteration itr with probability $1 - \varrho_1$. If the change in objective value is positive, then we set this

Table 4.2: RS based algorithm for (G1).

a) Initialize $itr \leftarrow 0$, $itr_{\max} > 1$, $1/2 < \varrho_1 \leq 1$, $0 \leq \varrho_2 < 1/2$, $O_{best} = \infty$, and set $\pi_{RS}^{(0)}$ as an arbitrary pint satisfying the constraints given in (4.5) and (4.6).

b) **While** $itr < itr_{\max}$ **do**:

1) Set $itr \leftarrow itr + 1$.

2) **For all** $h \in \mathcal{H}$ in order of $h = 1$ to $h = H$ **do**:

- **For all** $n \in \mathcal{N}_0$ in order of $n = n_0$ to $n = N$ **do**:
- Set the discounted electricity price $\tilde{\boldsymbol{x}}_h = [\boldsymbol{x}_{h,n_0,RS}^{(itr)}, \ldots, x_{h,n-1,RS}^{(itr)}, x'_{h,n}, x_{h,n+1,RS}^{(itr-1)}, \ldots, x_{h,N,RS}^{(itr-1)}]^T$, where $x'_{h,n}$ is randomly chose from $\underline{x}_n \leq x'_{h,n} \leq \dot{x}_{h,n}$.
- Given $\boldsymbol{x}_h = \tilde{\boldsymbol{x}}_h$, solve (DR$-h$) and save its optimal solution (rescheduled demand of aggregator h) as $\tilde{\boldsymbol{y}}_h = [\tilde{y}_{h,n_0}, \ldots, \tilde{y}_{h,N}]^T$.
- Compute Δ based on (4.21).
- **If** $\Delta < 0$ **then** set $(\boldsymbol{x}_{h,RS}^{(itr)}, \boldsymbol{y}_{h,RS}^{(itr)}) = (\tilde{\boldsymbol{x}}_h, \tilde{\boldsymbol{y}}h)$ with probability ϱ_1 or $(\boldsymbol{x}_{h,RS}^{(itr)}, \boldsymbol{y}_{h,RS}^{(itr)}) = (\boldsymbol{x}_{h,RS}^{(itr-1)}, \boldsymbol{y}_{h,RS}^{(itr-1)})$ with probability $1 - \varrho_1$.
- **If** $\Delta \geq 0$ **then** set $(\boldsymbol{x}_{h,RS}^{(itr)}, \boldsymbol{y}_{h,RS}^{(itr)}) = (\tilde{\boldsymbol{x}}_h, \tilde{\boldsymbol{y}}_h)$ with probability ϱ_2 or $(\boldsymbol{x}_{h,RS}^{(itr)}, \boldsymbol{y}_{h,RS}^{(itr)}) = (\boldsymbol{x}_{h,RS}^{(itr-1)}, \boldsymbol{y}_{h,RS}^{(itr-1)})$ with probability $1 - \varrho_2$.

3) **If** $C_{res}(\boldsymbol{y}_{1,RS}^{(itr)}, \ldots, \boldsymbol{y}_{H,RS}^{(itr)}) < O_{best}$ **then** set $O_{best} \leftarrow C_{res}(\boldsymbol{y}_{1,RS}^{(itr)}, \ldots, \boldsymbol{y}_{H,RS}^{(itr)})$ and $\pi_{best} \leftarrow (\{\boldsymbol{x}_{h,RS}^{(itr)}\}_{h\in\mathcal{H}}, \{\boldsymbol{y}_{h,RS}^{(itr)}\}_{h\in\mathcal{H}})$.

c) Return π_{best} as the solution to (G1).

particular decision variable for iteration itr as the given randomly generated point with probability $0 \leq \varrho_2 < 1/2$ or we set it the same as its value at iteration $itr - 1$ with probability $1 - \varrho_2$. The algorithm continues until a presumed stopping criterion is satisfied. In the following, we provide the details of our RS based algorithm to solve (G1).

Denote $\pi_{RS}^{(itr-1)} = (\{\boldsymbol{x}_{h,RS}^{(itr-1)}\}_{h\in\mathcal{H}}, \{\boldsymbol{y}_{h,RS}^{(itr-1)}\}_{h\in\mathcal{H}})$ as the set of decision variables of (G1) at the beginning of each iteration itr, where $\pi_{RS}^{(0)}$ is a given initial point at the beginning of iteration 1. Starting from $h = 1$ to $h = H$, we derive decision variables for iteration itr, one by one, according to the following procedure. For a particular aggregator h, starting from $n = n_0$ to $n = N$, we first set

$\tilde{\boldsymbol{x}}_h = [x^{(itr)}_{h,n_0,RS}, \ldots, x^{(itr)}_{h,n-1,RS}, x'_{h,n}, x^{(itr-1)}_{h,n+1,RS}, \ldots, x^{(itr-1)}_{h,N,RS}]^T$, where $x'_{h,n}$ is randomly generated over $\underline{x}_n \leq x'_{h,n} \leq \dot{x}_{h,n}$. Given $\boldsymbol{x}_h = \tilde{\boldsymbol{x}}_h$, we solve (DR$-h$) and denote its optimal solution as $\tilde{\boldsymbol{y}}_h = [\tilde{y}_{h,n_0}, \ldots, \tilde{y}_{h,N}]^T$. Accordingly, we evaluate the change in the objective value of (G1) as

$$\Delta = C_{res}(\boldsymbol{y}^{(itr)}_{1,RS}, \ldots, \boldsymbol{y}^{(itr)}_{h-1,RS}, \tilde{\boldsymbol{y}}_h, \boldsymbol{y}^{(itr-1)}_{h+1,RS}, \ldots, \boldsymbol{y}^{(itr-1)}_{H,RS}) - C_{res}(\boldsymbol{y}^{(itr)}_{1,RS}, \ldots, \boldsymbol{y}^{(itr)}_{h-1,RS}, \boldsymbol{y}^{(itr-1)}_{h,RS}, \boldsymbol{y}^{(itr-1)}_{h+1,RS}, \ldots, \boldsymbol{y}^{(itr-1)}_{H,RS}). \quad (4.21)$$

If $\Delta < 0$, we set $(\boldsymbol{x}^{(itr)}_{h,RS}, \boldsymbol{y}^{(itr)}_{h,RS}) = (\tilde{\boldsymbol{x}}_h, \tilde{\boldsymbol{y}}_h)$ with probability ϱ_1 or $(\boldsymbol{x}^{(itr)}_{h,RS}, \boldsymbol{y}^{(itr)}_{h,RS}) = (\boldsymbol{x}^{(itr-1)}_{h,RS}, \boldsymbol{y}^{(itr-1)}_{h,RS})$ with probability $1-\varrho_1$. Otherwise, if $\Delta \geq 0$, we set $(\boldsymbol{x}^{(itr)}_{h,RS}, \boldsymbol{y}^{(itr)}_{h,RS}) = (\tilde{\boldsymbol{x}}_h, \tilde{\boldsymbol{y}}_h)$ with probability ϱ_2 or $(\boldsymbol{x}^{(itr)}_{h,RS}, \boldsymbol{y}^{(itr)}_{h,RS}) = (\boldsymbol{x}^{(itr-1)}_{h,RS}, \boldsymbol{y}^{(itr-1)}_{h,RS})$ with probability $1 - \varrho_2$. Furthermore, we can track the best achieved solution to (G1) and its resulted objective value, denoted by π_{best} and O_{best}, respectively, as follows. At the end of iteration itr, if $C_{res}(\boldsymbol{y}^{(itr)}_{1,RS}, \ldots, \boldsymbol{y}^{(itr)}_{H,RS}) < O_{best}$, we update both $\pi_{best} = (\{\boldsymbol{x}^{(itr)}_{h,RS}\}_{h\in\mathcal{H}}, \{\boldsymbol{y}^{(itr)}_{h,RS}\}_{h\in\mathcal{H}})$ and $O_{best} = C_{res}(\boldsymbol{y}^{(itr)}_{1,RS}, \ldots, \boldsymbol{y}^{(itr)}_{H,RS})$. Otherwise, no update is needed. Last, the algorithm terminates when $itr = itr_{\max}$, where $itr_{\max} > 1$ is a given stopping threshold. Our RS based algorithm is summarized in Table 4.2. As a concluding remark, note that due to the randomized nature of the RS based algorithm for setting $\boldsymbol{x}_h$'s, this algorithm cannot ensure the fairness among different aggregators, i.e., some aggregators may receiver higher discount as compared to the others.

Note that by relying on a bidirectional communication system, we can deploy the RS based algorithm to solve BDPP even without any presumed knowledge about behavior of aggregators, which is discussed in the following remark.

Remark 4.6.1. At each iteration itr, given $\tilde{\boldsymbol{x}}_h$ announced by the system operator (distributed via the communication system), aggregator h solves its rescheduling problem (DR$-h$) by setting $\boldsymbol{x}_h = \tilde{\boldsymbol{x}}_h$, which is required in Step b.1, bullet 3, in Table 4.2. Then, aggregator h returns its rescheduled demand, i.e., $\tilde{\boldsymbol{y}}_h$, via the

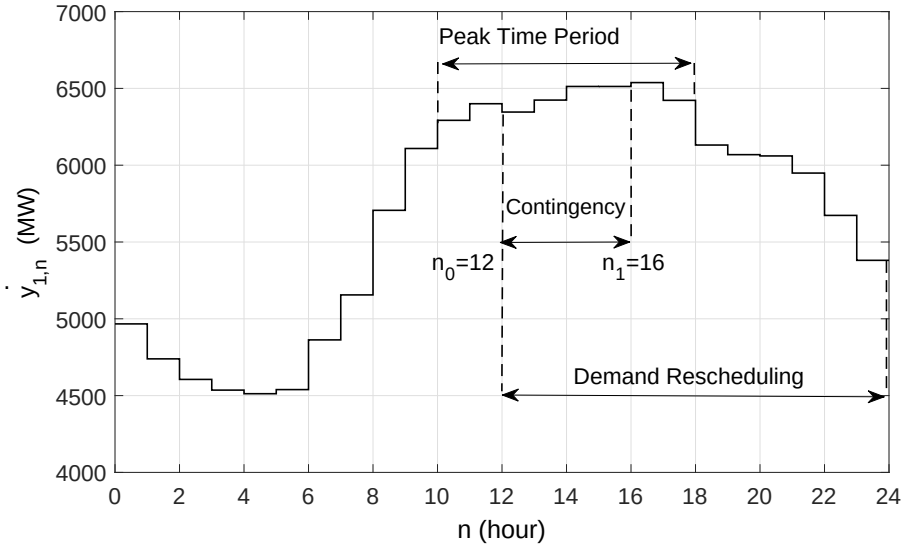

Figure 4.2: Hourly day-ahead demand of aggregator 1.

communication system to the system operator. Accordingly, the system operator sets the new price and the above is repeated until the algorithm terminates.

4.7 Simulation Results

We consider a power system consisting of a single aggregator $H = 1$ with $N = 24$ time slots (each slot duration is 1 hour). We set the day-ahead electricity price for aggregator 1 to be time-invariant as $\dot{x}_{1,n} = 257.3\$/\text{MWh}$ ($\underline{x}_n = 253\$/\text{MWh}$), $\forall n \in \mathcal{N}$, according to the electricity tariff for household users in Singapore (announced in 01 January, 2014) [101]. We set the day-ahead demand $\dot{\boldsymbol{y}}_1$ to be the hourly demand over one day (03 March, 2014) in the Singapore power grid [102], which is plotted in Fig. 4.2. We also model the service quality index of aggregator 1 as $Q_1(\boldsymbol{y}_1) = 1 - \sum_{n=n_0}^{N}(1 - y_{1,n}/\dot{y}_{1,n})^2$ [67] and set $\theta_1 = 0.8 \times 10^{-4}$, $\underline{y}_{1,n} = 0.75\dot{y}_{1,n}$, and $\overline{y}_{1,n} = 1.25\dot{y}_{1,n}$, $\forall n \in \mathcal{N}$, which means that aggregator 1 can change the day-ahead demand of its users within $\pm 25\%$ at each time slot, but the total demand $y_{1,tot}$ should be satisfied by time slot $N = 24$. Furthermore, we model the operational

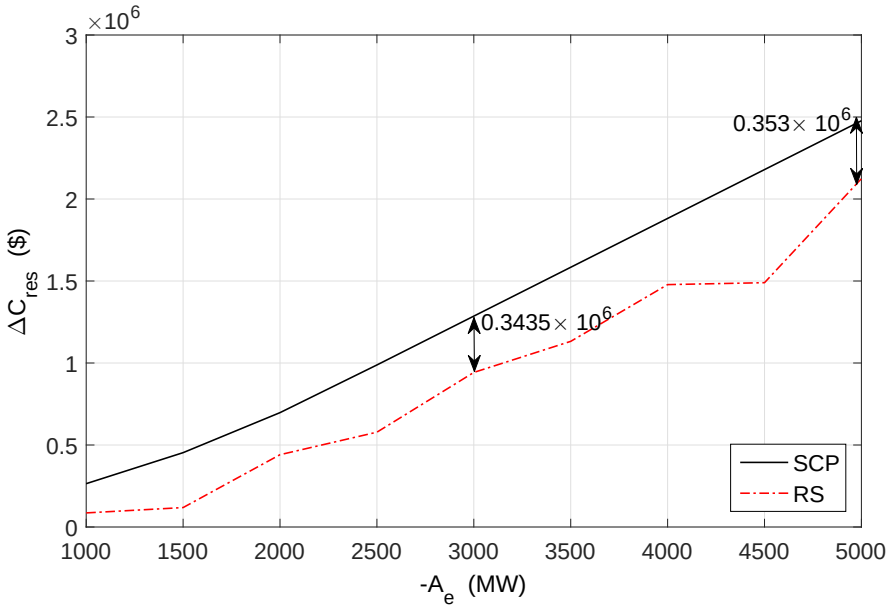

Figure 4.3: Changes in the residual cost of the system operator.

costs of the system operator over time slots by $C_n(g_n) = 0.037g_n^2 + 2.4g_n\$$, $\forall n \in \mathcal{N}$, with g_n in MW.

We assume that the power system experiences a contingency from time slot $n_0 = 12$ till time slot $n_1 = 16$, which results in A_e amount of supply deficit, with $A_e \in [-5000, -1000]$MW. Given the above system setup, we solve ODPP, i.e. (G2), locally optimally via our SCP based algorithm given in Table 4.1 by setting $\rho = 100$ (small as compared to the demand range), $\xi = 10^8$, and $\epsilon = 10^{-3}$. We also use our RS based algorithm given in Table 4.1 to heuristically solve BDPP, i.e. (G1), by setting $itr_{\max} = 2 \times 10^3$, $\varrho_1 = 0.95$, and $\varrho_2 = 0.1$.

Fig. 4.3 plots saving in the residual cost of the system operator, defined as $\Delta C_{res} = C_{res}(\boldsymbol{y}_1') - C_{res}(\boldsymbol{y}_1)$ with $\boldsymbol{y}_1' = [\dot{y}_{1,n_0}, \ldots, \dot{y}_{1,N}]$. It is observed that both algorithms help reduce the system operator's residual cost significantly, e.g., 4.68% ($1.28 \times 10^6\$$) and 7.02% ($2.48 \times 10^6\$$) for $A_e = -3000$MW and $A_e = -5000$MW, respectively, for the SCP based algorithm. However, the saving resulted from deploying the RS based algorithm is lower than that by the SCP based algorithm

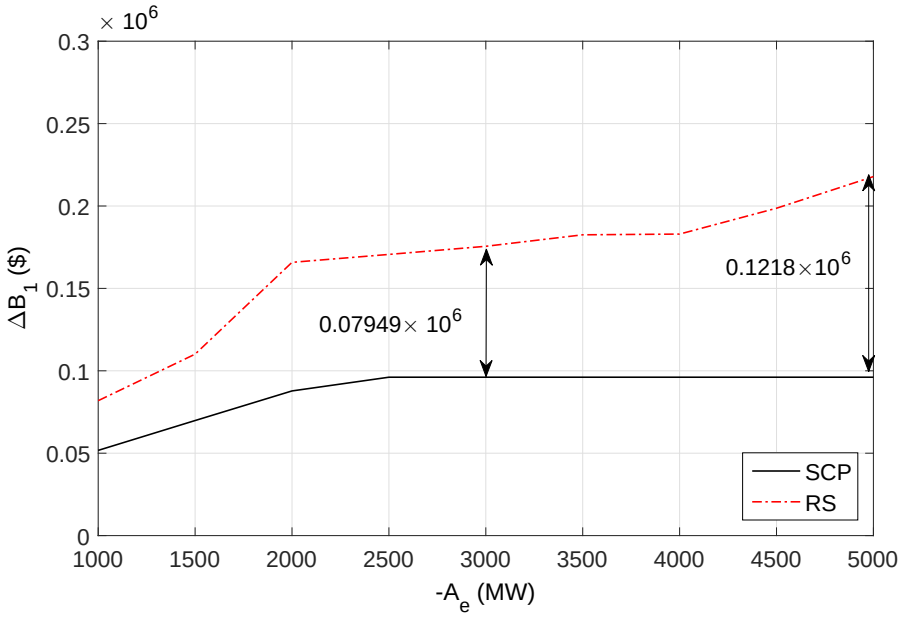

Figure 4.4: Reduction in the residual bill of aggregator 1.

consistently. This is expected since the RS based algorithm randomly searches over the set of feasible values of decision variables regardless of the results obtained in previous iterations. In contrast, the SCP based algorithm modifies the direction of searching at each iteration according to the results of previous iterations to find a solution with a lower objective value.

Figs. 4.4 shows reduction in the residual bill of aggregator 1, defined as $\Delta B_1 = B_1(\boldsymbol{x}_1', \boldsymbol{y}_1') - B_1(\boldsymbol{x}_1, \boldsymbol{y}_1)$ with $\boldsymbol{x}_1' = [\dot{x}_{1,n_0}, \ldots, \dot{x}_{1,N}]$. Fig. 4.5 also depicts changes in the profit of the system operator, defined as $\Delta P = \Delta C_{res} - \Delta B_1$. By comparing two figures, it is observed that although aggregator 1 pays less bill after demand rescheduling, the residual profit of the system operator increases. This can be explained by considering the fact that offering the discounted electric price $\boldsymbol{x}_1$ motivates aggregator 1 to shift a portion of its demand from time slots $12 \leq n \leq 16$ to time slots $17 \leq n \leq 24$ with lower electricity prices. Thus, as shown in Fig. 4.3, the residual cost of the system operator reduces remarkably, which offsets the reduction in the bill of aggregator 1, i.e., $\Delta C_{res} > \Delta B_1$. Moreover, it is observed that

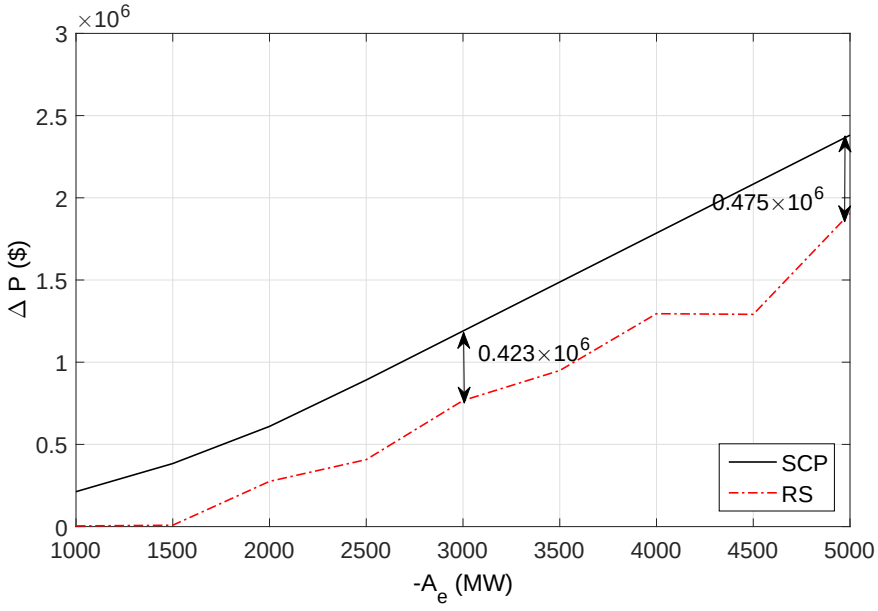

Figure 4.5: Changes in the profit of the system operator.

SCP based algorithm results in higher profit than the RS based algorithm. This is due to the fact that RS based algorithm offers over-discounted electricity prices to aggregator 1, which reduce the total bill of aggregator 1 more than that of the SCP based algorithm, while these over-discounted electricity prices cannot help reduce the residual cost of the system operator more than that of the SCP based algorithm.

Fig. 4.6 shows the impact of the weight coefficient θ_1, which controls the trade-off between the residual bill of aggregator 1 and its service quality index, on the profit of the system operator ΔP, given $A_e = -3000$MW. It is observed that the profit of system operator increases over θ_1. This is due to the fact that when θ_1 increases, aggregator 1 pays less attention to its service quality index as compared to its residual bill (see (4.2)); therefore, the system operator can motivate the aggregator to reschedule its demand by offering lower discounts. This increases the revenue of the system operator from selling energy to the aggregator and hence its profit increases.

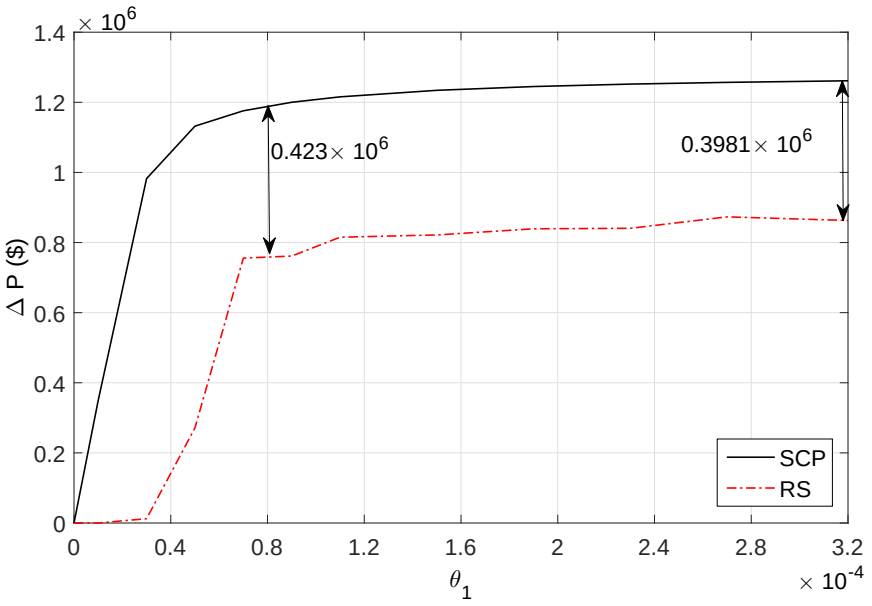

Figure 4.6: Impact of wight coefficient θ_1 on the profit of system operator.

Table 4.3: Average convergence time of algorithms.

A_e (MW)	Convergence time (Second)	
	SCP based algorithm	RS based algorithm
-1000	82.37	78.31
-3500	82.12	79.16

Last, we set $\theta_1 = 0.8 \times 10^{-4}$ again, and compare the average convergence time of th two algorithms under $A_e = -1000/-3500$MW in Table 4.3.[3] To derive the average convergence time, we use 10^3 randomly generated initial points for each algorithm. It is observed that SCP based and RS based algorithms solve the problem in approximately 82 and 79 seconds on average, respectively, which are largely shorter than the activation time limit for the secondary reserve service, typically, 5–10 minutes. As a result, our proposed pricing scheme can be implemented in real time as both secondary/tertiary reserve services for achieving balanced supply and demand for long term after the contingency. Note that for the RA based algorithm,

[3]Simulations are implemented on MATLAB R2011a and tested on a PC with a Core i7-2600 CPU,3.4-GHz processor, 8-GB RAM, and Windows 7.

it is assumed that any data exchanges between the system operator and aggregator 1 over the communication system in both directions incur a 0.2 millisecond delay (0.1 millisecond for each direction).

4.8 Chapter Summary

In this chapter, we proposed a real-time pricing scheme for the system operator to balance the supply and demand in long term, say, a couple of hours, after a contingency of supply deficit. Under our proposed scheme, the system operator is aimed to minimize the operational costs of the power grid by offering discounted electricity prices to self-interested aggregators in order to incentivize them to reschedule their day-ahead demand for frequency control. We formulated BDPP and ODPP problem to design discounted electricity prices for the system operator, for which two efficient algorithms were proposed. Based on the Singapore power grid data, it was shown that the real-time pricing scheme proposed is beneficial for both the system operator and aggregators upon the contingency, i.e, the cost of the system operator decreases (7% saving at 5000MW amount of supply deficiency), while each aggregator pays less bill than the case without demand rescheduling (1% saving correspondingly). It was also shown that our proposed algorithms for solving BDPP and ODPP converge in an efficient time, e.g., nearly 80 seconds by considering the processing delay of the communication system. Hence, our proposed pricing scheme can manage DR of aggregators in real time to provide cost-efficient secondary/tertiary reserve services.

Chapter 5

Conclusion and Future Work

5.1 Conclusion

This thesis has pursued a comprehensive and in-depth investigation of deploying distributed DR for frequency control, which can be used in replacement of the conventional primary/secondary/tertiary reserve services in smart grid. We summarize the main contributions of this thesis as follows.

- In Chapter 2, we proposed a demand-side frequency control algorithm via randomized on-off operation of distributed SAPPs. We characterized the impacts of SAPPs' randomized responses on the system frequency upon a contingency of supply shortfall. Moreover, we verified the performance of our proposed frequency control via extensive simulations based on the IEEE 9-Bus test system as well as the aggregate model of the Ireland power grid. It was observed that with our proposed frequency control algorithm, SAPPs' responses can replace the conventional primary reserve service to restore the system frequency reliably and cost-efficiently.

- In Chapter 3, we proposed a randomized frequency control algorithm via distributed EVs, where both the charging and discharging control of EVs was used for frequency recovery. We characterized the system frequency upon a contingency of supply deficit by taking EVs' randomized responses into account. Based on the derived analytical results, we formulated an optimization problem to design EVs' response rates so as to minimize the expected cost of

deploying our proposed frequency control algorithm subject to the given power grid requirements. An efficient algorithm was proposed to efficiently solve the formulated problem under certain practical assumptions. Last, we validated our analysis via simulations, from which it was observed that our distributed frequency control algorithm via EVs can be a promising low-cost solution to help maintain the power system stability.

- In Chapter 4, we proposed a real-time pricing scheme to manage DR in a group of self-interested aggregators to provide inexpensive secondary/tertiary reserve services. Specifically, we formulated a bilevel optimization problem to design discounted electricity prices for the system operator, where efficient algorithms were developed to solve the problem. We compared the performance of various algorithms via a numerical example based on the Singapore power grid data. It was observed that the demand rescheduling of aggregators can reduce the frequency recovery cost remarkably, while aggregators also pay less electricity bills than the case without demand rescheduling.

5.2 Future Work

Last, we point out some future work directions in the following which we deem important and worthy of further investigations by extending the results presented in this thesis.

In Chapters 2 and 3, we characterized the impacts of randomized responses of distributed frequency-responsive loads, i.e., SAPPs and EVs, on the system frequency dynamics by assuming a simplified model of the power system. However, to achieve a more detailed assessment of DR on a power system with a certain network topology, we need to use a more complex power system representation, as proposed in [89]. Moreover, the joint design of our proposed DR-enable frequency control

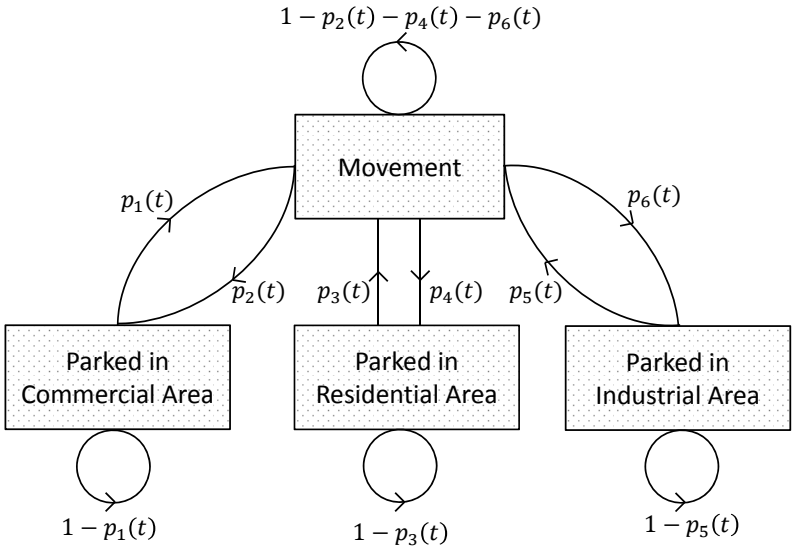

Figure 5.1: Markov process illustrating the motion of an EV over time.

together with the conventional generation-side controllers is practically important and worthy of future investigation.

In our analysis in Chapter3, we assumed that the number of EVs that are connected to the grid as well as their initial operational modes are known perfectly. However, this assumption may not be practically valid due to, e.g., the random deployment of EVs. Recently, Soares *et al.* [106] used a Markovian model with time-varying transient probabilities to represent the stochastic nature of motion of an EV over time. This model with the state transient probabilities $p_i(t)$, $i = 1, \ldots, 6$, at each time slot t, $t \in \{1, \ldots, 24\}$, is shown in Fig. 5.1. A similar model can be also developed to express the operational mode of an EV over time. Based on these stochastic models, we can extend the theoretical results given in Chapter 3 to consider the impacts of random number of grid-connected EVs as well as their randomized operational modes on the system frequency.

In Chapter 4, we assumed that each aggregator can adjust the power consumption of its users in real time, but at the cost of degrading the service quality. In practice, users can also be modelled as selfish entities and thus the aggregators need

to motivate them to defer their loads, e.g., by offering some monetary rewards in return. Accordingly, the real-time pricing problem of the system operator can be formulated as a general three-level optimization problem with two-sided energy trading, where the first two layers are the same as our formulated bilevel optimization problem in Chapter 4, while the third layer is the users' utility maximization.

Appendix A

Proof of Proposition 2.5.1

Given $A_e < A_{e,\min}$ and $A_a \geq A_{a,\min}$, it follows that there exist $t_0 > 0$ and consequently $T_r > t_0$. Over time $t_0 \leq t \leq T_r$, all SAPPs that respond by switching off their loads will remain in the off state since $f(t) \leq f_{\min}$. Since it is assumed that $S_i(0) = 1,\ i = 1, \ldots, M$, the system frequency given in (2.7) can be simplified as follows

$$f(t) = f_0 + \frac{f_0}{K_f A_0}\left(A_e \left(1 - e^{-\alpha t}\right) + \sum_{i=1}^{M} A_i \left(1 - e^{-\alpha (t - t_0 - T_i^*)^+}\right) \right), \tag{A.1}$$

where $T_i^* = t_i^* - t_0 \geq 0$ denotes the duration between t_0 and the first response (monitoring event) by SAPP i after t_0, denoted by t_i^*. From (A.1) and by considering the fact that SAPPs respond independently, it follows that the mean value of the system frequency function is given by

$$\mathbb{E}\left[f(t)\right] = f_0 + \frac{f_0}{K_f A_0}\left(A_e \left(1 - e^{-\alpha t}\right) + \sum_{i=1}^{M} \mathbb{E}\left[A_i \left(1 - e^{-\alpha (t - t_0 - T_i^*)^+}\right)\right] \right). \tag{A.2}$$

We rewrite each of the summation term on the RHS of (A.2) as follows

$$\begin{aligned} \mathbb{E}\left[A_i \left(1 - e^{-\alpha (t - t_0 - T_i^*)^+}\right)\right] &= A_i \mathbb{E}\left[\left(1 - e^{-\alpha (t - t_0 - T_i^*)^+}\right)\right] \\ &= A_i \left(1 - \mathbb{E}\left[e^{-\alpha (t - t_0 - T_i^*)^+}\right]\right). \end{aligned} \tag{A.3}$$

Due to the memoryless property of the Poisson process [81], it follows that T_i^* is exponentially distributed with mean of $1/\lambda_i$. Therefore, we obtain $\mathbb{E}[e^{-\alpha (t - t_0 - T_i^*)^+}]$

as follows

$$\begin{aligned}
\mathbb{E}[e^{-\alpha(t-t_0-T_i^*)^+}] &= \int_0^\infty e^{-\alpha(t-t_0-z)^+}\lambda_i e^{-\lambda_i z}dz \\
&= \int_0^{t-t_0} \lambda_i e^{-\alpha(t-t_0-z)}e^{-\lambda_i z}dz + \int_{t-t_0}^\infty \lambda_i e^{-\lambda_i z}dz \\
&= \begin{cases} \dfrac{\lambda_i}{\lambda_i-\alpha}e^{-\alpha(t-t_0)} - \dfrac{\alpha}{\lambda_i-\alpha}e^{-\lambda_i(t-t_0)}, & \text{if } \lambda_i \neq \alpha \text{ and } t > t_0 \\ \lambda_i(t-t_0)e^{-\alpha(t-t_0)} + e^{-\lambda_i(t-t_0)}, & \text{if } \lambda_i = \alpha \text{ and } t > t_0 \\ 1, & \text{if } t = 0. \end{cases}
\end{aligned} \tag{A.4}$$

From (A.3) and (A.4), the proof of Proposition 2.5.1 is thus completed.

Appendix B

Proof of Proposition 2.5.2

Similar to the proof of Proposition 2.5.1, overt time $t_0 \leq t \leq T_r$, since it is assumed that $S_i(0) = 1,\ i = 1, \ldots, M$, the variance of the system frequency is expressed as

$$\begin{aligned}\mathbb{V}\mathrm{ar}\left[f(t)\right] &= \left(\frac{f_0}{K_f A_0}\right)^2 \mathbb{V}\mathrm{ar}\left[\sum_{i=1}^{M} A_i \left(1 - e^{-\alpha(t-t_0-T_i^*)^+}\right)\right] \\ &\overset{(\star)}{=} \left(\frac{f_0}{K_f A_0}\right)^2 \sum_{i=1}^{M} A_i^2\ \mathbb{V}\mathrm{ar}\left[1 - e^{-\alpha(t-t_0-T_i^*)^+}\right] \end{aligned} \tag{B.1}$$

where $(\star)$ is due to the fact that T_i^*'s are independent over i. In the following, we can derive each of the variance terms on the RHS of (B.1) as follows

$$\mathbb{V}\mathrm{ar}\left[1 - e^{-\alpha(t-t_0-T_i^*)^+}\right] = \mathbb{E}\left[\left(1 - e^{-\alpha(t-t_0-T_i^*)^+}\right)^2\right] - \left(\mathbb{E}\left[1 - e^{-\alpha(t-t_0-T_i^*)^+}\right]\right)^2. \tag{B.2}$$

First, we derive

$$\begin{aligned}\mathbb{E}\left[\left(1 - e^{-\alpha(t-t_0-T_i^*)^+}\right)^2\right] &= \mathbb{E}\left[1 + e^{-2\alpha(t-t_0-T_i^*)^+} - 2e^{-\alpha(t-t_0-T_i^*)^+}\right] \\ &= 1 - 2\mathbb{E}\left[e^{-\alpha(t-t_0-T_i^*)^+}\right] + \mathbb{E}\left[e^{-2\alpha(t-t_0-T_i^*)^+}\right] \\ &= 1 - 2u_\alpha(\lambda_i, t-t_0) + u_{2\alpha}(\lambda_i, t-t_0). \end{aligned} \tag{B.3}$$

Next, we derive

$$\left(\mathbb{E}\left[1-e^{-\alpha(t-t_0-T_i^*)^+}\right]\right)^2 = \left(1-\mathbb{E}\left[e^{-\alpha(t-t_0-T_i^*)^+}\right]\right)^2$$
$$= 1-2u_\alpha(\lambda_i, t-t_0)+\left(u_\alpha(\lambda_i, t-t_0)\right)^2. \tag{B.4}$$

By substituting (B.3) and (B.4) into (B.2), we then obtain

$$\mathbb{V}\mathrm{ar}\left[1-e^{-\alpha(t-t_0-T_i^*)^+}\right] = u_{2\alpha}(\lambda_i, t-t_0)-\left(u_\alpha(\lambda_i, t-t_0)\right)^2 \tag{B.5}$$

By defining $v(\alpha,\lambda,s) = u_{2\alpha}(\lambda,s)-\left(h(\alpha,\lambda,s)\right)^2$ and substituting (B.5) into (B.1), the proof of Proposition 2.5.2 is thus completed.

Appendix C

Proof of Proposition 2.5.4

The probability that an SAPP in Class j has responded by switching off its load by time t, $t_0 \leq t \leq T_r$, is obtained as $1 - e^{-\tilde{\lambda}_j(t-t_0)}$. Note that since it is assumed that all SAPPs in Class j are initially in an on state, they will respond by switching off their loads at their first frequency monitoring event after t_0. The mean value of $N_j(t)$, over time $t_0 \leq t \leq T_r$, can be thus derived as

$$\begin{aligned}
\mathbb{E}[N_j(t)] &= \sum_{m=1}^{M_j} m \binom{M_c}{j} \left(1 - e^{-\tilde{\lambda}_j(t-t_0)}\right)^m \left(1 - e^{-\tilde{\lambda}_j(t-t_0)}\right)^{M_j - m} \\
&= M_j \left(1 - e^{-\tilde{\lambda}_j(t-t_0)}\right) \sum_{m=1}^{M_j} \binom{M_j - 1}{m-1} \left(1 - e^{-\tilde{\lambda}_j(t-t_0)}\right)^{m-1} \left(e^{-\tilde{\lambda}_j(t-t_0)}\right)^{M_j - m} \\
&= M_j \left(1 - e^{-\tilde{\lambda}_j(t-t_0)}\right) \left(1 - e^{-\tilde{\lambda}_j(t-t_0)} + e^{-\tilde{\lambda}_j(t-t_0)}\right)^{M_j - 1} \\
&= M_j \left(1 - e^{-\tilde{\lambda}_j(t-t_0)}\right). \qquad \text{(C.1)}
\end{aligned}$$

The proof of Proposition 2.5.4 is thus completed.

Appendix D

Proof of Proposition 2.5.5

Let $P_{os|s}$ denote the conditional probability of frequency overshoot due to over-responses of SAPPs given a frequency recovery time $T_r = s$, with $s > t_0$. Since SAPPs respond independently, we thus have

$$P_{os|s} = \sum_{\boldsymbol{n}\in\mathcal{O}} \prod_{j=1}^{J} \mathbb{P}\mathrm{r}\{\tilde{N}_j(T_r) = n_j \mid T_r = s\} \tag{D.1}$$

$$= \sum_{\boldsymbol{n}\in\mathcal{O}} \prod_{j=1}^{J} \binom{M_j}{n_j} \left(1 - e^{-\tilde{\lambda}_j(s-t_0)}\right)^{n_j} \left(e^{-\tilde{\lambda}_j(s-t_0)}\right)^{M_j-n_j}, \tag{D.2}$$

where (D.1) follows from (2.20) and (D.2) follows from (2.21). Note that $P_{os|s}$ is the probability of frequency overshoot conditioned given $T_r = s$, which should be averaged over the distribution of T_r to obtain the exact value of the probability of frequency overshoot. Similar to Proposition 2.5.3, since the distribution of T_r is difficult to be obtained, we use the average frequency recovery time $\overline{T}_r$ to obtain an approximation for P_{os}. By replacing T_r by $\overline{T}_r$ in (D.2), Proposition 2.5.5 thus follows.

Appendix E

Proof of Proposition 3.5.1

First, we consider the case of $V_I = 0$ and $V_D = 0$. Based on (3.1), over time $t_0 \leq t \leq T_r$, each EV in the charging mode responds by first switching to the idle mode and then to the discharging mode at its first and second frequency monitoring events after t_0, respectively. Hence, we simplify (3.4) as

$$f(t) = f_0 + \frac{f_0}{K_f A_0}\Bigg(A_e \left(1 - e^{-\alpha t}\right) + \sum_{v \in \mathcal{V}_C} A_{C,v} \left(1 - e^{-\alpha (t - t_0 - \hat{T}^*_{1,v})^+}\right) + \sum_{v \in \mathcal{V}_C} A_{D,v} \left(1 - e^{-\alpha (t - t_0 - \hat{T}^*_{3,v})^+}\right)\Bigg), \quad \text{(E.1)}$$

where $\hat{T}^*_{3,v} = \hat{T}^*_{1,v} + \hat{T}^*_{2,v}$. Specifically, $\hat{T}^*_{1,v} = \hat{t}^*_{1,v} - t_0$ denotes the time duration between t_0 and the first monitoring event of EV v after t_0, while $\hat{T}^*_{2,v} = \hat{t}^*_{2,v} - \hat{t}^*_{1,v}$ denotes the time duration between the first and second monitoring events of EV v after t_0. Since all EVs respond independently, the mean value of the given system frequency given in (E.1) can be expressed as

$$\mathbb{E}[f(t)] = f_0 + \frac{f_0}{K_f A_0}\Bigg(A_e \left(1 - e^{-\alpha t}\right) + \sum_{v \in \mathcal{M}_C} A_{C,v} \left(1 - \mathbb{E}\left[e^{-\alpha (t - t_0 - \hat{T}^*_{1,v})^+}\right]\right) + \sum_{v \in \mathcal{V}_C} A_{D,v} \left(1 - \mathbb{E}\left[e^{-\alpha (t - t_0 - \hat{T}^*_{3,v})^+}\right]\right)\Bigg). \quad \text{(E.2)}$$

Due to the memoryless property of Poisson processes [81], it can be readily verified that both $\hat{T}^*_{1,v}$ and $\hat{T}^*_{2,v}$ are exponentially distributed with respective mean values of $1/\lambda_{C,v}$ and $1/\lambda_{I,v}$ for EV v. As a result, the probability distribution

function (PDF) of $\hat{T}^*_{3,v}$ assuming $\lambda^*_{C,v} \neq \lambda^*_{I,v}$ (the sum of two exponential variables with different mean values) is given by

$$f_{\hat{T}^*_{3,v}}(z) = \frac{\lambda_{C,v}\lambda_{I,v}}{\lambda_{I,v} - \lambda_{C,v}} \left(e^{-\lambda_{C,v}z} - e^{-\lambda_{I,v}z}\right), \ z \geq 0. \tag{E.3}$$

On the other hand, the distribution function of $\hat{T}^*_{3,v}$ assuming $\lambda_{C,v} = \lambda_{I,v}$ (the sum of two exponential variables with the same mean value) is given by

$$f_{\hat{T}_{3,v}}(z) = \lambda^2_{C,v} z e^{-\lambda_{C,v}z}, \ z \geq 0. \tag{E.4}$$

Accordingly, we simplify (E.2) by showing

$$\begin{aligned}
\mathbb{E}\left[e^{-\alpha(t-t_0-\hat{T}^*_{1,v})^+}\right] &= \int_0^\infty e^{-\alpha(t-t_0-z)^+}\lambda_{C,v}e^{-\lambda_{C,v}z}dz \\
&= \int_0^{t-t_0} e^{-\alpha(t-t_0-z)}\lambda_{C,v}e^{-\lambda_{C,v}z}dz + \int_{t-t_0}^\infty \lambda_{C,v}e^{-\lambda_{C,v}z}dz \\
&= \begin{cases}
\dfrac{\lambda_{C,v}e^{-\alpha(t-t_0)} - \alpha e^{-\lambda_{C,v}(t-t_0)}}{\lambda_{C,v} - \alpha}, & \text{if } \lambda_{C,v} \neq \alpha \text{ and } t > t_0 \\
\lambda_{C,v}(t-t_0)e^{-\alpha(t-t_0)} + e^{-\lambda_{C,v}(t-t_0)}, & \text{if } \lambda_{C,v} = \alpha \text{ and } t > t_0 \\
1, & \text{if } \ t = 0.
\end{cases}
\end{aligned} \tag{E.5}$$

For our convenience, $u_\alpha(\lambda, s)$ has been previously defined in (2.14). Assuming $\lambda_{C,v} \neq \lambda_{I,v}$, we then have

$$\begin{aligned}
&\mathbb{E}\left[e^{-\alpha(t-t_0-\hat{T}^*_{3,v})^+}\right] \\
&= \int_0^\infty e^{-\alpha(t-t_0-z)^+}\frac{\lambda_{C,v}\lambda_{I,v}}{\lambda_{I,v} - \lambda_{C,v}}\left(e^{-\lambda_{C,v}z} - e^{-\lambda_{I,v}z}\right)dz \\
&= \frac{\lambda_{I,v}}{\lambda_{I,v} - \lambda_{C,v}}\int_0^\infty e^{-\alpha(t-t_0-z)^+}\lambda_{C,v}e^{-\lambda_{C,v}z}dz + \frac{\lambda_{C,v}}{\lambda_{C,v} - \lambda_{I,v}}\int_0^\infty e^{-\alpha(t-t_0-z)^+}\lambda_{I,v}e^{-\lambda_{I,v}z}dz \\
&= \frac{\lambda_{I,v}}{\lambda_{I,v} - \lambda_{C,v}}u_\alpha(\lambda_{C,v}, t-t_0) + \frac{\lambda_{C,v}}{\lambda_{C,v} - \lambda_{I,v}}u_\alpha(\lambda_{I,v}, t-t_0).
\end{aligned} \tag{E.6}$$

Similarly, assuming $\lambda_{C,v} = \lambda_{I,v}$, we have

$$\begin{aligned}
\mathbb{E}\left[e^{-\alpha(t-t_0-\hat{T}^*_{3,v})^+}\right] &= \int_0^\infty e^{-\alpha(t-t_0-z)^+}\lambda_{C,v}^2\ z\ e^{-\lambda_{C,v}z}dz \\
&= \int_0^\infty e^{-\alpha(t-t_0-z)^+}\lambda_{C,v}e^{-\lambda_{C,v}z}dz - \lambda_{C,v}\frac{\partial}{\partial\lambda_{C,v}}\int_0^\infty \lambda_{C,v}e^{-\lambda_{C,v}z}dz \\
&= u_\alpha(\lambda_{C,v}, t-t_0) - \lambda_{C,v}\frac{\partial}{\partial\lambda_{C,v}}u_\alpha(\lambda_{C,v}, t-t_0). \qquad \text{(E.7)}
\end{aligned}$$

By substituting (E.5), (E.6), and (E.7) into (E.2), the proof is thus completed for the case of $V_I = 0$ and $V_D = 0$. The obtained results hold (without any changes) for the case of $V_D \neq 0$ due to the fact that EVs that are initially in the charging mode do not respond over time $t_0 \leq t \leq T_r$ since $f(t) < f_{\min}$. The above proof can also be easily extended to the case of $V_I \neq 0$, for which the details are omitted for brevity. Proposition 3.5.1 is thus proved.

Appendix F

Proof of Proposition 3.5.2

First, we consider the case of $V_I = 0$ and $V_D = 0$. Similar to the proof of Proposition 3.5.1, over time $t_0 \leq t \leq T_r$, by considering the fact that $\hat{T}^*_{1,v}$ and $\hat{T}^*_{3,v}$ are independent over v (see Appendix E), the variance of the system frequency is expressed as

$$\mathbb{V}\text{ar}\left[f(t)\right] = \left(\frac{f_0}{K_f A_0}\right)^2 \left(A^2_{C,v} \sum_{v\in\mathcal{V}_c} \mathbb{V}\text{ar}\left[\left(1 - e^{-\alpha(t-t_0-\hat{T}^*_{1,v})^+}\right)\right] + A^2_{D,v} \sum_{v\in\mathcal{V}_c} \mathbb{V}\text{ar}\left[\left(1 - e^{-\alpha(t-t_0-\hat{T}^*_{3,v})^+}\right)\right]\right). \tag{F.1}$$

We simplify (F.1) by showing that

$$\begin{aligned}
&\mathbb{V}\text{ar}\left[1 - e^{-\alpha(t-t_0-\hat{T}^*_{1,v})^+}\right] \\
&= \mathbb{E}\left[\left(1 - e^{-\alpha(t-t_0-\hat{T}^*_{1,v})^+}\right)^2\right] - \left(\mathbb{E}\left[1 - e^{-\alpha(t-t_0-\hat{T}^*_{1,v})^+}\right]\right)^2 \\
&= \mathbb{E}\left[1 - 2e^{-\alpha(t-t_0-\hat{T}^*_{1,v})^+} + e^{-2\alpha(t-t_0-\hat{T}^*_{1,v})^+}\right] - \left(\mathbb{E}\left[1 - e^{-\alpha(t-t_0-\hat{T}^*_{1,v})^+}\right]\right)^2 \\
&= 2\mathbb{E}\left[1 - e^{-\alpha(t-t_0-\hat{T}^*_{1,v})^+}\right] - \mathbb{E}\left[1 - e^{-2\alpha(t-t_0-\hat{T}^*_{1,v})^+}\right] - \left(\mathbb{E}\left[1 - e^{-\alpha(t-t_0-\hat{T}^*_{1,v})^+}\right]\right)^2 \\
&= 2h_\alpha(1, 0, \lambda_{C,v}, \lambda_{I,v}, t - t_0) \\
&\qquad - h_{2\alpha}(1, 0, \lambda_{C,v}, \lambda_{I,v}, t - t_0) - \left(h_\alpha(1, 0, \lambda_{C,v}, \lambda_{I,v}, t - t_0)\right)^2.
\end{aligned} \tag{F.2}$$

Moreover, we can show that

$$
\begin{aligned}
&\mathbb{V}\mathrm{ar}\left[1-e^{-\alpha(t-t_0-\hat{T}^*_{3,v})^+}\right] \\
&=\mathbb{E}\left[\left(1-e^{-\alpha(t-t_0-\hat{T}^*_{3,v})^+}\right)^2\right]-\left(\mathbb{E}\left[1-e^{-\alpha(t-t_0-\hat{T}^*_{3,v})^+}\right]\right)^2 \\
&=\mathbb{E}\left[1-2e^{-\alpha(t-t_0-\hat{T}^*_{3,v})^+}+e^{-2\alpha(t-t_0-\hat{T}^*_{3,v})^+}\right]-\left(\mathbb{E}\left[1-e^{-\alpha(t-t_0-\hat{T}^*_{3,v})^+}\right]\right)^2 \\
&=2\mathbb{E}\left[1-e^{-\alpha(t-t_0-\hat{T}^*_{3,v})^+}\right]-\mathbb{E}\left[1-e^{-2\alpha(t-t_0-\hat{T}^*_{3,v})^+}\right]-\left(\mathbb{E}\left[1-e^{-\alpha(t-t_0-\hat{T}^*_{3,v})^+}\right]\right)^2 \\
&=2h_\alpha(0,1,\lambda_{C,v},\lambda_{I,v},t-t_0) \\
&\qquad -h_{2\alpha}(0,1,\lambda_{C,v},\lambda_{I,v},t-t_0)-\left(h_\alpha(0,1,\lambda_{C,v},\lambda_{I,v},t-t_0)\right)^2. \qquad \text{(F.3)}
\end{aligned}
$$

By substituting (F.2) and (F.3) into (F.1), the proof of Proposition 3.5.2 is thus completed for the case of $V_I = 0$ and $V_D = 0$. The obtained results hold for the case of $V_D \neq 0$ due to the fact that EVs that are initially in the charging mode do not respond over time $t_0 \leq t \leq T_r$ since $f(t) \leq f_{\min}$. The above proof also can be easily extended to the case of $V_I \neq 0$, for which the details are omitted for brevity. Proposition 3.5.2 is thus proved.

Appendix G

Proof of Proposition 3.5.4

First, we consider the case of $V_{I,k} = 0$ and $V_{D,k} = 0$. By assuming $\tilde{\lambda}_{C,k} \neq \tilde{\lambda}_{I,k}$, the probability that an EV from Class k has switched from the charging mode to the idle mode by time t, $t_0 \leq t \leq T_r$, is derived as

$$\begin{aligned}
&\mathbb{P}\mathrm{r}\left\{t_0 + \hat{T}^*_{1,k} < t \ \cap \ t_0 + \hat{T}^*_{1,k} + \hat{T}^*_{2,k} > t\right\} \\
&= \int_0^{t-t_0} \int_{t-t_0-z_1}^{+\infty} \tilde{\lambda}_{C,k} e^{-\tilde{\lambda}_{C,k} z_1} \tilde{\lambda}_{I,k} e^{-\tilde{\lambda}_{I,k} z_2} dz_2 \ dz_1 \\
&= \begin{cases} \dfrac{\tilde{\lambda}_{C,k}\left(1 - e^{-\tilde{\lambda}_{C,k}(t-t_0)}\right) - \tilde{\lambda}_{C,k}\left(1 - e^{-\tilde{\lambda}_{I,k}(t-t_0)}\right)}{\tilde{\lambda}_{C,k} - \tilde{\lambda}_{I,k}}, & \text{if } t > t_0 \\ 0, & \text{otherwise,} \end{cases}
\end{aligned} \tag{G.1}$$

while the probability of switching from the charging mode to the discharging mode is given by

$$\begin{aligned}
&\mathbb{P}\mathrm{r}\left\{t_0 + \hat{T}^*_{1,k} + \hat{T}^*_{2,k} < t\right\} \\
&= \int_0^{s} \int_0^{s-z_1} \tilde{\lambda}_{C,k} e^{-\tilde{\lambda}_{C,k} z_1} \tilde{\lambda}_{I,k} e^{-\tilde{\lambda}_{I,k} z_2} dz_2 \ dz_1 \\
&= \begin{cases} \dfrac{\tilde{\lambda}_{I,k}\left(1 - e^{-\tilde{\lambda}_{C,k} s}\right) - \tilde{\lambda}_{C,k}\left(1 - e^{-\tilde{\lambda}_{I,k} s}\right)}{\tilde{\lambda}_{I,k} - \tilde{\lambda}_{C,k}}, & \text{if } t > t_0 \\ 0, & \text{otherwise.} \end{cases}
\end{aligned} \tag{G.2}$$

Similarly, we can derive the aforementioned probabilities for the case of $\tilde{\lambda}_{C,k} = \tilde{\lambda}_{I,k}$. For convenience, we define $p_2(\lambda_C, \lambda_I, s)$ and $p_3(\lambda_C, \lambda_I, s)$ in (3.14) and (3.15) to represent the results given in (G.1) and (G.2), respectively. The probability that an

EV from Class k remains in the charging mode by time t, $t_0 \leq t \leq T_r$, is thus given by $1 - p_2(\tilde{\lambda}_{C,k}, \tilde{\lambda}_{I,k}, t - t_0) - p_3(\tilde{\lambda}_{C,k}, \tilde{\lambda}_{I,k}, t - t_0)$. For convenience, we also define $p_1(\lambda_C, \lambda_I, s) = 1 - p_2(\lambda_C, \lambda_I, s) - p_3(\lambda_C, \lambda_I, s)$.

Next, we show the expected number of EVs from Class k which remain in the charging mode by time t, $t_0 \leq t \leq T_r$, is given by

$$
\begin{aligned}
&\mathbb{E}[N_{C,k}(t)] \\
&= \sum_{m=1}^{V_{C,k}} m \binom{V_{C,k}}{m} \Big(p_1(\tilde{\lambda}_{C,k}, \tilde{\lambda}_{I,k}, t - t_0)\Big)^m \Big(1 - p_1(\tilde{\lambda}_{C,k}, \tilde{\lambda}_{I,k}, t - t_0)\Big)^{V_{C,k}-m} \\
&= \sum_{m=1}^{V_{C,k}} V_{C,k} \binom{V_{C,k}-1}{m-1} \Big(p_1(\tilde{\lambda}_{C,k}, \tilde{\lambda}_{I,k}, t - t_0)\Big)^m \Big(1 - p_1(\tilde{\lambda}_{C,k}, \tilde{\lambda}_{I,k}, t - t_0)\Big)^{V_{C,k}-m} \\
&= V_{C,k} p_1(\tilde{\lambda}_{C,k}, \tilde{\lambda}_{I,k}, t - t_0) \Big(p_1(\tilde{\lambda}_{C,k}, \tilde{\lambda}_{I,k}, t - t_0) + 1 - p_1(\tilde{\lambda}_{C,k}, \tilde{\lambda}_{I,k}, t - t_0)\Big)^{V_{C,k}-1} \\
&= V_{C,k} p_1(\tilde{\lambda}_{C,k}, \tilde{\lambda}_{I,k}, t - t_0), \qquad \text{(G.3)}
\end{aligned}
$$

Then the average number of EVs from Class k which are in the idle and discharging modes can be obtained similarly. The above proof can be extended to the case of $V_{I,k} \neq 0$ and $V_{D,k} \neq 0$, from which the details are omitted for brevity. The proof of Proposition 3.5.4 is thus completed.

Appendix H

Proof of Proposition 3.5.6

Let $P_{os|s}$ denote the conditional probability of frequency overshoot due to over-responses of EVs given $T_r = s$, with $s > t_0$. Based on the fact that EVs respond independently, we thus have

$$P_{os|s} = \sum_{\mathbf{M}\in\mathcal{S}} \prod_{k=1}^{K} P_j(\boldsymbol{m}_j, s), \tag{H.1}$$

where $\mathbf{M} = [\boldsymbol{m}_1, \ldots, \boldsymbol{m}_K]^T$ and $P_j(\boldsymbol{m}_j, t)$ is given in (3.18). In general, we need the distribution of T_r to obtain the exact probability of frequency overshoot, P_{os}, by averaging (H.1) over the given distribution. Since the distribution of T_r is difficult to be obtained, the average frequency recovery time $\overline{T}_r$ given in Proposition 3.5.3 is used to find an approximation for P_{os} by replacing T_r with $\overline{T}_r$ in (H.1). The proof is thus completed.

Appendix I

Stackelberg Game

Stackelberg game was developed in 1934 by Heinrich Stackelberg [107], which was a breaking point in the history of market structure study. Stackelberg game is a model of imperfect competition based on a sequential non-cooperative game in which the leader, i.e., the system operator in this thesis, moves first and then the followers, i.e., aggregators in this thesis, move sequentially in response to the leader's decision.

Let us study a simple example of Stackelberg game consisting of two electric companies selling power in the real-time electricity market under a given price per unit function (given by the users), but different generation cost functions. In this example, we assume that Company 1 is a well-known brand in the market and hence plays the role of leader, while Company 2 is a newly established brand and hence plays the role of follower. First, Company 1 decides to sell $q_1 > 0$ unit of power. In response to this decision, Company 2 decides to sell $q_2 > 0$ unit of power. Let $P(q_1, q_2) = a - b(q_1 + q_2)$, with $a > 0$ and $b > 0$, denote the price per unit function given by the users. Furthermore, denote $C_1(q_1) = c_1 q_1^2$, with $c_1 > 0$, and $C_2(q_2) = c_2 q_2^2$, with $c_2 > 0$, as the cost functions of Companies 1 and 2, respectively. The net profits of Companies 1 and 2, are thus derived as $\Pi_1(q_1, q_2) = aq_1 - b(q_1 + q_2)q_1 - c_1 q_1^2$ and $\Pi_2(q_1, q_2) = aq_2 - b(q_1 + q_2)q_2 - c_2 q_2^2$, respectively, from which it is observed that the benefit of each individual company is a function of its selling power as well as that of the other company. To find the Nash equilibrium of the aforementioned game, we can use backward induction,

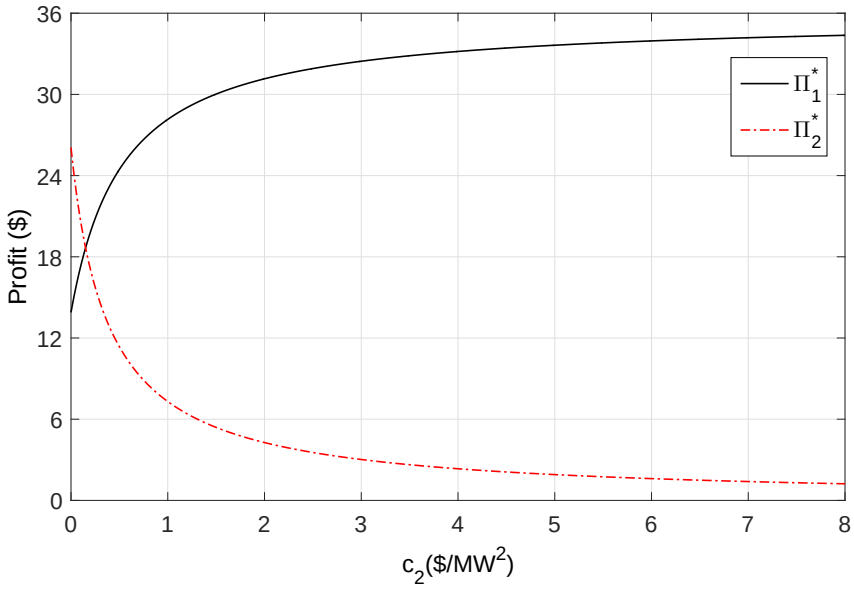

Figure I.1: Obtained Π_1^* and Π_2^* versus the cost coefficient c_2.

which is discussed in the following.

Given q_1, the Company 2 can maximize its profit by setting $q_2 = f(q_1) = [(a - bq_1)]^+/(2(b + c_2))$. By assuming that Company 1 knows (or predicts) the behavior of Company 2, i.e., $f(q_1)$ is known to Company 1, it can maximize its profit by setting $q_1 = q_1^* = \max\{0, z\}$, where z solves

$$a - \frac{b}{2(b + c_2)} [a - bz]^+ - 2(b + c_1)z = 0. \tag{I.1}$$

The Nash equilibrium is thus given by $(q_1, q_2) = (q_1^*, f(q_1^*))$. Given the Nash equilibrium, the achievable profits for the two companies are obtained as $\Pi_1^* = \Pi_1(q_1^*, f(q_1*))$ and $\Pi_2^* = \Pi_2(q_1^*, f(q_1^*))$.

For the purpose of exposition, we now consider a numerical example. Set $a = 10\$$, $b = 0.5\$/\text{MW}$, $c_1 = 0.2\$/\text{MW}^2$, and vary $0 < c_2 < 1.6\$/\text{MW}^2$ in the above example. Fig. I.1 compares Π_1^* and Π_2^* versus c_2, from which it is observed that Π_2^* monotonically decreases over c_2, while the opposite is true for Π_1^*. This can be

explained by considering the fact that the generation cot (per unit) of Company 2 increases when c_2 increases. As a result, Company 2 reduces selling power q_2 to moderate the increasing trend of its generation cot, which lowers its revenue from selling power to the users. On the other hand, the price per unit, i.e., $P(q_1, q_2) = 10 - 0.5(q_1 + q_2)$, increases when q_2 decreases, with q_1 fixed. Hence, the profit of Company 1 increases. This example verifies that in Stackelberg game, the followers' parameters can implicitly affect the decision/utility of the leader. The opposite is also true, i.e., the change in decision of the leader affects the followers' ultimate decisions.

Appendix J

Proof of Proposition 4.6.1

Let $itr^\star > 1$ denotes the iteration that algorithm terminates, as a result, the algorithm given in Table 4.1 returns $\pi_{SCP}^{(itr^\star)}$ as the solution to (G2). Herein, we prove that $\pi_{SCP}^{(itr^\star)}$ is a locally optimal solution to (G2). Our proof consists of two main steps. First, we show that $\pi_{SCP}^{(itr^\star)}$ is a feasible point to (G2). Second, we show that $\pi_{SCP}^{(itr^\star)}$ locally minimizes (G2).

First, due to the fact that the stopping criterion is satisfied at the iteration $itr^\star$, i.e., $\mathcal{E} \leq \epsilon$ holds, it thus follows that both the conditions $\sum_{h=1}^{H} \phi_h^{(itr^\star)}(\boldsymbol{x}_{h,SCP}^{(itr^\star)}, \boldsymbol{y}_{h,SCP}^{(itr^\star)}, \underline{\boldsymbol{v}}_{h,SCP}^{(itr^\star)}, \overline{\boldsymbol{v}}_{h,SCP}^{(itr^\star)}, w_{h,SCP}^{(itr^\star)}) \leq \epsilon$ and $ED(\pi_{SCP}^{(itr^\star-1)}, \pi_{SCP}^{(itr^\star)}) \leq \epsilon$ hold simultaneously. Due to the fact that $\phi_h^{(itr)}(\cdot)$, $h = 1, \ldots, H$, and $ED(\cdot)$ are all non-negative functions, given $\epsilon \to 0$ and $\xi \gg 1$, we obtain

$$\phi_h^{(itr^\star)}(\boldsymbol{x}_{h,SCP}^{(itr^\star)}, \boldsymbol{y}_{h,SCP}^{(itr^\star)}, \underline{\boldsymbol{v}}_{h,\mathrm{SCP}}^{(itr^\star)}, \overline{\boldsymbol{v}}_{h,SCP}^{(itr^\star)}, w_{h,SCP}^{(itr^\star)}) = 0, \ \forall h \in \mathcal{H}, \tag{J.1}$$

$$ED(\pi_{SCP}^{(itr^\star-1)}, \pi_{SCP}^{(itr^\star)}) = 0. \tag{J.2}$$

From (J.1), it follows that $|q_{h,n}(\boldsymbol{y}_{h,SCP}^{(itr^\star-1)}) + \nabla q_{h,n}(\boldsymbol{y}_{h,SCP}^{(itr^\star-1)})^T(\boldsymbol{y}_{h,SCP}^{(itr^\star)} - \boldsymbol{y}_{h,SCP}^{(itr^\star-1)}) - \theta_h x_{h,n,SCP}^{(itr^\star)} + \underline{t}_{h,n,SCP}^{(itr^\star)} - \overline{t}_{h,n,SCP}^{(itr^\star)} - r_{h,SCP}^{(itr^\star)}| = 0$, $|\underline{v}_{h,n,SCP}^{(itr^\star)}(y_{h,n,SCP}^{(itr^\star-1)} - \underline{y}_{a,h}) + \underline{v}_{h,n,SCP}^{(itr^\star-1)}(y_{h,n,SCP}^{(itr^\star)} - y_{h,n,SCP}^{(itr^\star-1)})| = 0$, and $|\overline{v}_{h,n,SCP}^{(itr^\star)}(\overline{y}_{h,n} - y_{h,n,SCP}^{(itr^\star-1)}) - \overline{v}_{h,n,SCP}^{(itr^\star-1)}(y_{h,n,SCP}^{(itr^\star)} - y_{h,n,SCP}^{(itr^\star-1)})| = 0$, $n = n_0, \ldots, N$, $h = 1, \ldots, H$. From (J.2), it also follows that $\|\boldsymbol{x}_{h,SCP}^{(itr^\star-1)} - \boldsymbol{x}_{h,SCP}^{(itr^\star)}\|_2 = 0$, $\|\boldsymbol{y}_{h,SCP}^{(itr^\star-1)} - \boldsymbol{y}_{h,SCP}^{(itr^\star)}\|_2 = 0$, $\|\underline{\boldsymbol{v}}_{h,SCP}^{(itr^\star-1)} - \underline{\boldsymbol{v}}_{h,SCP}^{(itr^\star)}\|_2 = 0$, $\|\overline{\boldsymbol{v}}_{h,SCP}^{(itr^\star-1)} - \overline{\boldsymbol{v}}_{h,SCP}^{(itr^\star)}\|_2 = 0$, $h = 1, \ldots, H$, and $\|\boldsymbol{w}_{SCP}^{(itr^\star-1)} - \boldsymbol{w}_{SCP}^{(itr^\star)}\|_2 = 0$. According to the above results obtained

from (J.1) and (J.2), we thus have

$$q_{h,n}(\boldsymbol{y}_{h,SCP}^{(itr^\star)}) - \theta_h x_{h,n,SCP}^{(itr^\star)} + \underline{v}_{h,n,SCP}^{(itr^\star)} - \overline{v}_{h,n,SCP}^{(itr^\star)} - w_{h,SCP}^{(itr^\star)} = 0,\ \forall n \in \mathcal{N}_0,\ \forall h \in \mathcal{H}, \tag{J.3}$$

$$\underline{v}_{h,n,SCP}^{(itr^\star)}(y_{h,n,SCP}^{(itr^\star)} - \underline{y}_{h,n}) = 0,\ \forall n \in \mathcal{N}_0,\ \forall h \in \mathcal{H}, \tag{J.4}$$

$$\overline{v}_{h,n,SCP}^{(itr^\star)}(\overline{y}_{h,n} - y_{h,n,SCP}^{(itr^\star)}) = 0,\ \forall n \in \mathcal{N}_0,\ \forall h \in \mathcal{H}. \tag{J.5}$$

Since $\pi_{SCP}^{(itr^\star)}$ is a feasible point of (G2$-itr$), it holds the constraints given in (4.5) and (4.11)–(4.13). Furthermore, $\pi_{SCP}^{(itr^\star)}$ satisfies the constraint given in (J.3), (J.4), and (J.5), which are equivalent to those given in (4.8), (4.9), and (4.9), respectively. Therefore, it follows that $\pi_{SCP}^{(itr^\star)}$ is a feasible point to (G2).

Next, we want to show that $\pi_{SCP}^{(itr^\star)}$ is a locally optimal solution to (G2). Since $\pi_{\text{SCP}}^{(itr^\star)}$ is the optimal solution to (G2$-$ $itr^\star$), it follows that for any feasible point $(\{\boldsymbol{x}_h\}_{h\in\mathcal{H}}, \{\boldsymbol{y}_h\}_{h\in\mathcal{H}}, \{\underline{\boldsymbol{v}}_h\}_{h\in\mathcal{H}}, \{\overline{\boldsymbol{v}}_h\}_{h\in\mathcal{H}}, \boldsymbol{w})$ to (G2$-$ $itr^\star$), we have

$$C_{res}(\boldsymbol{y}_{1,SCP}^{(itr^\star)}, \ldots, \boldsymbol{y}_{H,SCP}^{(itr^\star)}) + \sum_{h=1}^{H} \phi_h^{(itr^\star)}(\boldsymbol{x}_{h,SCP}^{(itr^\star)}, \boldsymbol{y}_{h,SCP}^{(itr^\star)}, \underline{\boldsymbol{v}}_{h,SCP}^{(itr^\star)}, \overline{\boldsymbol{v}}_{h,SCP}^{(itr^\star)}, w_{h,SCP}^{(itr^\star)}) \leq$$
$$C_{res}(\boldsymbol{y}_1, \ldots, \boldsymbol{y}_H) + \sum_{h=1}^{H} \phi_h^{(itr)}(\boldsymbol{x}_h, \boldsymbol{y}_h, \underline{\boldsymbol{v}}_h, \overline{\boldsymbol{v}}_h, w_h). \tag{J.6}$$

Moreover, from (J.2), it follows that $\sum_{h=1}^{H} \phi_h^{(itr^\star)}(\boldsymbol{x}_h, \boldsymbol{y}_h, \underline{\boldsymbol{v}}_h, \overline{\boldsymbol{v}}_h, w_h) = 0$ for any point $(\{\boldsymbol{x}_h\}_{h\in\mathcal{H}}, \{\boldsymbol{y}_h\}_{h\in\mathcal{H}}, \{\underline{\boldsymbol{v}}_h\}_{h\in\mathcal{H}}, \{\overline{\boldsymbol{v}}_h\}_{h\in\mathcal{H}}, \boldsymbol{w})$ in the close vicinity of $\pi_{SCP}^{(itr^\star)}$. Accordingly, we can simplify (J.6) as follows

$$C_{res}(\boldsymbol{y}_{1,SCP}^{(itr^\star)}, \ldots, \boldsymbol{y}_{H,SCP}^{(itr^\star)}) \leq C_{res}(\boldsymbol{y}_1, \ldots, \boldsymbol{y}_H), \tag{J.7}$$

where $C_{res}(\cdot)$ is the objective function of (G2). Last, since $\pi_{SCP}^{(itr^\star)}$ is a feasible point to (G2) and (J.7) is valid for $\boldsymbol{y}_h$'s nearby $\boldsymbol{y}_{h,SCP}^{(itr^\star)}$ (neighboring points only), it follows that $\pi_{SCP}^{(itr^*)}$ locally minimizes (G2). The proof is thus completed.

References

[1] A. Zidan, and E. F. El-Saadany, "A cooperative multiagent framework for self-healing mechanisms in distribution systems, *IEEE Trans. Smart Grid*, vol. 3, no. 3, pp. 1525-1539, Sept. 2012.

[2] Operation statistics, available online at `https://www.ema.gov.sg/cmsmedia/Publications_and_Statistics/Publications/SES\%202014\%20Chapters/Chapter\%206\%20Solar.pdf`, May 2015.

[3] K. Rahbar, J. Xu, and R. Zhang, "Real-time energy storage management for renewable integration in microgrid: an Off-Line optimization approach, *IEEE Trans. Smart Grid*, vol. 6, no. 1, pp. 124-134, Jan. 2015.

[4] Technical Report, available online at `http://energy.gov/sites/prod/files/oeprod/DocumentsandMedia/DOE_Benefits_of_Demand_Response_in_Electricity_Markets_and_Recommendations_for_Achieving_Them_Report_to_Congress.pdf`, Feb. 2006.

[5] S. Mohagheghi, J. Stoupis, Z. Y. Wang, Z. Li, and H. Kazemzadeh, "Demand response architecture: integration into the distribution management system," *IEEE Int. Conf. Smart Grid Communications (SmartGridComm)*, pp. 501-506, Oct. 2010.

[6] S. C. Chan, K. M. Tsui, H. C. Wu, Y. Hou, Y. Wu, and F. F. Wu, "Load/price forecasting and managing demand response for smart grids: methodologies and challenges," *IEEE Sig. Process. Mag.*, vol. 29, no. 5, pp. 68-85, Sept. 2012.

[7] C. O. Adika and F. Wang, "Autonomous appliance scheduling for household energy management, *IEEE Trans. Smart Grid*, vol. 5, no. 2, pp. 673-682, Mar. 2014.

[8] P. Snchez-Martn, G. Snchez, and G. Morales-Espaa, "Direct load control decision model for aggregated EV charging points," *IEEE Trans. Power Sys.*, vol. 27, no. 3, pp. 1577-1584, June 2013.

[9] M. Alizadeh, A. Scaglione, and R. J. Thomas, "From packet to power switching: digital direct load scheduling," *IEEE J. Sel. Areas Commun.*, vol. 30, no. 6, pp. 1027-1036, July 2012.

[10] I. Koutsopoulos and L. Tassiulas, "Optimal control policies for power demand scheduling in the smart grid," *IEEE J. Sel. Areas Commun.*, vol. 30, no. 6, pp. 1049-1060, July 2012.

[11] A. Mohsenian-Rad and A. Leon-Garcia, "Optimal residential load control with price prediction in real-time electricity pricing environments," *IEEE Trans. Smart Grid*, vol. 1, no. 2, pp. 120-133, Sept. 2010.

[12] I. Atzeni, L. G. Ordez, G. Scutari, D. P. Palomar, and J. R. Fonollosa, "Non-cooperative and cooperative optimization of distributed energy generation and storage in the demand-side of the smart grid," *IEEE Trans. Sig. Process.*, vol. 61, no. 10, pp. 2454-2472, May 2013.

[13] L. P. Qian, Y. J. Zhang, J. Huang, and Y. Wu, "Demand response management via real-time electricity price control in smart grids," *IEEE J. Sel. Areas Commun.*, vol. 31, no. 7, pp. 1268-1280, July 2013.

[14] P. Samadi, A. Mohsenian-Rad, R. Schober, V. W. S. Wong, and J. Jatskevich, "Optimal real-time pricing algorithm based on utility maximization for smart grid," *IEEE Int. Conf. Smart Grid Communications (SmartGridComm)*, pp. 320-331, Oct. 2010.

[15] C. Joe-Wong, S. Sen, S. Ha, and M. Chiang, "Optimized day-ahead pricing for smart grids with device-specic scheduling flexibility," *IEEE J. Sel. Areas Commun.*, vol. 30, no. 6, pp. 1075-1085, July 2012.

[16] A. Mohsenian-Rad, V. W. S. Wong, J. Jatskevich, R. Schober, and A. Leon-Garcia, "Autonomous demand-side management based on game-theoretic energy consumption scheduling for the future smart grid," *IEEE Trans. Smart Grid*, vol. 1, no. 3, pp. 320-331, Dec. 2010.

[17] S. Caron and G. Kesidis, "Incentive-based energy consumption scheduling algorithms for the smart grid," *IEEE Int. Conf. Smart Grid Communications (SmartGridComm)*, pp. 391-396, Oct. 2010.

[18] A. Sepulveda, L. Paull, W. G. Morsi, H. Li, C. P. Diduch, and L. Chang, "A novel demand side management program using water heaters and particle swarm optimization," *IEEE Int. Conf. Electric Power and Energy Conference (EPEC)*, pp. 1-5, Aug. 2010.

[19] J. Yi, P. Wang, P. C. Taylor, P. J. Davison, P. F. Lyons, D. Liang, S. Brown, and D. Roberts , "Distribution network voltage control using energy storage and demand side response," *IEEE Int. Conf. Innovative Smart Grid Technologies (ISGT)*, pp. 1-8, Oct. 2012.

[20] A. L. M. Mufaris and J. Baba , "Local control of heat pump water heaters for voltage control with high penetration of residential PV systems," *IEEE Int. Conf. Industrial and Information Systems (ICIIS)*, pp. 18-23, Dec. 2013.

[21] S. A. Pourmousavi and M. H. Nehrir, "Real-time central demand response for primary frequency regulation in microgrids," *IEEE Trans. Smart Grid*, vol. 3, no. 4, pp. 1988-1996, Dec. 2012.

[22] N. Lu, and Y. Zhang, "Design considerations of a centralized load controller using thermostatically controlled appliances for continuous regulation reserves," *IEEE Trans. Smart Grid*, vol. 4, no. 2, pp. 914-921, June 2013.

[23] O. Ma, N. Alkadi, P. Cappers *et al.*, "Demand response for ancillary services," *IEEE Trans. Smart Grid*, vol. 4, no. 4, pp. 1988-1995, Dec. 2013.

[24] Technical Report, "Basic criteria for design and operation of interconnected power systems," *Northeast Power Coordinating Council*, available online at `http://www.iso-ne.com/committees/comm_wkgrps/relblty_comm/relblty/mtrls/2004/nov12004/A8-1_A-02\%20old.pdf`, May 2004.

[25] G. Lalor, "Frequency control on an Island power system with evolving plant mix," *PhD Thesis*, University College Dublin, 2005.

[26] Transmission system map, available online at `http://smartgriddashboard.eirgrid.com/#all/transmission-map`.

[27] Technical report, "Alternative approaches for incentivizing the frequency responsive reserve ancillary service," *National Renewable Energy Laboratory (NREL)*, available online at `http://www.nrel.gov/docs/fy12osti/54393.pdf`, Mar. 2012.

[28] State of the Market Report for PJM, "Monitoring Analytics," *PJM Electricity Market*, available online at `http://www.monitoringanalytics.com/reports/PJM_State_of_the_Market/2014/2014-som-pjm-volume1.pdf`, Mar. 2015.

[29] V. V. Terzija, "Adaptive under-frequency load shedding based on the magnitude of the disturbance estimation," *IEEE Trans. Power Sys.*, vol. 21, no. 3, pp. 1260-1266, Aug. 2006.

[30] A. Ketabi and M. H. Fini, "An under-frequency load Shedding Scheme for Hybrid and Multiarea Power Systems," *IEEE Trans. Smart Grid*, vol. 6, no. 1, pp. 82-91, Jan. 2015.

[31] A. Saffarian and M. Sanaye-Pasand, "Enhancement of power system stability using adaptive combinational load shedding methods," *IEEE Trans. Power Sys.*, vol. 26, no. 3, pp. 1010-1020, Aug. 2011.

[32] H. Sekyung, H. Soohee, and K. Sezaki, "Development of an optimal vehicle-to-grid aggregator for frequency regulation," *IEEE Trans. Smart Grid*, vol. 1, no. 1, pp. 65-72, June 2010.

[33] M. D. Galus, S. Koch, and G. Andersson, "Provision of load frequency control by PHEVs, controllable loads, and a cogeneration unit," *IEEE Trans. Ind. Electron.*, vol. 58, no. 10, pp. 4568-4582, June 2010.

[34] L. Chang-Chien, L. N. An, T. Lin, and W. Lee, "Incorporating demand response with spinning reserve to realize an adaptive frequency restoration plan for system contingencies," *IEEE Trans. Smart Grid*, vol. 3, no. 3, pp. 1145-1153, Sept. 2012.

[35] G. Sharma, L. Xie, and P. R. Kumar, "Large population optimal demand response for thermostatically controlled inertial loads," *IEEE Int. Conf. Smart Grid Communications (SmartGidComm)*, pp. 259 - 264 , Oct. 2013.

[36] M. A. Ortega-Vazquez, F. Bouffard, and V. Silva, "Electric vehicle aggregator/system operator coordination for charging scheduling and services procurement," *IEEE Trans. Power Sys.*, vol. 28, no. 2, pp. 1806-1815, May 2013.

[37] F. Kennel, D. Gorges, and S. Liu, "Energy management for smart grids with electric vehicles based on hierarchical MPC," *IEEE Trans. Ind. Informat.*, vol. 9, no. 3, pp. 1528-1537, Aug. 2013.

[38] A. Papavasiliou and S. S. Oren, "Large-scale integration of deferrable demand and renewable energy sources," *IEEE Trans. Power Sys.*, vol. 29, no. 1, pp. 489-499, Jan. 2014.

[39] J. Lin, K. Leung, and V. O. K. Li, "Online scheduling with vehicle-to-grid regulation service," *IEEE Trans. Smart Grid*, vol. 1, no. 6, pp. 556-569, Dec. 2014.

[40] Z. Liu, D. Wang, H. Jia, N. Djilali, and W. Zhang, "Aggregation and bidirectional charging power control of plug-in hybrid electric vehicles: generation system adequacy analysis," *IEEE Trans. Sustain. Energy*, vol. 6, no. 2, pp. 325-335, Apr. 2015.

[41] Technical Report, "Pacific northwest gridwise testbed demonstration projects – part II: grid friendly appliance project," *Pacific Northwest National Labolatory (PNNL)*, available online at `http://www.pnl.gov/main/publications/external/technical_reports/PNNL-17079.pdf`, Oct. 2007.

[42] J. A. Short, D. G. Infield, and L. L. Freris, "Stabilization of grid frequency through dynamic demand control," *IEEE Trans. Power Sys.*, vol. 22, no. 3, pp. 1284-1293, Aug. 2007.

[43] A. Molina-Garcia, F. Bouffard, and D. S. Kirschen, "Decentralized demand-side contribution to primary frequency control," *IEEE Trans. Power Sys.*, vol. 26, no. 1, pp. 411-418, Feb. 2011.

[44] X. Zhao, J. Østergaard, and M. Togeby, "Demand as frequency controlled reserve," *IEEE Trans. Power Sys.*, vol. 26, no. 3, pp. 1062-1071, Aug. 2011.

[45] K. Samarakoon, J. Ekayanake, and N. Jenkins, "Investigation of domestic load control to provide primary frequency response using smart meters," *IEEE Trans. Smart Grid*, vol. 3, no. 1, pp. 282-292, Mar. 2012.

[46] P. J. Douglass, R. Garcia-Valle, P. Nyeng, J. Ostergaard, M. Togeby "Smart demand for frequency regulation," *IEEE Trans. Smart Grid*, vol. 4, no. 3, pp. 1713-1720, Sept. 2013.

[47] A. Molina-Garcia, I. Munoz-Benavente, A. D. Hansen, F. Gomez-Lazaro, "Demand-side contribution to primary frequency control with wind farm auxiliary control," *IEEE Trans. Power Sys.*, vol. 29, no. 5, pp. 2391-2399, Sept. 2014.

[48] S. Hild, S. Leavey, C. Graf, and B. Sorazu, "Smart charging technologies for portable electronic devices," *IEEE Trans. Smart Grid*, vol. 5, no. 1, pp. 328-336, Jan. 2014.

[49] D. Angeli and P. A. Kountouriotis, "A stochastic approach to dynamic-demand refrigerator control," *IEEE Trans. Control Sys. Tech.*, vol. 20, no. 3, pp. 581-592, May 2012.

[50] Y. Ota, H. Taniguchi, T. Nakajima, K. M. Liyanage, J. Baba, and A. Yokoyama, "Autonomous distributed V2G (vehicle-to-grid) satisfying scheduled charging, " *IEEE Trans. Smart Grid*, vol. 3, no. 1, pp. 559-564, Mar. 2012.

[51] J. A. P. Lopes, F. J. Soares, and P. M. R. Almeida, "Integration of electric vehicles in the electric power system," *IEEE Proc.*, vol. 99, no. 1, pp. 168-183, Jan. 2011.

[52] H. Yang, Member, C. Y. Chung, and J. Zhao, "Application of plug-in electric vehicles to frequency regulation based on distributed signal acquisition via limited communication, " *IEEE Trans. Power Sys.*, vol. 28, no. 2, pp. 1017-1026, May 2013.

[53] J. Pahasa and I. Ngamroo, "PHEVs bidirectional charging/discharging and SoC control for microgrid frequency stabilization using multiple MPC", *IEEE Trans. Smart Grid*, vol. 6, no. 2, pp. 526-533, Mar. 2015.

[54] M. Aunedi, P. A. Kountouriotis, J. E. O. Calderon, D. Angeli and G. Strbac, "Economic and environmental benefits of dynamic demand in providing frequency regulation", *IEEE Trans. Smart Grid*, vol. 4, no. 4, pp. 2036-2048, Dec. 2013.

[55] K. Dehghanpour and S. Afsharnia, "Electrical demand side contribution to frequency control in power systems:a review on technical aspects," *Renewable and Sustainable Energy Reviews*, vol. 41, pp. 1267-1276, Jan. 2015.

[56] Power systems test case archive, available online at `http://publish.illinois.edu/smartergrid/wscc-9-bus-system/`.

[57] C. Zhao, U. Topcu, and S. H. Low, "Frequency-based load control in power systems," *IEEE American Control Conference (ACC)*, pp. 4423-4430, June 2012.

[58] R. G. Gallager, "A perspective on multiaccess channels," *IEEE Trans. Inf. Theory*, vol. 31, no. 2, pp. 124-142, Mar. 1985.

[59] Y. Yang and T. P. Yum,"Delay distributions of slotted ALOHA and CSMA," *IEEE Trans. Commun.*, vol. 51, no. 11, pp. 1846-1857, Nov. 2003.

[60] P. Zhou, H. Hu, H. Wang, and H. Chen,"An efficient random access scheme for OFDMA systems with implicit message transmission," *IEEE Trans. Wireless Commun.*, vol. 7, no. 7, pp. 2790-2797, July 2008.

[61] P. Samadi, A. Mohsenian-Rad, R. Schober, V. W. S. Wong, and J. Jatskevich, "Optimal real-time pricing algorithm based on utility maximization for smart grid," *IEEE Int. Conf. Smart Grid Communications (SmartGridComm)*, pp. 415-420, Oct. 2010.

[62] R. Yu, W. Yang, and S. Rahardja, "A statistical demand-price model with its application in optimal real-time price," *IEEE Trans. Smart Grid*, vol. 3, no. 4, pp. 1734-1742, Dec. 2012.

[63] J. Chen, B. Yang, and X. Guan, "Optimal demand response scheduling with Stackelberg game approach under load uncertainty for smart grid," *IEEE Trans. Smart Grid*, pp. 546-551, Nov. 2012.

[64] F. Meng and X. Zeng, "A stackelberg game approach to maximise electricity retailer's profit and minimse customers' bills for future smart grid," *IEEE Workshop Computational Intelligence*, pp. 1-7, Sept. 2012.

[65] F. Meng and X. Zeng, "An Optimal Real-time Pricing Algorithm for the Smart Grid: A Bi-level Programming Approach," *Imperial College Computing Student Workshop (ICCSW)*, pp. 81-88, Sept. 2013.

[66] L. P. Qian, Y. J. Zhang, J. Huang, and Y. Wu, "Demand response management via real-time electricity price control in smart grids," *IEEE J. Sel. Areas Commun.*, vol. 31, no. 7, pp. 1268-1280, July 2013.

[67] L. Gkatzikis, I. Koutsopoulos, and T. Salonidis, "The role of aggregators in smart grid demand response markets," *IEEE J. Sel. Areas Commun.*, vol. 31, no. 7, pp. 1247-1257, July 2013.

[68] B. Kim, S. Ren, M. Schaar, and J. Lee, "Bidirectional energy trading and residential load scheduling with electric vehicles in the smart grid," *IEEE J. Sel. Areas Commun.*, vol. 31, no. 7, pp. 1219-1234, July 2013.

[69] P. Samadi, A. Mohsenian-Rad, V. W. S. Wong, and R. Schober, "Real-time pricing for demand response based on stochastic approximation," *IEEE Trans. Smart Grid*, vol. 5, no. 2, pp. 789-798, Mar. 2014.

[70] C. Vivekananthan, Y. Mishra, G. Ledwich, and F. Li, "Demand response for residential appliances via customer reward scheme," *IEEE Trans. Smart Grid*, vol. 5, no. 2, pp. 809-820, Mar. 2014.

[71] A. G. Vlachos and P. N. Biskas, "Demand response in a real-time balancing market clearing with pay-as-bid pricing," *IEEE Trans. Smart Grid*, vol. 4, no. 4, pp. 1966-1975, Dec. 2015.

[72] P. Kundur, *Power System Stability and Control*, McGraw-Hill, 1994.

[73] Z. Chen, Z. Sahinoglu, and H. Li, "Fast frequency and phase estimation in three phase power systems," *IEEE Power and Energy Society General Meeting*, pp. 1-5, July 2013.

[74] Computer software, "PowerWorld simulator," Ver. 16, available online at `www.powerworld.com`.

[75] G. Xiao, C. Li, Z. Yu, Y. Cao, and B. Fang, "Review of the impact of electric vehicles participating in frequency regulation on power Grid," *IEEE Chinese Automation Congress (CAC)*, pp. 75-80, Nov. 2013.

[76] Technical Report, "Environmental assessment of plug-in hybrid electric vehicles, volume 1: nationwide greenhouse gas emissions," *Electric Power Research Institute*, available online at `http://www.epri.com/abstracts/pages/ProductAbstract.aspx?productId=000000000001015325`, July 2007.

[77] F. Rassaei, W. Sohc, and K. C. Chua, "A Statistical modelling and analysis of residential electric vehicles' charging demand in smart grids," available online at `http://arxiv.org/pdf/1408.2320v1.pdf`, Aug. 2014.

[78] M. F. Shaaban, M. Ismail, E. F. El-Saadany, and W. Zhuang, "Real-time PEV charging/discharging coordination in smart distribution systems," *IEEE Trans. Smart Grid*, vol. 5, no. 4, pp. 1797-1807, July 2014.

[79] J. Machowski, J. W. Bialek, and J. R. Bumby, *Power System Dynamics: Stability and Control*, Wiley, 2008.

[80] G. Kasal and B. Singh, "Decoupled voltage and frequency controller for isolated asynchronous generators feeding three-phase four-wire loads," *IEEE Trans. Power Delivery*, vol. 23, no. 2, pp. 966-973, Apr. 2008.

[81] A. Papoulis and S. U. Pillai, *Probability, Random Variables, and Stochastic Processes*, McGraw-Hill, 2002.

[82] D. T. Nguyen and L. B. Le, "Joint optimization of electric vehicle and home energy scheduling considering user comfort preference," *IEEE Trans. Smart Grid*, vol. 5, no. 1, pp. 188-199, Jan. 2014.

[83] J. Donadee and M D. Ilic, "Stochastic optimization of grid to vehicle frequency regulation capacity bids," *IEEE Trans. Smart Grid*, vol. 5, no. 2, pp. 1061-1069, Mar. 2014.

[84] W. Hu, C. Su, Z. Chen, and B. Bak-Jensen, "Optimal operation of plug-in electric vehicles in power systems with high wind power penetrations," *IEEE Trans. Sustain. Energy*, vol. 4, no. 3, pp. 577-585, July 2013.

[85] Y. Cao, S. Tang, C. Li, P. Zhang, Y. Tan, Z. Zhang, and J. Li, "An optimized EV charging model considering TOU price and SOC curve," *IEEE Trans. Smart Grid*, vol. 3, no. 1, pp. 388-393, Mar. 2012.

[86] K. Mets, R. D'hulst, and C. Develder, "Comparison of intelligent charging algorithms for electric vehicles to reduce peak load and demand variability in a distribution grid," *J. Commun. and Net.*, vol. 14, no. 6, pp. 672-681, Dec. 2012.

[87] S. Deilami, A. S. Masoum, P. S. Moses, and M. A. S. Masoum,"Real-time coordination of plug-in electric vehicle charging in smart grids to minimize power losses and improve voltage prole," *IEEE Trans. Smart Grid*, vol. 2, no. 3, pp. 456-467, Sept. 2011.

[88] G. Delille, B. Franois, and G. Malarange, "Dynamic frequency control support by energy storage to reduce the impact of wind and solar generation on isolated power systems inertia," *IEEE Trans. Sustain. Energy*, vol. 3, no. 4, pp. 931-929, Oct. 2012.

[89] D. L. H. Aik, "A general-order system frequency response model incorporating load shedding: analytic modeling and applications," *IEEE Trans. Power Sys.*, vol. 21, no. 2, pp. 709-717, May 2006.

[90] S. Boyd and L. Vandenberghe, *Convex Optimization*, Cambridge University Press, 2004.

[91] M. Grant and S. Boyd, CVX: Matlab software for disciplined convex programming, Ver. 2.0 beta, available online at http://cvxr.com/cvx, Sept. 2012.

[92] Technical Report, "PEV charging standards status including AC, DC and wireless technologies," *Theodore Bohn Argonne National Laboratory*, available online at `http://www.sae.org/events/gim/presentations/2013/pev_charging_standards_status.pdf`, 2013.

[93] P. Yi, X. Dong, A. Iwayemi, C. Zhou, and S. Li, "Real-time opportunistic scheduling for residential demand response," *IEEE Trans. Smart Grid*, vol. 4, no. 1, pp. 227-234, Mar. 2013.

[94] C. Joe-Wong, S. Sen, S. Ha, and M. Chiang, "Optimized day-ahead pricing for smart grids with device-specific scheduling flexibility," *IEEE J. Sel. Areas Commun.*, vol. 30, no. 6, pp. 1075-1085, July 2012.

[95] J. H. Yoon, R. Baldick, and A. Novoselac, "Dynamic demand response controller based on real-time retail price for residential buildings," *IEEE Trans. Smart Grid*, vol. 5, no. 1, pp. 121-129, Jan. 2014.

[96] S. Li, D. Zhang, A. B. Roget, and Z. O'Neill, "Integrating home energy simulation and dynamic electricity price for demand response study," *IEEE Trans. Smart Grid*, vol. 5, no. 2, pp. 779-788, Mar. 2014.

[97] Technical Report, "Commercially available aggregator programs in California," available online at `http://www.pge.com/includes/docs/pdfs/mybusiness/energysavingsrebates/demandresponse/amp/fs_aggregatorprograms.pdf`, Aug. 2013.

[98] B. Colson, P. Marcotte, and G. Savard, "An overview of bilevel optimization," *Ann. Oper. Res.*, vol. 153, no. 1, pp. 235-256, Sept. 2007.

[99] S. Boyd, "Convex optimization II," Stanford University, available online at http://www.stanford.edu/class/ee364b/lectures.html

[100] P. J. M. Laarhoven and E. H. L. Aarts, *Simulated annealing: theory and applications*, Springer, 1987.

[101] Operation statistics, available online at `http://www.singaporepower.com.sg/irj/go/km/docs/wpccontent/Sites/SP\%20Services/Site\%20Content/Tariffs/documents/Historical\%20Electricity\%20Tariff.pdf`.

[102] Operation statistics, available online at `https://www.emcsg.com/MarketData/PriceInformation`.

[103] A. J. Wood and B. F. Wollenberg, *Power Generation, Operation, and Control*, Wiley, 1996.

[104] I. Maruta and Y. Takarada "Modeling of dynamics in demand response for real-time pricing," *IEEE Int. Conf. Smart Grid Communications (SmartGrtidComm)*, pp. 806-811, Nov. 2014.

[105] S. Zhao and Zhou Ming, "Modeling demand response under time-of-use pricing," *IEEE Int. Conf. Power System Technology (POWERCON)*, pp. 1948-1955, Oct. 2014.

[106] F. J. Soares, J. A. P. Lopes, P. M. R. Almeida, C. L. Moreira, and L. Seca, "A stochastic model to simulate electric vehicles motion and quantify the energy required from the grid," *IEEE Int. Conf. Power Systems Computation*, pp. 369-374, Aug. 2011.

[107] H. Stackelberg, *Market Structure and Equilibrium*, Springer, 2011.

List of Publications

Journal Publications

(J1) M. R. V. Moghadam and R. Zhang, "Multiuser wireless power transfer via magnetic resonant coupling: performance analysis, charging control, and power region characterization," *IEEE Transactions on Signal and Information Processing over Networks*, Dec. 2015. (early access on IEEE Xplore).

(J2) M. R. V. Moghadam, R. Zhang, and R. T. B. Ma, "Distributed frequency control in smart grid via randomized response of electric vehicles," *IEEE Transactions on Sustainable Energy*, Nov. 2015. (early access on IEEE Xplore)

(J3) M. R. V. Moghadam, R. T. B. Ma, and R. Zhang, "Distributed frequency control in smart grids via randomized demand response," *IEEE Transactions on Smart Grid*, pp. 2798-2809, Nov. 2014.

Conference Publications

(C1) M. R. V. Moghadam and R. Zhang, "Multiuser charging control in wireless power transfer via magnetic resonant coupling," *IEEE International Conference on Acoustics, Speech, and Signal Processing (ICASSP)*, pp. 1-5, Apr. 2015.

(C2) M. R. V. Moghadam, R. Zhang, and R. T. B. Ma, "Demand response for contingency management via real-time pricing in smart grids," *IEEE International Conference on Smart Grid Communications (SmartGridComm)*, pp. 632-637, Nov. 2014.

(C3) M. R. V. Moghadam, R. Zhang, and R. T. B. Ma, "Randomized response electric vehicles for distributed frequency control in smart grid," *IEEE International Conference on Smart Grid Communications (SmartGrtidComm)*, pp. 139-144, Oct. 2013.

(C4) M. R. V. Moghadam, R. T. B. Ma, and R. Zhang, "Distributed frequency control via demand responses in smart grids," *IEEE International Conference on Acoustics, Speech, and Signal Processing (ICASSP)*, May 2013.